TUM – Fakultät für Maschinenwesen

Conception of Advanced Driver Assistance Systems for Precise and Safe Control of Teleoperated Road Vehicles in Urban Environments

Seyed Amin Hosseini, M.Sc.

Vollständiger Abdruck der von der Fakultät für Maschinenwesen der Technischen Universität München zur Erlangung des akademischen Grades eines

Doktor-Ingenieurs (Dr.-Ing)

genehmigten Dissertation.

Vorsitzende: Prof. Dr. rer. nat. Sonja Berensmeier

Prüfende der Dissertation:

1. Prof. Dr.-Ing. Markus Lienkamp

2. Prof. Dr.-Ing. habil. Alois Knoll

Die Dissertation wurde am 20.12.2017 bei der Technischen Universität München eingereicht und durch die Fakultät für Maschinenwesen am 15.09.2018 angenommen.

Anhang I

Eidesstattliche Erklärung

Ich erkläre an Eides statt, dass ich die bei der promotionsführenden Einrichtung
Fakultät für Maschinenwesen
der TUM zur Promotionsprüfung vorgelegte Arbeit mit dem Titel
Conception of Advanced Driver Assistance Systems for Precise and Safe Control of Teleoperated Road Vehicles in Urban Environments
am **Lehrstuhl für Fahrzeugtechnik**
unter der Anleitung und Betreuung durch **Univ.-Prof. Dr.-Ing. Markus Lienkamp**
ohne sonstige Hilfe erstellt und bei der Abfassung nur die gemäß § 6 Ab. 6 und 7 Satz 2 angebotenen Hilfsmittel benutzt habe.

☒ Ich habe keine Organisation eingeschaltet, die gegen Entgelt Betreuerinnen und Betreuer für die Anfertigung von Dissertationen sucht, oder die mir obliegenden Pflichten hinsichtlich der Prüfungsleistungen für mich ganz oder teilweise erledigt.

☒ Ich habe die Dissertation in dieser oder ähnlicher Form in keinem anderen Prüfungsverfahren als Prüfungsleistung vorgelegt.

☐ Die vollständige Dissertation wurde in _____ veröffentlicht. Die promotionsführende Einrichtung _____ hat der Veröffentlichung zugestimmt.

☒ Ich habe den angestrebten Doktorgrad noch nicht erworben und bin nicht in einem früheren Promotionsverfahren für den angestrebten Doktorgrad endgültig gescheitert.

☐ Ich habe bereits am _____ bei der Fakultät für der Hochschule _____ unter Vorlage einer Dissertation mit dem Thema die Zulassung zur Promotion beantragt mit dem Ergebnis: _____

Die öffentlich zugängliche Promotionsordnung der TUM ist mir bekannt, insbesondere habe ich die Bedeutung von § 28 (Nichtigkeit der Promotion) und § 29 (Entzug des Doktorgrades) zur Kenntnis genommen. Ich bin mir der Konse-quenzen einer falschen Eidesstattlichen Erklärung bewusst.
Mit der Aufnahme meiner personenbezogenen Daten in die Alumni-Datei bei der TUM bin ich

☒ einverstanden, ☐ nicht einverstanden.

Ort, Datum, Unterschrift

Abstract

The current state of technology enables autonomous driving in simple environments such as freeways and parking garages. However, intelligent cars still cannot behave faultlessly in complex urban traffic scenarios.

Teleoperated driving is considered to be a transient technology for driverless driving in urban environments. Using this technology, data from the sensors of the unmanned vehicle are transmitted over a mobile network to a stationary call center, from which a human operator can control the car remotely. Thus, human intelligence can be used in situations in which machines cannot appropriately understand their environments or make robust decisions.

One of the main use cases of this technology would be car sharing, meaning that cars could be remotely provided to costumers. In addition, some other applications such as remote valet parking and remote driving of electric cars to charging stations can be realized using this technology.

Although this mobility concept benefits from retaining humans within vehicles' control loops, it faces challenges. This work focuses on low situational awareness and time delay in communication as two important challenges that arise during teleoperated driving and can cause obvious difficulties when attempting to precisely and safely control a remote car.

To address these challenges, this work proposes a package of advanced driver assistance systems. To improve the operator's situation awareness and increase his ability to precisely control a vehicle, a mixed reality human-machine interface (HMI) using a head-mounted display (HMD) is proposed. This HMI concept uses the data transmitted by the camera and the LiDAR sensors of a remote vehicle in order to depict the 360° vehicle's surroundings to the human operator as a mixture of the real and virtual environments.

In order to promote safety, two braking and haptic assistance systems that intervene in the longitudinal and lateral control of remote cars are proposed. The proposed brake assistance system reacts to upcoming hazards that the human operator may be unaware of due to communication time delay. In order to do so, this system predicts the motion trajectories of dynamic obstacles in the vehicle's surroundings using a stereo vision based track-before-detect approach and reacts autonomously to the predicted hazards through speed control.

The proposed haptic assistance system predicts lateral collisions and applies an assistance steering torque to the steering wheel of the operator's workstation. This steering assistance system supports the human operator in a generic way in challenging scenarios without the need for road information. Thus, it reduces the lateral collision risk that exists during the lateral control of a remote car as a result of communication time delay.

The proposed assistance systems are evaluated in several human-in-the-loop test drives, using experienced test persons. The results of these test drives show an overall increase in the precision and safety of teleoperated driving as a result of applying the proposed concepts.

Danksagung

Die vorliegende Arbeit entstand während meiner vierjährigen Tätigkeit von 2013 bis 2017 als wissenschaftlicher Mitarbeiter am Lehrstuhl für Fahrzeugtechnik der Technischen Universität München. Mein besonderer Dank gilt Herrn Prof. Dr.-Ing. Markus Lienkamp, der es mir ermöglicht hat, am spannenden Forschungsprojekt "Teleoperiertes Fahren" teilhaben zu können. Während unserer Zusammenarbeit habe ich viel von seiner pragmatischen Sicht in der Forschung gelernt.

Herrn Prof. Dr.-Ing. habil. Alois Knoll danke ich für die Übernahme der Zweitgutachtung dieser Dissertation, sowie Frau Prof. Dr. rer. nat. Sonja Berensmeier für die Übernahme des Prüfungsvorsitzes.

Meinen ehemaligen Kollegen in der Forschungsgruppe Fahrerassistenz und Sicherheit des Lehrstuhls für Fahrzeugtechnik danke ich für die zahlreichen Diskussionen und fachliche Anregungen für meine Forschungsarbeit. Mein besonderer Dank gilt hier meinem Gruppenleiter Dr.-Ing. Frank Diermeyer für seine Unterstützung und die hilfreichen Diskussionen. Ein zusätzlicher Dank geht an meine ehemaligen Kollegen, David Wittmann und Philip Feig, für das Gegenlesen dieser Dissertation und ihre wertvollen Anmerkungen.

Meinem Vorgänger im Projekt "Teleoperiertes Fahren", Dr.-Ing. Sebastian Gnatzig, danke ich für seine Forschungsarbeit, die eine passende Basis für die vorliegende Arbeit vorbereitet hat. Zusätzlich bedanke ich mich bei allen meinen Kollegen am Lehrstuhl für Fahrzeugtechnik, die durch eine super freundliche Stimmung die Freude an der Arbeit verdoppelt haben.

Ein großer Dank gilt auch den vielen Studenten, die mich durch studentische Arbeiten bei der Realisierung und Validierung meiner Ideen unterstützt haben. Besonders hervorheben möchte ich: Roland Kutka, Julian Sabielny, Thomas Wiedemann, Simon Bauer, Florian Richthammer und Jakob Porer für ihre hervorragende Unterstützung in verschiedenen Schritten meiner Arbeit.

Meinen Eltern und Brüdern danke ich für ihre grenzenlose Liebe und Unterstützung im ganzen Leben. Anschließend bedanke ich mich bei Ida für ihre Unterstützung während der Anfertigung dieser wissenschaftlichen Arbeit an der TUM.

Amin Hosseini
Stuttgart, im November 2017.

Contents

1 Introduction

1.1 Motivation

Over recent decades, remarkable efforts have been made to improve the intelligence of cars. While earlier efforts focused on promoting the driver's safety and comfort, more recent efforts have aimed at removing drivers altogether from a car's control loop.
This trend is a logical response to different requirements: On the one hand, drivers tend to demand greater safety and comfort while driving. Fully automated driving would provide greater comfort over long distances and could avoid the risk of inappropriate human decisions.
On the other hand, commercial users such as haulers have tended to decrease their fuel and personal costs through fully automated driving. The full automation of public transportation systems in cities could produce similar benefits.
Given the current state of technology, fully automated vehicles will soon be introduced to the market. However, at first this technology will only function in simple environments such as freeways or parking garages.
Despite the obvious progress that has been made toward automated driving, much work is still required before vehicles can operate autonomously in all driving scenarios. The main challenge is driverless operation in highly complex urban environments. Given the current state of machine intelligence, it cannot fully process complex environments and make appropriate decisions in all situations. For example, a recent report from the Google self-driving car project [1] indicated that $89\,\%$ of the disengagements of the autonomous mode occurred in complex street environments. The main causes for these disengagements were machine perception, software discrepancies and unwanted vehicle maneuvers.
Teleoperated driving [2] is a transient technology for realizing driving in urban environments without the need for a driver in the vehicle. This concept involves a human *operator* who controls the car remotely from a stationary workstation. The remote car or *teleoperator* is equipped with sensors that transmit data to the operator using a wireless communication unit. Figure 1.1 illustrates a schematic of this concept.
The operator's workstation is equipped with the conventional actuators, such as a steering wheel and brake and gas pedals, with which the human operator can send control signals to the teleoperator. In addition, the images received from the teleoperator are displayed to the operator using several monitors.
The main advantage of this concept is that a human remains in the control loop of the vehicle. In situations where a machine is unable to appropriately process its environment or make a robust decision, the human operator can demonstrate robust driving behavior, using his environment perception and decision-making abilities.

1.2 Use Cases

The main use case of teleoperated driving would be car-sharing in the megacities that have grown significantly over recent decades. Figure 1.2 illustrates the rapid growth of this market in recent years. Several studies predict that car sharing will be an increasingly common practice. For example, a case study in Germany has shown that $31\,\%$ of the population intended to increase their use of car-sharing services over the upcoming 10 years [3].
Currently, car-sharing customers park their hired cars in arbitrary parking spaces within a defined business area after using them. The next customer then needs to check an online map, find the nearest car and retrieve it. Furthermore, the companies that provide car-sharing services sometimes need to retrieve their cars in order to refuel or clean them.
Using teleoperated driving, vehicles can be remotely driven to customers, charging stations

or providers. In addition, a valet parking service that drives cars to the next parking garage can be realized.
In addition to car sharing, teleoperated driving would significantly affect conventional taxi services. Currently, taxi drivers need to wait long periods of time for their passengers. Thus, their vehicles are only in operation for limited periods of time each day.
To increase the efficiency of taxi services, taxi drivers can be replaced by human operators who can control taxis remotely. Using this approach, each taxi service would need a call center from which the taxis distributed throughout a city can be controlled. As analyzed in [141], based on the taxi fleet in Porto, teleoperation of taxi fleets would reduce the number of drivers hired by taxi services by 15 to 39 %.

1.3 General Challenges in Teleoperation

Although teleoperated driving benefits from keeping humans in the control loop, this practice has its own challenges. Generally, these challenges can be divided into the following categories:

1) Lack of situation awareness
When a human operator controls a car remotely, his situation awareness is lower than when controlling it from within the vehicle. This reduced situation awareness mainly results from the lack of information that the operator receives regarding the teleoperator and its surroundings as a result of his physical absence from the teleoperator. Reduced situation awareness may affect the driving performance of the human operator.

2) Time delay in communication
Time delay is always a factor in mobile communication. Ping tests for the transmission of small-sized amounts of control data from the operator's workstation to a car (downlink case) using LTE (4G) indicate a maximum time delay of 70 ms and an average time delay of 47 ms [5]. These tests indicate a longer time delay when transmitting larger amounts of data in the opposite direction (uplink case).

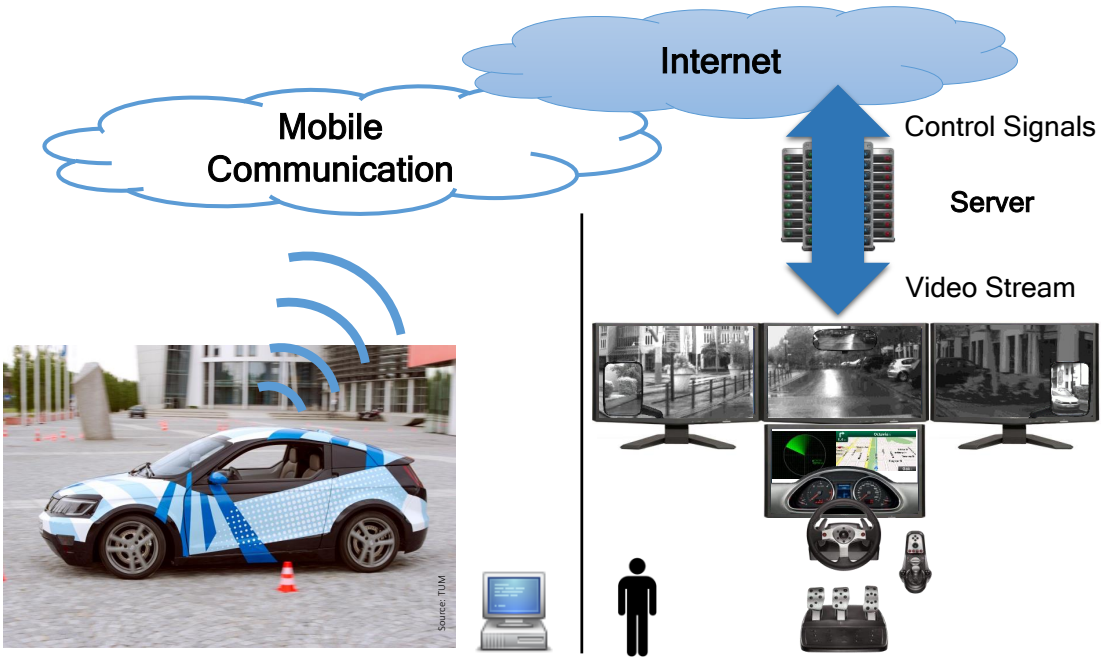

Figure 1.1 : System structure of the vehicle teleoperation using a mobile network [2]

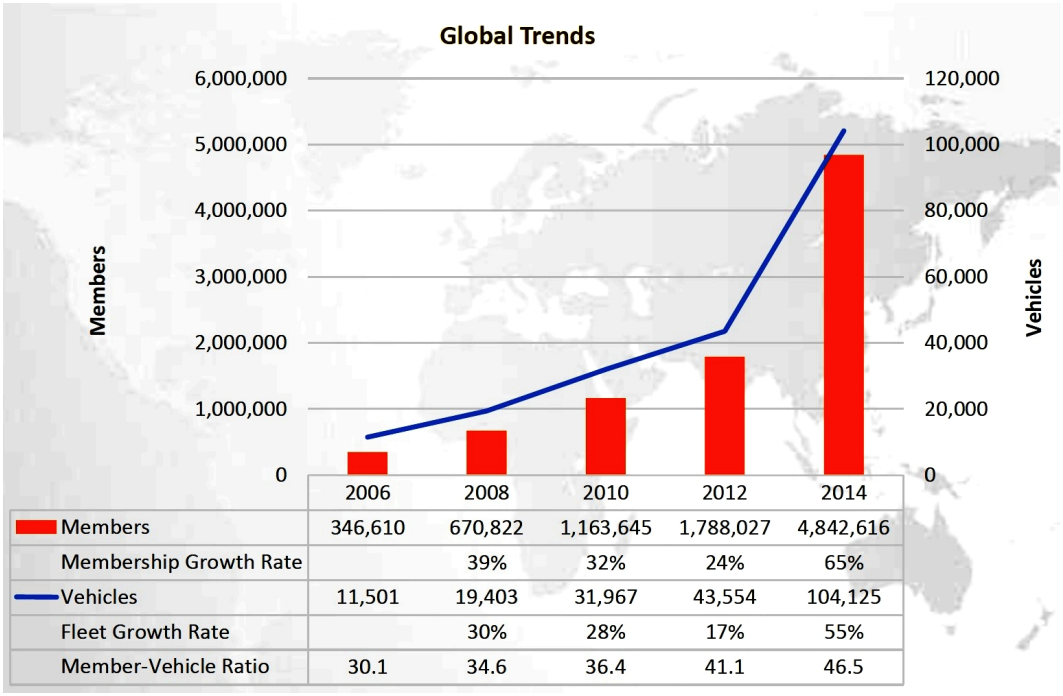

	2006	2008	2010	2012	2014
Members	346,610	670,822	1,163,645	1,788,027	4,842,616
Membership Growth Rate		39%	32%	24%	65%
Vehicles	11,501	19,403	31,967	43,554	104,125
Fleet Growth Rate		30%	28%	17%	55%
Member-Vehicle Ratio	30.1	34.6	36.4	41.1	46.5

Figure 1.2 : Rapid growth of the car sharing market in the world [4]

Since mobile networks have restricted bandwidth capacities, camera images must be encoded before transmission and decoded thereafter. Figure 1.3 shows the overall time delay when transmitting three encoded camera images at the speed of 3 Mbit/s from a teleoperator to the operator's workstation using a commercial LTE (4G) network. This measurement shows a maximum time delay of 445 ms and an average time delay of 138 ms. To ensure appropriate streaming quality for the human operator, images need to be buffered before visualization up to a constant time delay. Using this approach, image freezing during teleoperated driving can be prevented.

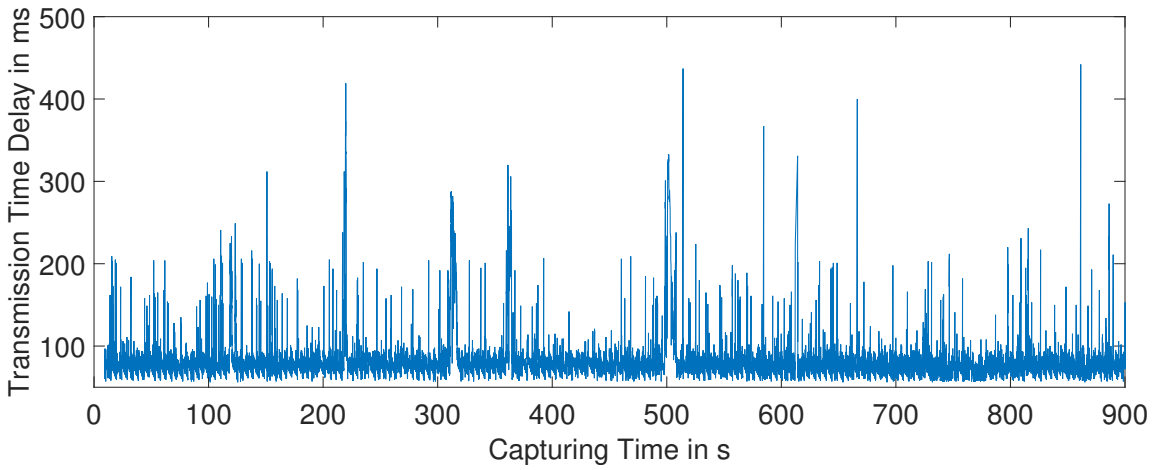

Figure 1.3 : Variable time delay during teleoperated driving using a commercial LTE network, including the spent time to transmitting the video images from the vehicle to the operator's workstation as well as the time spent to transmitting the control commands in the opposite direction [141]

To account for possible communication jitters and to ensure the fluidness of the illustrated video images, the received images need to be buffered by 500 ms at the operator's workstation [6]. When this is done, all of the received images at the operator's workstation are synchronized, the delayed video packets are aligned to their correct positions and an interruption-free video footage is displayed to the human operator [141].

Driving with such long delays between the human operator and teleoperator is one of the most significant challenges in the teleoperation of vehicles.

3) Loss of communication
Another significant challenge in vehicle teleoperation is possible loss of communication while driving. This challenge is always present in wireless communication and cannot be completely prevented. Hence, there is a need for an appropriate solution that will ensure the safety of a teleoperated vehicle when its connection to its operator is broken.

1.4 Aim of this Work

The challenges identified above cause various limits for a human operator when driving a vehicle remotely. When compared to the driver of a manned vehicle, a human operator may demonstrate lower levels of task performance and safety while driving a teleoperated vehicle. Since the challenges identified above affect the performance of tasks during vehicle teleoperation in different ways, they cannot be solved by means of a single solution.
This work aims at tackling these problems by developing a package of assistance systems for the human operator. Of the three challenges identified, this work focuses on lack of situation awareness and time delay in communication. To address the challenges posed by loss of communication, an existing solution is utilized and its performance is analyzed.
The remainder of this dissertation is organized as follows:
Chapter 2 briefly reviews the state of the art in the areas of automated and teleoperated driving. In addition, this chapter also presents the system setup used in this work.
Chapter 3 evaluates the existing concepts associated with the remote controlling of vehicles and identifies the challenges that they face.
Chapter 4 redesigns the conventional cockpit for vehicle teleoperation, incorporating a head-mounted display and using the sensor data provided by the remote vehicle. The proposed concept HMI in this chapter is intended to increase the situation awareness of human operators while engaged in teleoperated driving.
The following two chapters address the safety concerns in vehicle teleoperation that arise as a result of time delay in communication. These problems are addressed by means of autonomous intervention in the driving task.
Chapter 5 proposes a novel brake assistance system for autonomous intervention in the longitudinal control of a teleoperated vehicle and chapter 6 proposes a haptic assistance system for autonomous intervention in a vehicle's steering system during teleoperated driving.
Chapter 7 provides a general discussion of the concepts proposed in this work and considers the future of teleoperated driving. Chapter 8 summarizes the content of this work and presents its conclusion.

2 State of the Art

This chapter outlines the general state of the art in the fields of automated driving and teleoperation as two subjects that are highly relevant to the field of teleoperated driving. A more detailed discussion of the state of the art related to the proposed concepts in this work can be found at the beginning of each chapter. At the end of this chapter, the system setup used for teleoperated driving is presented.

2.1 Automated Driving

2.1.1 Automation Levels

In 2014, the Society of Automotive Engineers (SAE) released a new standard (J3016) that defines the levels of driving automation for on-road vehicles. As illustrated in Figure 2.1, based on this standard, driving automation can be categorized into five levels, which span a spectrum from driver assistance to full automation.

SAE Level	Name	Execution of Steering and Accelartion/ Decelartion	Monitoring of Driving Environment	Fallback Performance of *Dynamic Driving Task*	System Capability *(Driving Modes)*
Human driver monitors the driving environment					
0	**No Automation**	Human driver	Human driver	Human driver	n/a
1	**Driver Assistance**	Human driver and system	Human driver	Human driver	Some driving modes
2	**Partial Automation**	**System**	Human driver	Human driver	Some driving modes
Automated driving system („system“) monitors the driving environment					
3	**Conditional Automation**	System	**System**	Human driver	Some driving modes
4	**High Automation**	System	System	**System**	Some driving modes
5	**Full Automation**	System	System	System	**All driving modes**

Figure 2.1 : SAE standard J3016: Taxonomy and definitions for terms related to on-road motor vehicle automated driving systems [7]

At the lowest level of automation (level 1), the driver is responsible for all driving tasks and is only supported by advanced driver assistance systems (ADAS). At the level of partial automation (level 2), some driving tasks are executed by the automated driving system, but the human driver is responsible for monitoring the driving environment.
At the conditional automation level (level 3), the automated driving system is responsible for all aspects of the dynamic driving task, with the expectation that the human driver will respond appropriately to a request to intervene.
At the high automation level (level 4), the automated driving system is responsible for all

aspects of the dynamic driving task, even if the human driver does not respond appropriately to a request to intervene.
At the full automation level (level 5), all driving tasks under all roadway and environmental conditions that can be managed by a human driver are executed by the automated driving system. This level can be seen as the long-term goal of automated driving.
The approach to classifying automated driving systems adopted by the German Federal Highway Research Institute (BASt) is rather different from that used in the SAE standard J3016. In this system of classification [8], automated driving systems can be divided into four levels, namely "assisted", "partially automated", "highly automated" and "fully automated". Some parts of these definitions are slightly different from the similar terms used by the SAE.

2.1.2 Advanced Driver Assistance Systems

After successful development of vehicle stabilization systems, such as anti-lock braking system (ABS) and electronic stability program (ESP), advanced driver assistance systems (ADAS) were introduced to the market in the 1980s to improve safety and comfort while driving.
The ADAS for active safety are designed to avoid or mitigate collisions through warnings or intervening in the control of the vehicle. As two important systems of this field, autonomous emergency braking (AEB) and lane keeping assist (LKA) can be indicated, which respectively intervene in the longitudinal and lateral control of the car.
Some of the ADAS have been developed to promote driver's comfort through partial or complete takeover of the driving task. One of the most well-known systems developed in this field is adaptive cruise control (ACC), which automates longitudinal control of the vehicle. Another example is parking assist system, which autonomously executes the task of backing into a parking space.
To realize these systems, a variety of passive and active sensors, such as mono cameras, stereo vision, night vision, radar, LiDAR and ultrasonic sensors are used. In the next generation of environment perception sensors, more information about the environment will be gained by means of wireless communication with other traffic participants and road infrastructure.
In the recent decades, different interfaces have been developed to interact with a car's driver. Generally, these interfaces provide information to the driver through visual, acoustic and hap-

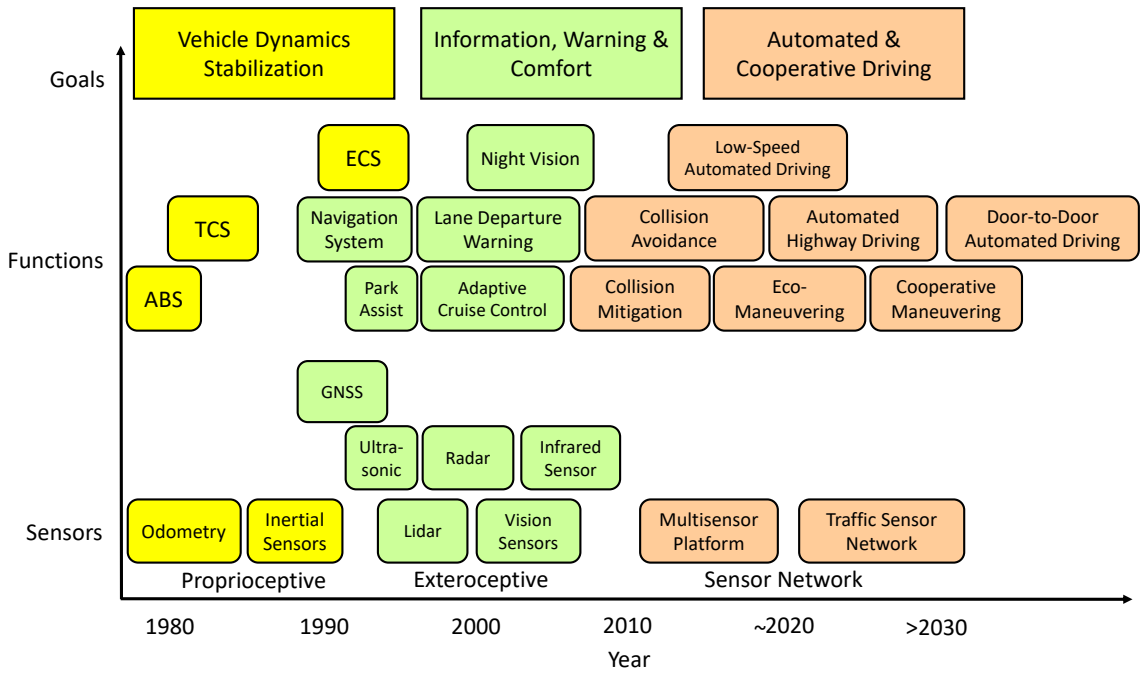

Figure 2.2 : Past and potential future evolution towards automated cooperative driving [9]

tic channels. In particular, there has been remarkable progress in the area of visual interfaces using head-up displays (HUDs) in cars, which provide information in a specific area of the windshield. The next generation of visual interfaces are likely to use the entire windshield as an augmented-reality screen [142].
Figure 2.2 illustrates the evolutionary progress of ADAS towards fully automated driving. As can be seen, the current technology is only capable of industrialization of automated driving at low speeds and, in the upcoming years, highly automated driving (automation level three based on the SAE standard J3016) in simple environments such as highways. A longer period of time will be required for the industrialization of door-to-door automated driving in all areas (automation level 5 based on the SAE standard J3016).

2.1.3 Autonomous Driving

Generally, the different tasks that machines perform in autonomous driving can be divided into several layers, which are listed in Table 1.

Table 1 Simplified hierarchical model of automated driving [143]

1. Navigation and Localization
2. Environment Perception
3. Situation Awareness and Decision Making
4. Path Planning
5. Vehicle Control

Although there has been remarkable progress in the field of autonomous driving, considerable challenges still exist in some of these layers.
The existing technologies used in autonomous driving rely on high-definition digital maps in order to obtain a priori knowledge about the environment. Using these maps, uncertainty about the static environment is reduced and a horizon, broader than the area that can be perceived by vehicle sensors, is provided.
After ego-localization on the digital map and determination of the destination, the way points that the car should follow are generated in the first step. To reduce the number of errors that arise as a result of relying on global navigation satellite systems (GNSS) in urban environments, ego-localization is performed through a fusion of GNSS-based and GNSS-free approaches [10]. GNSS-free ego-localization relies on recognizing local landmarks that are identified beforehand and saved in descriptors. However, since urban environments are permanently undergoing change, digital maps and local landmark descriptors must be frequently updated.
A variety of different sensors are used for environment perception. The majority of machine perception algorithms are based on machine learning, in which specific features need to be extracted and classified. In recent years, deep-learning techniques such as GoogLeNet [11], R-CNN [12] and their different extensions have demonstrated remarkable performance in the detection and classification of objects. However, the problems encountered when attempting to recognize complex objects, such as pedestrians, have still not been completely solved.
Since in several areas within urban environments no clear lane marking or curbs can be seen, free-space detection cannot be solely performed using vehicle sensors. To solve this problem, the support of high-definition digital maps is required. The greatest challenges in this area are environment perception at night and during poor weather conditions, both of which will require much effort before they are completely solved.
In addition, V2X communication technology is used to perceive those parts of the environment that cannot be seen by vehicle's sensors. The main challenge involved in using this technology in active safety systems is its high latency, which might be solved in the future by

the fifth generation of mobile communication networks.
Decision-making algorithms are mostly based on probabilistic approaches, and their performance in complex urban environments is still not comparable with human abilities.
Path-planning techniques such as heuristic search algorithms and numerical optimization approaches have been improved in recent years [13]. However, there is a need for further progress in real-time path planning when confronted with uncertainties within dynamic environments.

2.2 Teleoperation

2.2.1 Areas of Application

Teleoperation has a long history in robotics. This technology enables controlling a robot, including one or several of its actuators, that is located at a distance from a human operator. The main use case of this technology is where the human is not capable of or interested in being physically present at the robot's location.
One well-known application of teleoperation is the exploration of space using mobile robots. The first lunar rover was landed on the Moon in 1970 by the Soviet Union. Thereafter, several unmanned rovers have been developed to explore the surfaces of the Moon and Mars. An example of these Mars rovers is shown in Figure 2.3(a). This model is equipped with a chemistry and camera (ChemCam) instrument with which the composition of surfaces can be investigated.
A similar application can be seen in the teleoperation of submarines used for underwater operations. While in earlier versions of these submarines the teleoperator was connected to the operator's workstation using a cable, modern versions mostly use underwater wireless communication. An example of these robots, which are connected to the operator via a cable, is illustrated in Figure 2.3(b).
Surgery is another area in which human ability is still dominant. Telesurgery is a technology that enables surgeons to operate on their patients without being physically present in the operating room. Figure 2.3(c) shows an example of a telesurgery system developed by Intuitive Surgical Inc. [14].

(a) (b) (c)

Figure 2.3 : Some use cases of teleoperation: (a) Exploration of the Mars by the rover Curiosity of NASA's Mars Science Laboratory [15]; (b) Exploration and underwater teleoperation by H2000 of ECA Group Hytec [16]; (c) Telesurgery using "da Vinci" surgical system [17]

Another application of teleoperation is enabling remote presence in locations that are hazardous to humans. In this regard, different robots have been developed to locate mines, to explore hazardous locations or to clear radiated areas. Figure 2.4(a) depicts an example of a robot developed for remote inspection.
Similarly to other technologies, not all of the applications of teleoperation are civil. In recent decades, this technology has been intensively used for military purposes. This technology is used to teleoperate both armed ground vehicles and armed aerial drones. Figures 2.4(b) and 2.4(c) illustrate two examples of military robots.
Recently, teleoperation technology has been used for logistics purposes. For example, Amazon has announced that it intends to develop a "Prime Air" service which will deliver packages

(a) (b) (c)

Figure 2.4 : Some use cases of teleoperation: (a) remote inspection (b) Guardium as an unmanned ground vehicle (UGV) developed by G-NIUS (c) MQ-1 Predator as an unmanned aerial vehicle (UAV) built by General Atomics and employed by US Air Force [18]

to customers using remotely controlled drones. Some other applications of teleoperation can be found in [19].

2.2.2 Human-Machine Cooperation Levels

Generally, the level of human-machine cooperation in a teleoperation task can be categorized as direct, shared or supervisory control. This approach to classification is illustrated in Figure 2.5.

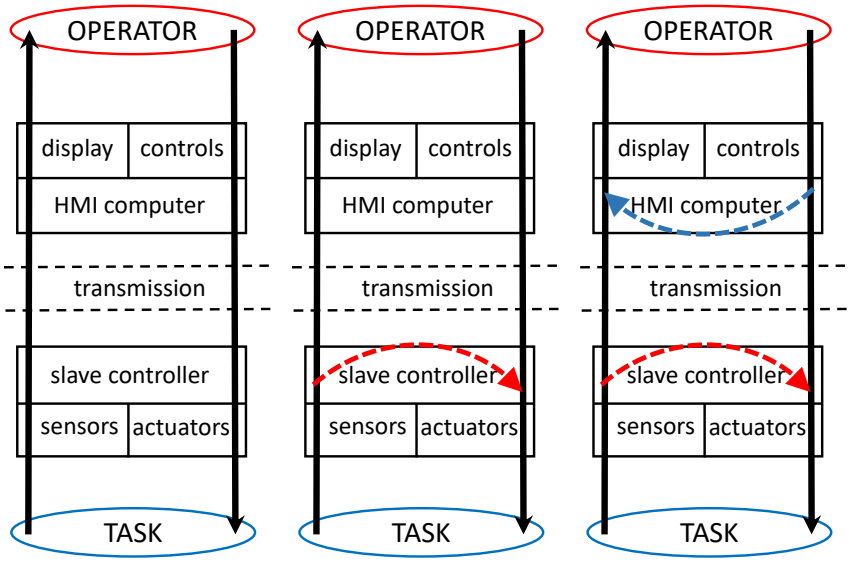

Figure 2.5 : Teleoperation strategies: (a) direct control, (b) shared control and (c) supervisory control [20]

In this classification, direct control or closed-loop control represents a level of teleoperation in which the remote system is continuously controlled by direct signals sent by the operator [21].

Shared control represents a level of human-machine interaction in which both, human intervention in programmed tasks and computer augmentation of manually controlled operation, are permitted [22]. Instead of a supervisor dictating to a subordinate, in shared control the human and the robot engage in dialogue in order to exchange ideas and resolve differences [23]. In this strategy, the control loops that cannot be controlled by the human operator are closed using internal loops in the teleoperator. This is illustrated in Figure 2.5(b) as a red dashed arrow on the teleoperator's side. A well-known application of this control concept as a H-metaphor for vehicle automation and interaction is provided by Flemisch *et al.* [24].

In supervisory control, the machine conducts the task autonomously, and the operator continually monitors and iteratively updates or modifies the program [25]. The blue dashed arrow on the operator's side in Figure 2.5(c) represents the feedback from the human-machine interface (HMI) [20].

2.2.3 Human-Machine Interfaces for Teleoperation

One of the main aspects to consider when designing a teleoperation system is its HMI, which enables the interaction of the human operator with the remote environment. An HMI should allow tasks to be adequately performed and increase the telepresence of the human operator. In addition, several other parameters, such as workload, building cost and size of the operator's workstation should be considered.

An HMI for teleoperation consists mainly of one or more feedback and one or more control channels. The feedback channels convey the received signals from the teleoperator to the operator, while the control channels transmit the control signals in the opposite direction.

To improve the telepresence of the human operator, different feedback and control channels can be used. These channels are mainly selected based on the task at hand. The most common feedback channel is the visual channel, which illustrates the video received from the teleoperator on the displays of the operator's workstation.

This channel has the ability to enhance the raw images received from the teleoperator by providing additional information. This can be achieved through processing the received images and projecting additional information onto them, representing a form of augmented reality.

In addition to visual feedback, the other human senses can be used in human-machine interaction. For example, through acoustic feedback the sounds of the remote environment can be presented to the operator. This would improve the human operator's impression of being present in the remote vehicle while he is engaged in teleoperated driving. This topic is investigated in [26] through simulation of the sound of the motor at the operator's workstation.

The sense of touch is another channel that is intensively used in order to increase the operator's telepresence. This channel conveys tactile or kinesthetic information about the remote environment to the human operator. To create this force feedback, the force that exists at the teleoperator is measured and then artificially generated using an actuator at the operator's workstation.

Based on the teleoperation task to be performed, different devices are used to generate the human operator's control signals. Figure 2.6(a) illustrates a HMI for telesurgery, in which the control signals are created using the surgical instruments provided on the operator's workstation. Fig. 2.6(b) shows the HMI of a military UAV, in which two joysticks and a keyboard are provided to control the drone.

(a) (b) (c)

Figure 2.6 : Some example HMIs for teleoperation: (a) an interface for telesurgery, (b) an operator's workstation to remotely control a military drone [19], (c) CAPIO upper-body dual-arm exoskeleton as an wearable interface for teleoperation using bio signals [27]

For more intensive interaction between the human operator and the remote environment, wearable interfaces can be used. Figure 2.6(c) illustrates an example of these HMIs, in which the control signals are created by the bodily motions of the human operator.

This technology can be enhanced through gaze tracking [28], head-pose estimation [29] or even the scanning of brain signals [30].

2.3 Teleoperated Driving

Teleoperated driving, a branch of telerobotics, refers to controlling a car from outside of it. Since given current state of the art driverless operation of vehicles cannot still be realized in all urban environments, this technology has received a remarkable degree of attention in recent years.
For example, in 2015 the American car manufacturer Ford officially announced that it would begin research on this technology [31]. The test vehicle used for this purpose was a golf cart, which was equipped with camera sensors and an LTE communication unit. The official demonstration presented low-speed remote control of this vehicle using a logitech actuator and three monitors. Figure 2.7 shows a scene from this demonstration.

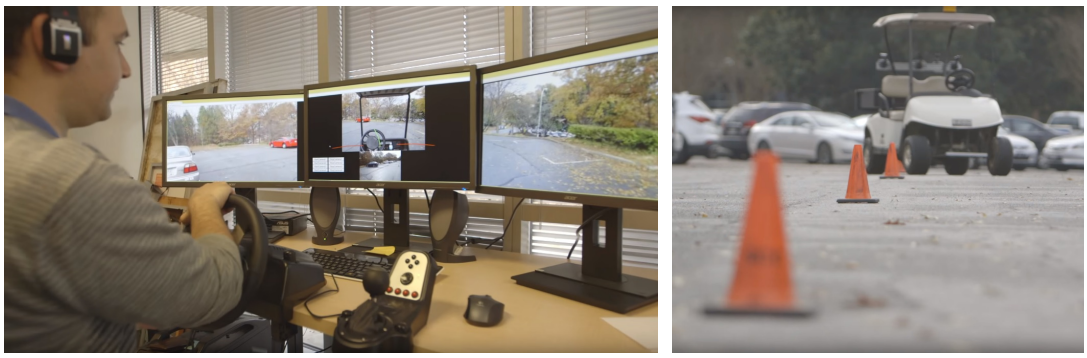

(a) (b)

Figure 2.7 : A scene from the Ford's official demonstration on teleoperated driving [31]

In addition to Ford, some other developers and car manufacturers have recently started to work on teleoperated driving. For example, the Renault-Nissan Alliance announced at the Consumer Electronics Show (CES) of 2017 its intension to use teleoperation technology in order to support driverless cars [32]. In addition, Telefónica and Ericsson demonstrated remote driving using a trial 5G network at the Mobile World Congress (MWC) 2017 in Tarragona, Spain [33]. While some of these companies consider teleoperated driving as a back-up to autonomous driving, some others consider it as an independent mobility concept. Chapter 7 discusses these approaches.

2.3.1 System Setup at TUM

The chair of automotive technology at the Technical University of Munich (TUM) has been engaged in research into the concept of teleoperated driving since 2010 [2]. The system architecture as well as the main system components developed are described below.

2.3.1.1 Teleoperator

An Audi Q7 was employed as the main experimental vehicle. This vehicle was first equipped with the required sensors and actuators for automated driving in the "*DFG Sonderforschungsbereich Transregio 28 Kognitive Automobile*" project and was developed further in the "*Teleoperated Driving*" project. Figure 2.8 depicts this car, which was equipped with several sensors and actuators, as well as a communication unit. Three camera sensors, mounted behind the vehicle's windscreen, capture approximately 240° of its surroundings. The rest of the car's environment are captured by two additional cameras, which are mounted in two side-mirrors as well as a rear camera.
The used cameras are CMOS Gigabit Ethernet (GiGE) cameras from Basler [34], with differ-

ent resolutions and fields of view (FOV). The middle camera is of the acA2000-50gc type, with a resolution of 2046 x 1086 pixels. This camera, together with a LM5JC1M lens from Kowa, provides a FOV of approximately $150°$. The captured camera images are compressed using H.264 video coding format and transmitted via an LTE mobile network to the operator's workstation.
For machine perception, a stereo vision system was developed and mounted in the car. This stereo vision system consists of two monocular acA640-100gc type cameras from Basler and a baseline with a length of 50 cm. The raw images of this camera system are not transmitted to the operator's workstation, but are processed in the car and are used by the vehicle's intelligence.
In addition to camera sensors, three SICK LMS 291 LiDAR sensors were mounted on the car. These LiDAR sensors scan $180°$ of the environment in one layer, with an angular resolution of $0.5°$ or $1°$. Two of these three sensors can be seen in Figure 2.8(a). In this work, only two of these three sensors, which are mounted on the front and the rear of the vehicle, are employed.
The experimental vehicle was equipped with an OxTS RT3003 precision inertial and GPS navigation systems from Oxford Technical Solutions [35], which measures motion, position and orientation at a frequency of 100 Hz. Highly accurate measurements can be made using the car's mounted DGPS antenna.

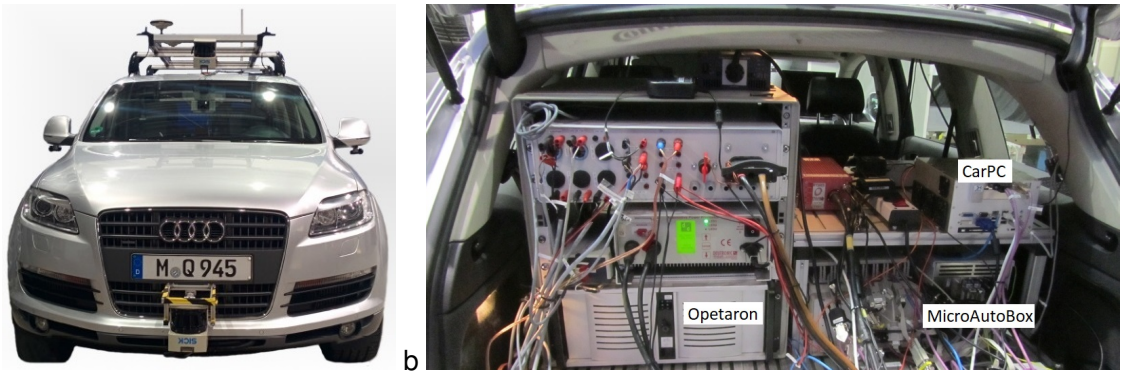

(a) b (b)

Figure 2.8 : The used experimental vehicle for teleoperated driving equipped with different sensors, actuators and computing units

In order to remotely steer the car, a hollow shaft motor was mounted on its steering column. To ensure safety during test drives, this additional actuator could be over-steered at any time by the safety driver. Pushing the gas and brake pedals, as well some secondary driving tasks such as honking the horn or switching the lights on or off, were controlled over the car's CAN bus. Shifting was carried out using a shift-by-wire system mounted in the car. To ensure the safety of the braking system, an additional pneumatic system was installed in the car, which can directly push the brake pedal using the air stored in a tank.
Several computation units with different tasks were installed in the experimental vehicle. The main computation unit, called CarPC, is an industrial PC which serves as the main interface between sensors, actuators and the communication unit. Another computation unit, called Opteron, captures the sensor measurement data and sends them to CarPC via Ethernet. A Gigabit Ethernet switch serves as the interface between the GigE cameras and Opteron. For rapid control prototyping (RCP), a MicroAutoBox from dSPACE [36] is used, that translates the received commands from CarPC to the actuators. Figure 2.8(b) shows the mounting positions of these computation units in the experimental Audi Q7 vehicle.

2.3.1.2 Communication Channel

A commercial LTE router serves as the communication unit in the experimental vehicle. The LTE router employed is a Speedport LTE from Telekom, which can be adjusted to connect in either GSM, UMTS or LTE modes. During the test drives, two different LTE SIM cards, from Telekom and Vodafone were used. A secure connection between the teleoperator and the operator's workstation was created using a VPN connection. To reduce the communication time delay as much as possible, the connectionless UDP protocol was used to transfer the data in both directions.

2.3.1.3 Operator Workstations

Two operator's workstations, illustrated in Figure 2.9, were developed for teleoperated driving. Both workstations were equipped with three monitors for visualizing the video received from the remote vehicle. They were also fitted with conventional actuators to control the car, such as steering wheels, gas and brake pedals. Both workstations are connected to a PC, which is responsible for receiving the sensor data from the teleoperator and sending the control commands to it.
The main differences between these two workstations lie in the size of their displays and their control actuators. The workstation shown in Figure 2.9(a) has three 24 inch monitors, as well as a G25 steering wheel and racing pedals from Logitech.
The workstation shown in Figure 2.9(b) has three 55 inch monitors, a SENSO-Wheel SD-LC [37] steering wheel and pedals from SENSODRIVE [38]. This workstation's larger displays enable the visualization of the vehicle's surroundings at their real-world size, which a driver would see from the inside of the vehicle. In addition, the steering wheel of this workstation enables the generation of force feedback.

(a) (b)

Figure 2.9 : The used operator workstations for teleoperated driving

2.3.1.4 Software Platform

Both of the car's main computing units are equipped with the ADTF framework [39], which enables the modular development of software functions as C++ classes.
The operator's interface was developed using the QT framework, which enables the development of graphical user interfaces (GUIs) in C++.
The driving dynamics model of the car used for trajectory control as well as the connections between sensors and actuators on the rapid control prototyping unit were developed using MATLAB/Simulink. The ControlDesk software from dSPACE was used to develop a GUI for several of the car's actuating units.

2.3.2 Control Concepts for Teleoperated Driving

The communication time delay results in a high level of inconsistency in control of the vehicle during teleoperated driving. This challenge needs to be addressed using a specific control concept. With reference to the human-machine cooperation levels discussed in Chapter

2.2.2, different solutions for this problem can be proposed.
For direct control of the teleoperator in space despite existing of communication time delay, Sheridan [25] proposed the *predictive display*. The application of this concept in the direct control of road vehicles was investigated in [40] and [5]. Based on this concept, the vehicle's driving dynamics are modeled as a non-linear single-track model and the model's states are predicted over the time delay. After prediction of the current states of the remote car, its front is illustrated as a rectangle within the delayed images. Figure 2.10(a) shows an example of this concept.
Since this concept does not provide a solution for situations in which communication is lost, it needed to be combined with another solution developed specifically for this purpose. Tang [26] proposed the "free corridor" concept, which is based on the idea of full braking after a possible communication loss. This concept calculates brake path in the form of Euler spirals and permanently visualizes it as part of the augmented reality displayed to the operator. The operator has the responsibility to keep this corridor free of obstacles while engaged in teleoperated driving. After a possible communication loss, the remote vehicle will brake autonomously along the latest corridor displayed to the operator. Figure 2.10(b) depicts this corridor in a simulated environment.
Figure 2.10(c) illustrates a driving scene with a speed of 50 km/h and a communication time delay of 500 ms. As can be seen, both the predictive display and free corridor concepts are depicted as part of the augmented reality that is displayed to the operator.

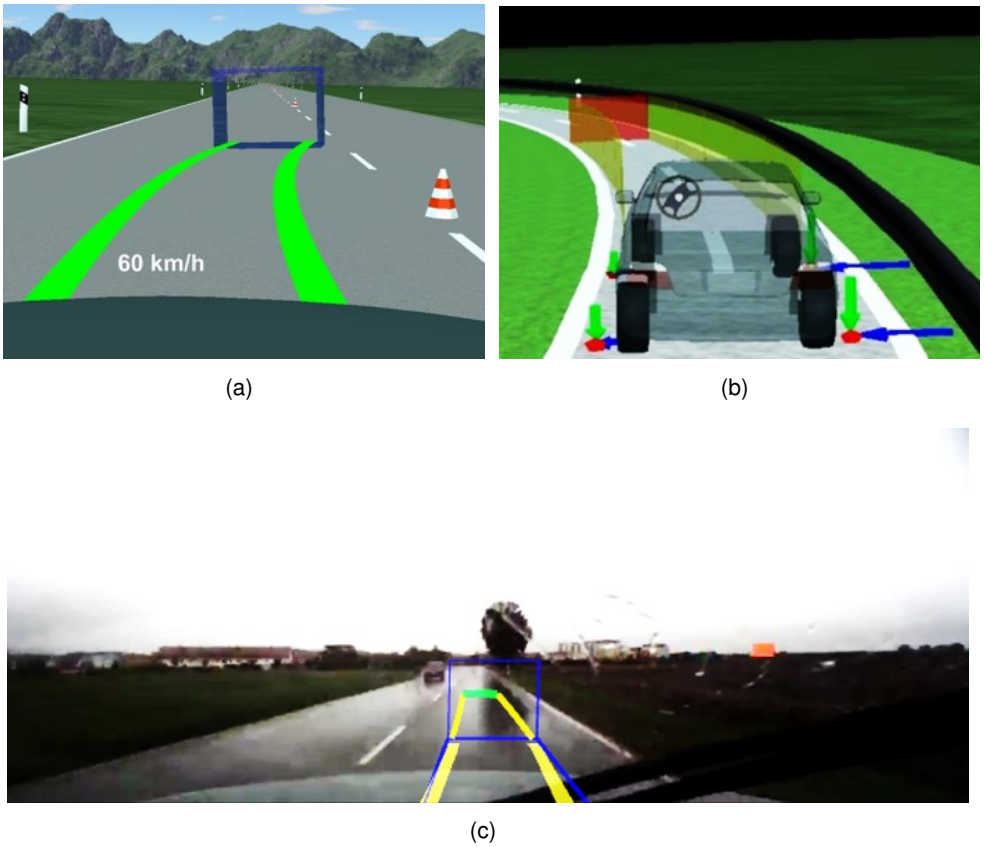

(a) (b)

(c)

Figure 2.10 : (a) The predictive display [5] to handle the communication time delay and (b) the free corridor [26] to ensure collision avoidance through full braking after a possible communication loss; (c) a real test drive on a rainy day with the HMI concept direct control using the predictive display and the free corridor

The challenge posed by time delay can be minimized by the use of shared control as a higher level of automation. As an example for teleoperated driving, the concept of trajectory-based control [41] can be indicated, which gives a part of the control over to the vehicle itself. With this approach, the human operator manually generates the driving paths in the form of Euler spirals and sends them to the remote car. These paths are then autonomously driven by the

remote car. The curvature of an Euler spiral is formulated as follows:

$$\kappa = C_0 + C_1 l, \qquad \text{with } 0 \leq l \leq L, \tag{2.1}$$

in which C_0 and C_1 represent the initial curvature and the change of the curvature, l represents the path coordinates and L stands for the length of the segment.
The change of the curvature is set using the steering wheel and the length of the segment is set using the gas pedal of the operator's workstation. Based on these inputs, a path with the following coordinates is produced:

$$x(l) = x_0 + \int_0^l \sin \Psi(\tau) d\tau, \qquad \text{with } 0 \leq l \leq L \tag{2.2}$$

$$y(l) = y_0 + \int_0^l \cos \Psi(\tau) d\tau, \qquad \text{with } 0 \leq l \leq L \tag{2.3}$$

$$\Psi(l) = \Psi_0 + C_0 l + \frac{1}{2} C_1 l^2, \tag{2.4}$$

in which x and y represent the Cartesian coordinates of the segment and Ψ represents the course angle. The required initial states of $[x_0, y_0, \Psi_0, C_0]$ for each segment are adopted from the final states of the previous segment.
Figure 2.11 illustrates the generated trajectories in both a simulated and a real environment. After the operator generates a trajectory and ensures that it is suitable, he confirms it by pressing a button on the steering wheel mounted on the operator's workstation. The trajectory generated is then sent to the remote car and visualized in green.

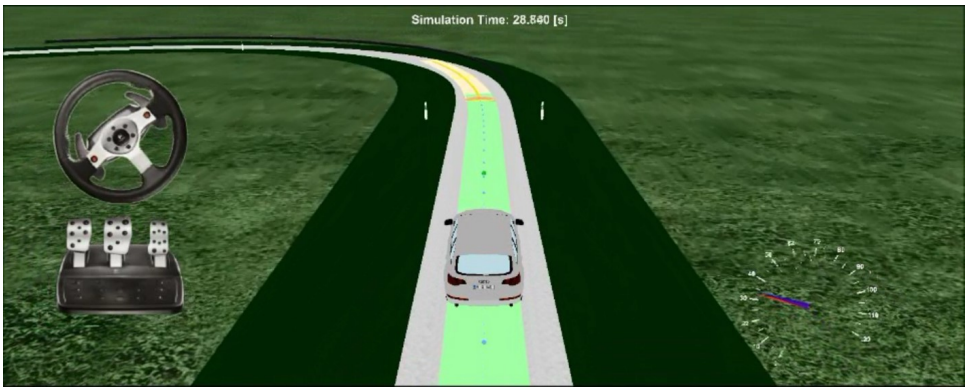

(a)

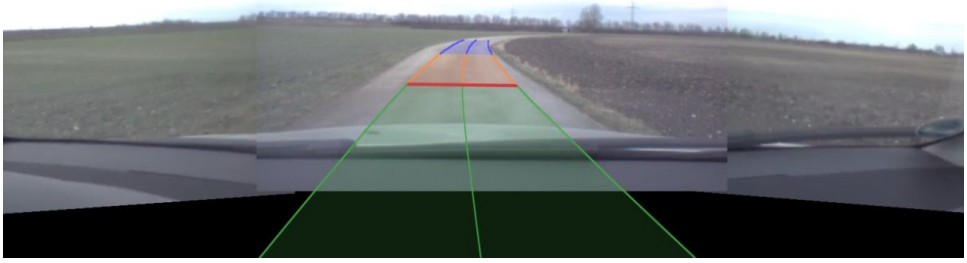

(b)

Figure 2.11 : Trajectory-based control as a kind of shared control of teleoperated vehicles (a) in the simulation and (b) during a real test drive [41]

Should a possible communication loss occur, the vehicle will stop at the end point of the last trajectory received. Hence, this concept handles both, the challenges posed by communication time delay and loss of communication simultaneously.
The control concepts described in this chapter are analyzed further in Chapter 3 and discussed in Chapter 7.

3 Analysis of the Existing Control Concepts for Teleoperated Driving

3.1 Trajectory-based Control vs. Direct Control

The control concepts discussed in Chapter 2.3.2 have different strengths and weaknesses. Some of these strengths and weaknesses are described in this chapter.

3.1.1 Trajectory-based Control

As an example of shared control, this concept has the advantage that it assigns part of the driving task to the machine. This human-machine cooperation may lead to the human operator being partially relieved of the responsibility for the driving task.
In addition, this control concept takes into account the challenges posed by communication time delay and loss of communication simultaneously. Hence, the operator does not need to take into account two different HMI concepts while driving.
Since driving with a communication time delay decreases the operator's performance in terms of controlling the car, this concept divides the driving task into trajectory planning and trajectory control. The human operator is responsible for the former task and the vehicle is responsible for the latter.
Although this concept would be suitable for teleoperated driving in off-road environments, utilizing it in urban environments presents some challenges.
The first challenge is that there is a time delay in displaying the vehicle's environment to the human operator. Thus, the operator will not have current information about the vehicle's surroundings. Since urban environments are highly dynamic, decision-making based on delayed information about the vehicle's surroundings may lead to generation of a trajectory that is not appropriate for the driving scenario.
Since the human operator cannot predict the motion behavior of other traffic participants over a long time horizon, he must generate short trajectories and send them to the remote vehicle one after the other. For example, when driving at a speed of 50 $\frac{km}{h}$, the operator would need to generate and send several trajectories per second, which does not seem to be possible.
In addition to the points identified above, lateral control of a remote vehicle using this concept represents a challenge. Figure 3.1 illustrates an example of a static driving scene, in which the operator needs to send four command steps, using Euler spirals, in order to navigate. Since this scenario could not be negotiated by means of a single Euler spiral as described in [41], the human operator would need to generate several short trajectories in several stages, in order to successfully complete the driving task. This example indicates the low agility of this control concept in some challenging scenarios, such as cases in which evasions may be required in order to avoid collisions.
In order to create a drivable path using several manually generated trajectories, the teleoperated car must have a highly accurate positioning system. Such a positioning system enables connecting the short received trajectories within a global coordination system. The high cost of such a positioning system would be an economic barrier to implement this control concept for mass-produced autonomous vehicles.
Based on this control concept, the teleoperated vehicle would stop after a communication loss at the end of the last trajectory received from the operator. However, stopping a vehicle on the street does not seem to be an optimal solution when driving in urban environments.

3.1.2 Direct Control using Predictive Display

The concept of direct control using predictive display [5] has the advantage of providing the possibility of an intuitive driving experience that uses a steering wheel as well as gas and brake pedals. When compared to the shared control concept, directly controlling a remote

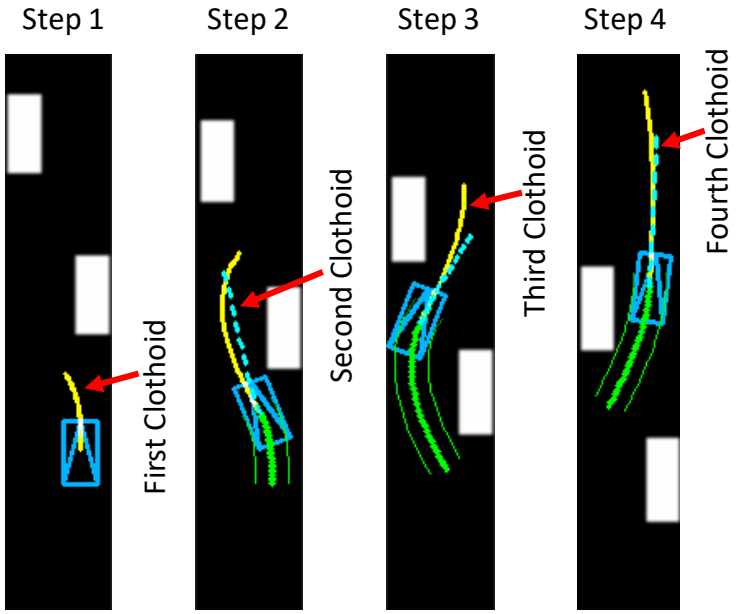

Figure 3.1 : Several required steps to drive through a curve using the concept "trajectory-based control"

car is more similar to driving a vehicle from its inside. This would lead to easier and faster learning of this control concept by human operators.
In addition, this control concept provides higher agility while driving when compared to the trajectory-based control concept. Since the human operator has the vehicle fully under his or her control, he can better make use of evasion maneuvers to avoid collisions in hazardous situations.
Since no highly accurate positioning system is required for the realization of this concept, its large-scale adoption would offer an economic advantage compared to the trajectory-based control concept.
Despite these advantages, this control concept suffers some problems. The main challenge is high instability of the remote car while it is being laterally controlled. Figure 3.2 shows the driving trajectories in a human-in-the-loop test, in which 22 test persons without prior experience of teleoperated driving were asked to drive along the middle lane of a test track using a predictive display. The driving velocity for this handling course was set to 50 $\frac{km}{h}$. For the human-in-the-loop test, the teleoperator and the test track were simulated using the DYNA4 software [42], and an artificial round-trip time delay of 500 ms was created between the operator and the simulated teleoperator.
As can be seen, even when using a predictive display some test participants were unable to demonstrate stable lateral control of the remote car on the curves and to avoid obvious deviation from the middle lane of the test track. A lack of situation awareness while laterally controlling the remote car, even when using a predictive display, could be one of the main reasons behind these difficulties. This topic is discussed in more detail in Chapter 6.1.
Through additional visualization of the predictive display of other traffic participants, this control concept conveys the actual positions of dynamic obstacles in the vehicle's surroundings to the human operator. Simultaneous visualization of the predictive display of the remote car together with the predictive displays of other traffic participants, may result in a high workload for the human operator when attempting to understand the actual state of a situation. This would lead to the human operator being overburdened or even overwhelmed when navigating urban areas with a high number of traffic participants.
In addition, as a result of communication time delays, only the visualization of the current positions of other traffic participants using the predictive display cannot guarantee the safety while teleoperated driving. This challenge is discussed in more detail in Chapter 5.1.

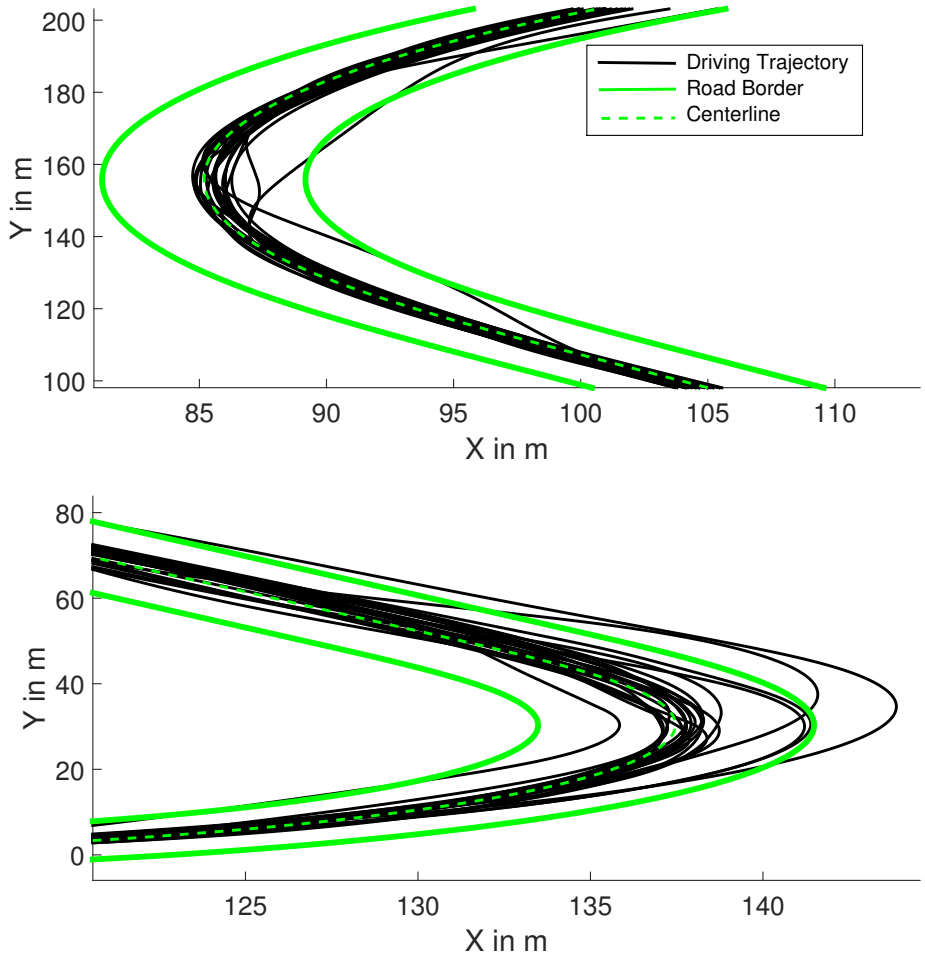

Figure 3.2 : The driving trajectories of 22 test persons without prior experience of teleoperated driving on two sample curves of a handling course. The test drives were conducted with a constant round-trip time delay of 500 ms and at a velocity of 50 $\frac{km}{h}$. The test's participants used a predictive display while driving.

3.1.3 Shared or Direct Control? Choosing a Control Concept

The above-mentioned strengths and weaknesses of both control concepts do not indicate that one approach clearly outperforms the other. The choice of implementing one of these concepts in teleoperated driving depends on several criteria, such as the use case, the driving environment, communication time delay, the existing level of the vehicle's intelligence, safety, comfort and the final cost of realization.

In order to use teleoperated driving as a transient technology toward autonomous driving in urban environments, the direct control concept using predictive display seems the superior choice. This concept is more appropriate for driving with a round-trip time delay of under 500 ms and shows greater agility in urban environments. In addition, it is realizable on the large scale, using low-cost sensors that the automotive industry already produces.

The shared control concept would seem to be more appropriate after the realization of a highly reliable intelligence within a remotely controlled vehicle, which is still not available for all urban environments.

Hence, this work mainly focuses on the direct control concept using predictive display as a basis for teleoperated driving. However, it does not exclude the utilization of the shared control concept and introduces some novel concepts for its further development in chapters 7.2.1 and 7.2.2. In addition, chapters 4.5 and 5.5 discuss how the concepts developed in this work could be applied to the shared control concept.

3.2 Impact of Training on Driving Performance

Due to the presence of a human operator in the control loop of a teleoperated vehicle, human factors play an important role in task performance. Several factors, such as driving experience and experience with the operator's workstation, as well as several other personal factors, may affect the driving performance of human operators.
The exact determination of the weights of all of the human factors relevant to teleoperated driving is not within the scope of this work. However, to emphasize the impact of training on teleoperated driving performance, the results of one of the many test drive conducted for this research are summarized, illustrated and discussed below.
In this study, two test persons with little experience of teleoperated driving were asked to drive on a simulated handling course, which is illustrated in Figure 3.3. For this human-in-the-loop test, the test track and the vehicle were simulated using the SILAB [43] software. The test subjects used the conventional operator's workstation for teleoperated driving, which is shown in Figure 2.9(b).

Figure 3.3 : Top view of the test track to investigate the driving performance of the test persons

Both test persons were asked to drive in the middle of the test track, maintaining a constant speed of 50 $\frac{km}{h}$, once without a time delay and once with an artificial communication time delay of 500 ms between the operator's workstation and the teleoperator. The test drive without the time delay served as the baseline of the driving performance of the test person using the operator's workstation.
After these two test drives, the test persons were trained for about two hours in several different driving scenarios. Thereafter, the test persons were asked to repeat the test drive, again with an artificial communication time delay of 500 ms. In all of the test drives conducted with the time delay, the predictive display was used to control the simulated remote car.
Figure 3.4 illustrates the test results of the first test person. When comparing the lateral deviation from the desired trajectory in Figures 3.4(a) and 3.4(c), it can be seen that the time delay obviously reduced the driving performance. When comparing this objective parameter in Figures 3.4(c) and 3.4(e), it can be seen that with the same system configuration, the reduced driving performance was improved with training. However, it did not match the performance demonstrated when driving without a time delay.
The same phenomenon can be detected when investigating the steering angle while driving, which is another important objective parameter when evaluating driving performance on a handling course. This parameter is depicted in Figures 3.4(b), 3.4(d) and 3.4(f).
The overall number of lane departures as well as the average number of deviations from the centerline while driving with three different constellations are illustrated in Table 2.
The test results of the second test person are illustrated in Figure 3.5. As can be seen, a similar trend can be identified in these test results.

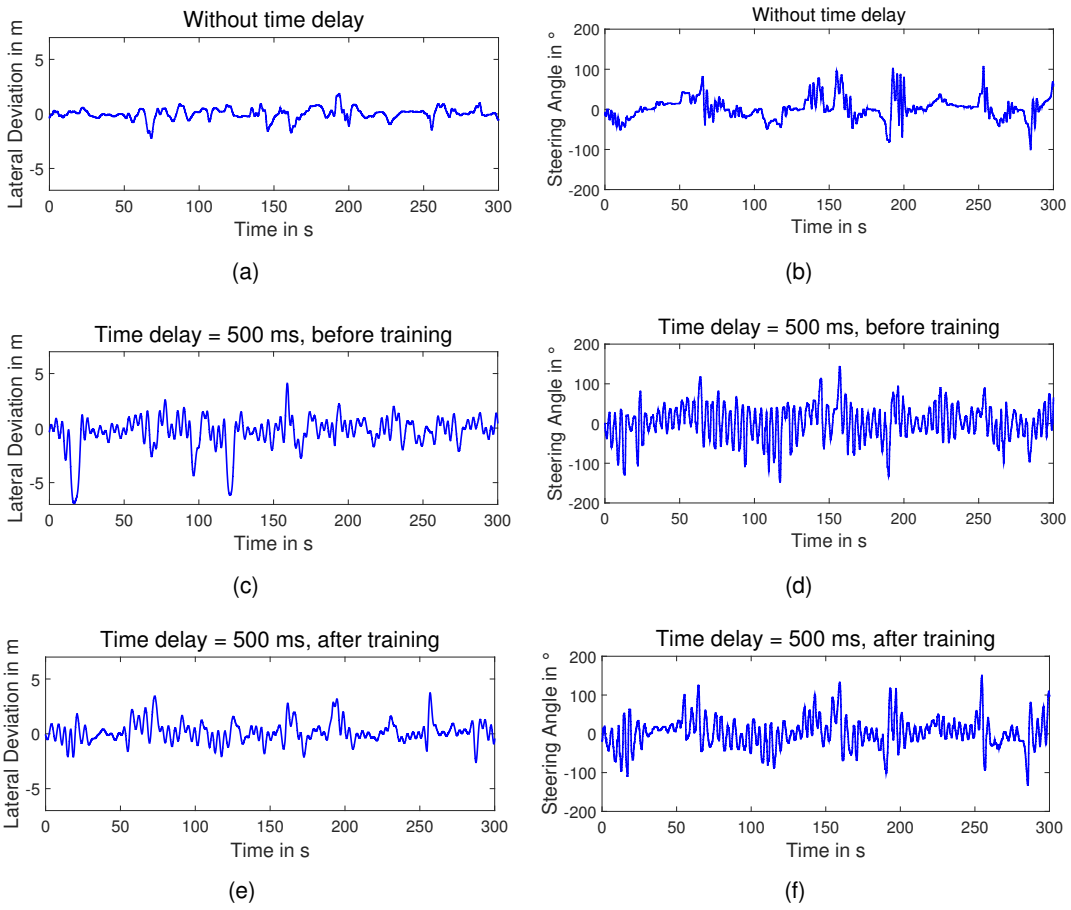

Figure 3.4 : The effect of training on the driving performance of the first test person: (a) and (b) show the measured lateral deviation and steering angle while driving without a time delay; (c) and (d) show the results, with a time delay of 500 ms, before training; and (e) and (f) show the results, with a time delay of 500 ms, after training.

Table 2 The overall number of lane departures and average deviation from the centerline in all three conducted test drives by the first test person.

	Number of Lane Departures	Average Deviation from the Centerline
Without time delay	9	0.38 m
With time delay, before training	60	0.96 m
With time delay, after training	37	0.67 m

Table 3 illustrates the overall number of lane departures and the average number of deviations from the centerline in all three constellations produced by the second test person. As this table shows, while driving with a time delay of 500 ms after training, the test results of this participant are even better than the results of his test drive without the time delay.
This study cannot offer all-encompassing conclusions regarding the effects of training and learning on all human operators. Based on his or her personal background, every test person will require different training times in order to reach a level after which driving performance does not improve significantly.
However, this study indicates the importance of using trained operators for teleoperated driving. Hence, the remaining test drives in this work were conducted using only trained and experienced test persons.

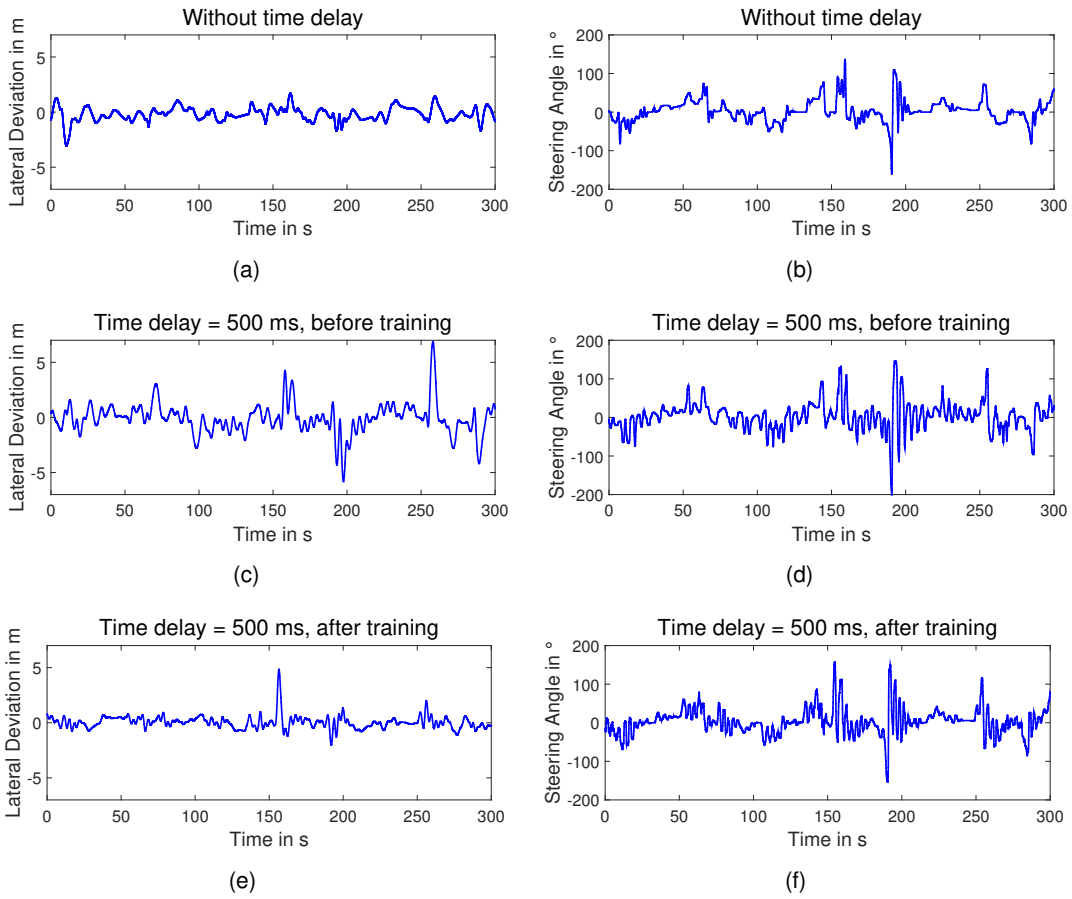

Figure 3.5 : The effect of training on the driving performance of the second test person: (a) and (b) show the measured lateral deviation and steering angle while driving without a time delay; (c) and (d) show the results, with a time delay of 500 ms, before training; and (e) and (f) show the results, with a time delay of 500 ms, after training.

Table 3 The overall number of lane departures and average deviation from the centerline in all three conducted test drives by the second test person.

	Number of Lane Departures	Average Distance to the Centerline
Without time delay	20	0.51 m
With time delay, before training	42	0.92 m
With time delay, after training	11	0.39 m

3.3 Derivation of the Research Focus

Several of the test drives conducted using the control concepts introduced in Chapter 2.3.2 illustrate two main challenges encountered in teleoperated driving.
The first challenge appears when the human operator attempts to precisely control the remote vehicle when negotiating a narrow passage. The difficulty here lies in the low situation awareness of the human operator when using existing HMI concepts.
The second and more important challenge is the low level of safety that exists when driving with a time delay. The absence of an appropriate solution to this difficulty makes the realization of this mobility concept in urban environments impossible.
Since these challenges do not arise from the same source, they cannot be solved by means of a single solution. Hence, this work proposes a package of HMI and driver assistance

systems for overcoming the existing limitations of teleoperated driving.
The HMI proposed in Chapter 4 is aimed at enhancing the situation awareness and improving the task performance of the human operator in terms of precisely controlling the remote car.
The safety challenge should be addressed through increased onboard autonomy. Because of the various influences that communication time delay can have on the driving behavior of a human operator in terms of longitudinal and lateral control of a remote car, the safety risks encountered in teleoperated driving should be addressed by means of interventions in both, braking and steering systems. For this purpose, two driver assistance systems that autonomously intervene in the braking and steering systems during hazardous situations are proposed in Chapters 5 and 6.
The development of the proposed package is based on the V-Model [44], which is a well-known approach for system development. Figure 3.6 illustrates the variant of the V-Model used in this work, in which the covered development steps are shaded in gray.

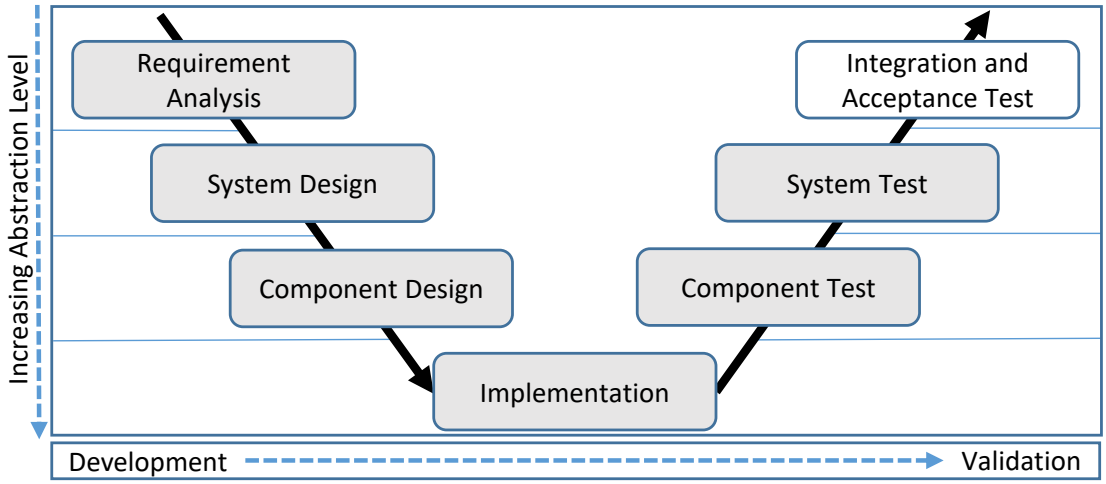

Figure 3.6 : The used V-Model to develop the required HMI and ADAS package for teleoperated driving in urban environments. The covered development steps in this work are filled in gray.

As the first step of this process model, the existing problems in precisely and safely controlling a remote car are analyzed and detailed requirements are defined. Thereafter, based on the defined requirements, solution concepts and the software components required to realize them are developed.
To demonstrate the feasibility of the developed concepts, the designed software components are implemented using the system setup presented in Chapter 2.3.1. For this purpose, the existing sensors, actuators and computation units of the teleoperator and the operator's workstations are used.
Using this system setup, the developed software components such as the modules for environment perception are validated using real measurement data.
The system test aims at validating the developed concepts by means of human-in-the-loop test drives. In addition to the real-life test drives performed at a restricted level, a driving simulator is employed, with which the remote vehicle and the desired urban environments can be simulated. Using this simulator, the safety limits of the developed concepts are validated in a safe manner and the driving behavior of different test persons are studied under the same conditions.
The final step in validating the proposed HMI and ADAS for teleoperated vehicles is subjecting them to intensive examination by means of test drives on public roads. This work provides the required inputs for this validation step, which needs to be handled intensively in subsequent studies.

4 HMD-based Mixed Reality HMI for Enhancing Telepresence

The main content of the concept introduced in this chapter was previously presented in [144] and [145]. This chapter provides a description of this concept.

4.1 Problem Description

As mentioned in Chapter 1, one of the main challenges in the teleoperation of vehicles is the lack of situation awareness, as this degrades the task performance of the human operator. This challenge is particularly pronounced in situations in which the operator needs to precisely control a vehicle.
Figure 4.1 depicts a typical operator's workstation for teleoperated driving, which is equipped with three monitors for visualizing the environment on the real-life scale. Because of communication time delays, the displayed images do not correspond to the current reality. Thus, the actual position of the vehicle is predicted regarding time delay and visualized as a see-through augmented reality. This *predictive display* is depicted in Figure 4.1 as a blue rectangle within the visualized images.

Figure 4.1 : A human operator controls the remote vehicle using the conventional operator's workstation.

Although the conventional approach to visualization of the vehicle's surroundings using several displays may be suitable for various teleoperation applications, its ability to depict the environment is not adequate for teleoperated driving in all urban environments.
As illustrated in Figure 4.2, when using the conventional HMI concepts, only a fraction of a 360° vehicle's surroundings can be visualized simultaneously. The low level of situation awareness provided by the conventional HMI leads to inadequate task performance on the part of the human operator when he needs to control a remote car precisely. Examples of such scenarios are driving within narrow passages or precisely controlling a vehicle in parking garages.
Capturing the entirety of a vehicle's surroundings by means of several camera sensors and transmitting all of these images from the vehicle to the operator requires a considerable communication bandwidth which is not always available.

Figure 4.2 : Top view of a conventional operator's workstation. Using the conventional HMI, the human operator can see only a fraction of the 360° vehicle surroundings simultaneously.

Even with sufficient communication bandwidth to transmit all of these data, simultaneous visualization of the 360° vehicle's surroundings requires several displays, resulting in high costs and the operator's workstation taking up large amounts of space. In addition, switching between several displays to perform a specific driving task may pose ergonomic challenges to the human operator.
To solve these challenges, the operator's workstation needs to be redesigned. For this purpose, this chapter introduces a novel HMI concept for vehicle teleoperation that uses a head-mounted display (HMD).

4.2 State of the Art: Improvement of Telepresence

4.2.1 Telepresence and Performance

Telepresence is defined by Sheridan as "the sense of being at a real location other than where one actually is" [45]. This sense is distinct from immersion, which is defined as "the degree to which a virtual environment submerges the perceptual systems of the user in computer stimuli" [46].
As described in Chapter 2.2.3, several approaches exist for enhancing telepresence. However, there is no unique objective parameter for measuring telepresence. Hence, its improvement is usually evaluated by comparison of different HMIs.
The relationship between telepresence and situational awareness has been investigated in several studies. Endsley [47] defined situation awareness as the "perception of elements in the environment within a volume of time and space, the comprehension of their meaning and the projection of their status in the near future." Draper *et al.* [48] distinguish between situation awareness of the local and remote environment. Based on this division, they assert that "telepresence may be considered the maximization of situation awareness in the remote environment accompanied by loss of situation awareness for the local environment." Therefore, they conclude that "if all of the information needed for task performance is located in the remote environment, maximization of remote situation awareness should improve telepresence and performance."
Riley *et al.* [49] developed the following regression model for measuring telepresence:

$$\text{Telepresence} = \beta_0 + \beta_1 \text{LOD} + \beta_2 \text{SA} + \beta_3 \text{ATTENTION} + \beta_4 \text{ITQ} + \epsilon, \tag{4.1}$$

in which situation awareness (SA), the level of difficulty (LOD) of a task, attention allocation and the results of the immersive tendencies questionnaire (ITQ) are assumed as constituting components of telepresence.
The relationship between telepresence and task performance has been the subject of much

speculation within the field of teleoperation. Several studies such as [50], [51] and [52] show that telepresence improves task performance [48]. However, Zeltzer [53] believes that, while telepresence might improve performance, it might also make tasks more difficult and fatiguing [48]. In addition, some studies, such as that of [54], assert that no clear relationship can be identified between telepresence and task performance.

4.2.2 Virtual Reality

Virtual reality is considered to be a novel form of HMI that could be used to increase telepresence. One of the many definitions of this HMI concept states that "virtual reality refers to immersive, interactive, multi-sensory, viewer-centered, three-dimensional computer generated environments and the combination of technologies required to build these environments" [55].

One of the main advantages of such an impressive virtual environment is that the user can perceive and interact with the three-dimensional environment, which enables the development of more natural and effective HMIs [56].

To immerse the user in a completely virtual world, a specific user interface is required. A HMD is one of the main components required in order to develop such an interface. Such a device would cover the user's eyes and display a virtual environment constructed using computer graphics to him or her. Using such an approach, decoupling the user from the real world becomes possible.

Ivan Sutherland [57] developed the idea of an "ultimate display," which "would, of course, be a room within which the computer can control the existence of matter. A chair displayed in such a room would be good enough to sit in. Handcuffs displayed in such a room would be confining, and a bullet displayed in such a room would be fatal. With appropriate programming such a display could literally be the Wonderland into which Alice walked".

Later, in 1968, he invented the first prototype of a HMD at MIT's Lincoln Laboratory [58]. This prototype is illustrated in Figure 4.3(a). Due to the weight of the developed HMD, it could not be easily worn. Hence, it was mounted to the ceiling, and a mechanical device was used to set the user's line of sight. He then developed his prototype further by incorporating stereoscopy and further improved its hardware and software at the University of Utah during the 1970s.

In 1984, NASA Ames Research Center developed the first stereoscopic HMD, intended for use in space operations. The LCDs used in this HMD had a resolution of 100 x 100 pixels and its design was partially based on the prototype developed by Ivan Sutherland. Figure 4.3(b) illustrates this HMD, which was designed to be worn as a helmet.

A few decades after the invention of HMD, innovations in display and tracking technologies, as well as the appearance of high-performance graphical and computing units on the market, led to this technology spreading. Through technological developments and mass production of these HMDs, their prices were significantly reduced. Figure 4.3(c) illustrates one of the HMDs currently available on the market, developed by HTC.

Contemporary HMDs are usually equipped with several sensors such as gyroscopes and acceleration sensors for measuring their rotation. In addition, some external sensors such as camera sensors are used to track the user's head position. Such an external sensor for head-tracking can be seen in Figure 4.4(a), near an Oculus Rift. As illustrated in Figure 4.4(b), visualization of the virtual environment occurs through two displays, with a lateral shift in the images providing stereoscopy for the user.

Meanwhile, some VR devices have been developed that can be used as head-mounted displays in combination with a smartphone. These gadgets use the display and the processing units of the inserted smartphone and can thus be produced at a low cost. In addition, some wearable devices that enable the dynamic visualization of the hand or other parts of the body in a virtual environment have been developed. An example of one of these wearable interfaces for visualizing the user's hands can be seen in Figure 4.4(c).

One of the main applications of HMD is training by means of simulating real conditions in a virtual space. For example, such devices are used for training surgeons [61], pilots [62] and

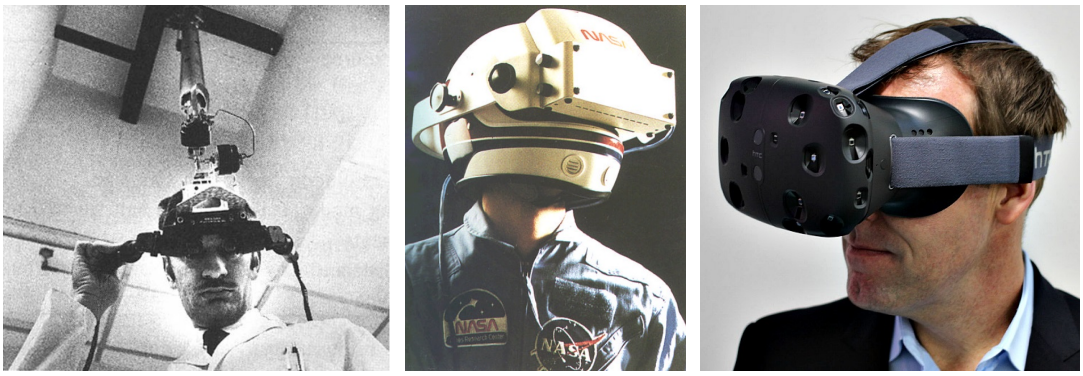

(a) (b) (c)

Figure 4.3 : Evolutionary development of head-mounted displays, (a) the first developed HMD by Ivan Sutherland in 1968 [59], (b) the developed HMD by NASA in 1984 and (c) an example of current HMDs.

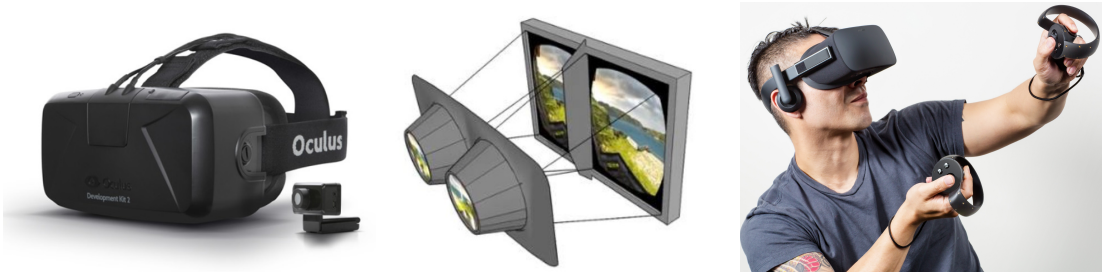

(a) (b) (c)

Figure 4.4 : (a) an Oculus Rift with its external infrared sensor for head-tracking; (b) stereoscopic visualization of the images within the HMD; (c) Oculus Touch as an example of wearable devices to visualize the hands in the virtual environment [60].

soldiers [63]. Another area of application for HMDs is computer games, which encouraged the private use of this technology. Several novel game consoles include a HMD in order to exploit the benefits offered by virtual reality.
In the automotive industry, HMDs are often used for design, production and vehicle-in-the-loop test [64] purposes. Similar applications can be found in the building industry, in which HMDs are used to check the design of a building before it is constructed.
In telerobotics, HMD is mainly used to improve the user's immersion. Several research works in this area have attempted to do so using stereoscopy [65], [66] or the head-tracking ability of HMDs [67] [68] [69].

4.2.3 Mixed Reality

Milgram *et al.* [70] defined the Reality-Virtuality (RV) continuum as a wide spectrum between the real and the virtual environments. This definition describes the mixed reality environment as "one in which real world and virtual world objects are presented together within a single display, that is, anywhere between the extrema of the RV-continuum."
Figure 4.5 illustrates this definition. As can be seen, mixed reality includes "augmented reality", the enhancement of the real environment with additional information and "augmented virtuality," referring to enhancement of the virtual environment with information from the real environment.
Depending on the use case, the weight of the reality or virtuality within a mixed reality environment can be adjusted. Examples of different adjustments of reality and virtuality can be found in [71] and [72].

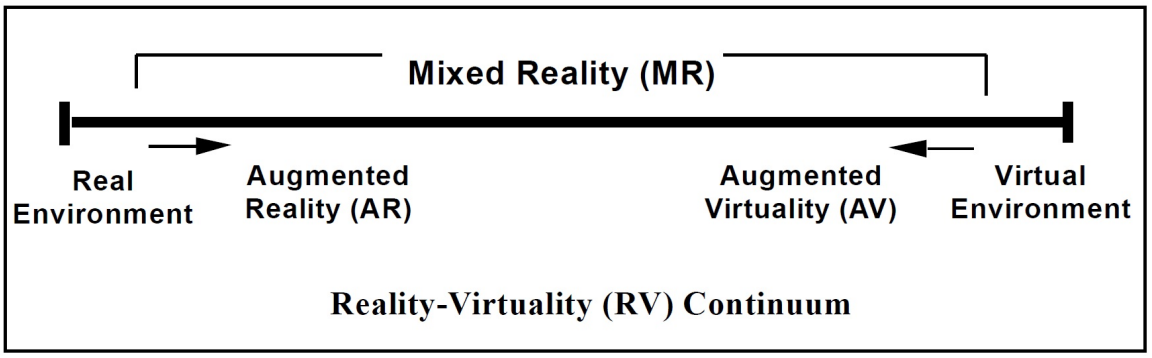

Figure 4.5 : Reality-Virtuality (RV) Continuum as a wide spectrum between the real and the virtual environment [70]

4.3 Approach

4.3.1 Enhancing Telepresence Using Mixed Reality

To improve the situation awareness of the human operator and consequently enhance his telepresence, more information about the vehicle's surroundings needs to be provided. Enhanced telepresence would improve his task performance while engaged in teleoperated driving.

A simple solution for satisfying this requirement would be mounting a surround-view camera system on the remote car, transmitting its images to the operator's workstation and displaying them alongside the footage from the front camera in the operator interface.

Using such a solution, the human operator would need to compare several images from different points of view in order to extract the required information. Although this solution would provide the human operator with more information about the vehicle's surroundings, it may lead to him or her becoming distracted from the driving task and would thus not be appropriate for teleoperated driving in urban environments.

To increase the amount of information available to the human operator about the vehicle's surroundings and to improve his telepresence, the 360° vehicle's surroundings need to be visualized in a uniform environment. This can be realized through reconstruction of the missing information about the vehicle's surroundings at the operator's workstation and the creation of a mixed reality environment for the human operator.

To achieve this goal, the displays of the conventional operator's workstation would need to be replaced by a HMD. Using this approach, the camera images received at the operator's workstation could be combined with a virtual environment that includes additional information about the vehicle's surroundings provided by the vehicle's sensors.

Figure 4.6 illustrates the general structure of vehicle teleoperation using this novel HMI. When compared to Figure 1.1, only the visualization unit changes, while the other cockpit components remain the same.

Using this HMI, the human operator is decoupled from his real environment at the operator's workstation and can imagine being in the remote car. This leads to an increase of his telepresence during teleoperation of the vehicle.

To realize this HMI, the vehicle's surroundings need to be modeled for the remote car. Thereafter, this model must be transmitted to the operator's workstation. Transmission of this environment model from the teleoperator to the operator's workstation would only add a negligible load to the transmission channel. The steps required to realize this HMI are described below.

4.3.2 360° Modeling of the Vehicle's Environment Using Occupancy Grid

The vehicle's environment can be modeled as an occupancy grid, which is a two-dimensional tessellation of space into cells, where each cell stores a probabilistic estimation of its occu-

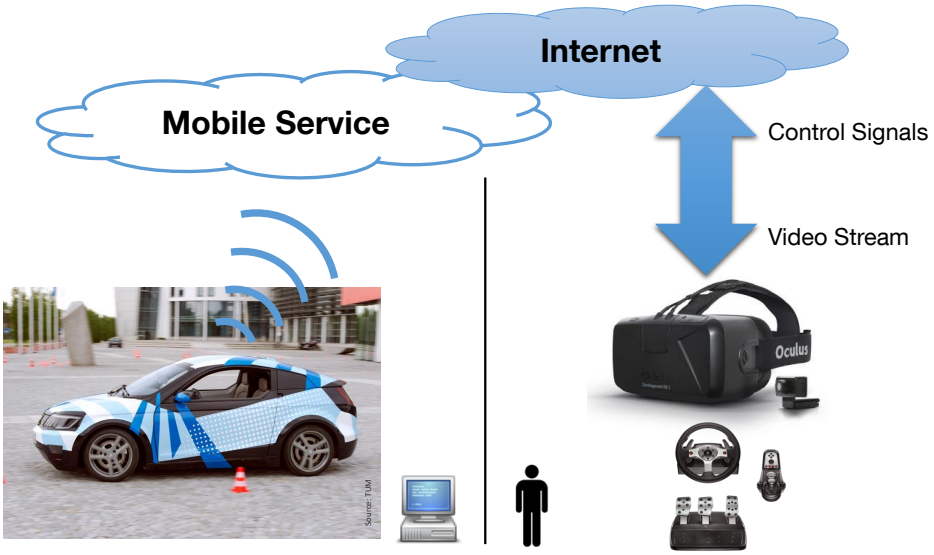

Figure 4.6 : Using HMD to create a mixed reality environment for vehicle teleoperation [144]

pation state [73].
An occupancy grid can be created using a ranging sensor, such as a stereo camera system or LiDAR, that measures the distance of an obstacles from the remote vehicle. Since the LiDAR sensors have a greater scanning angle and higher accuracy in distance measurement, these sensors are used in this work to create a 360° environment model. The sensors employed to create the occupancy grid and their mounting positions on the car have been introduced in Chapter 2.3.1.1.
The occupancy grid consists of certain number of cells of the same size. A probabilistic value between 0 and 1 is assigned to each cell, where 0 represents the free state and 1 represents the occupied state. The occupation state is visualized using a color spectrum between black and white, where black represents the free state and white represents the occupied state.
Each cell is initialized with a value of 0.5, which means the occupation state of the cell is unknown. This is also the case when a cell is located behind an occupied cell and no information about its occupation state is available. These cells are shaded in gray on the occupancy grid.
Calculation of an occupancy grid consists of prediction and update steps. In the prediction step, the current state of each cell is predicted using the measured data obtained during the last calculation step. For this purpose, the occupancy grid of the last calculation step is rotated and shifted according to the changes in the position and the heading angle of the vehicle within the most recent measurement step.
During the update step, the new measurement data from the LiDAR sensors are fed to the occupancy grid. This occurs using two increasing and decreasing maps which are added to and subtracted from the occupancy grid, respectively. The increasing map projects the obstacles newly detected by LiDAR into the grid cells and sets their occupation state to 1. The decreasing map calculates the free space between the vehicle and the occupied cells based on the newest LiDAR measurement data and draws lines that connect the sensor positions to the occupied cells. With the subtraction of this map from the occupancy grid, the previously calculated free spaces are updated.
Figure 4.7 illustrates these calculation steps using the measurement data supplied by LiDAR. With regard to the calculation steps discussed above, the value of each cell in the time stamp t can be estimated as follows:

$$v_t(x,y) = v_{t-1}(x + \Delta x, y + \Delta y) + \alpha.v_{I,t}(x,y) - \beta.v_{D,t}(x,y), \tag{4.2}$$

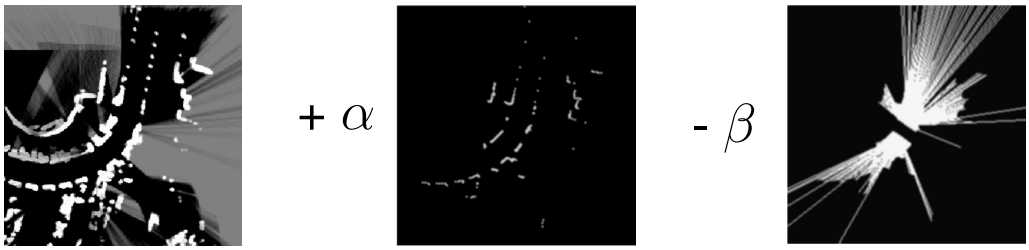

Figure 4.7 : Calculation of the occupancy grid using the LiDAR measurement data

where x and y represent the coordinates of the cell on the occupancy grid, v_t and v_{t-1} represent the value of the cell in the current and last time stamps and $v_{I,t}$ and $v_{D,t}$ represent the value of the same cell on the increasing and decreasing maps in the current time stamp, respectively. α and β represent the weights of the increasing and decreasing maps in the update step, respectively.
Figure 4.8(a) shows the raw LiDAR data captured by two LiDAR sensors mounted on the front and rear of the test vehicle. Figure 4.8(b) illustrates the resulting occupancy grid by this raw data. On this grid, the occupied and free cells are illustrated in white and black, respectively. Those cells whose occupancy status cannot be determined are illustrated in gray. These cells are normally located behind the occupied cells.

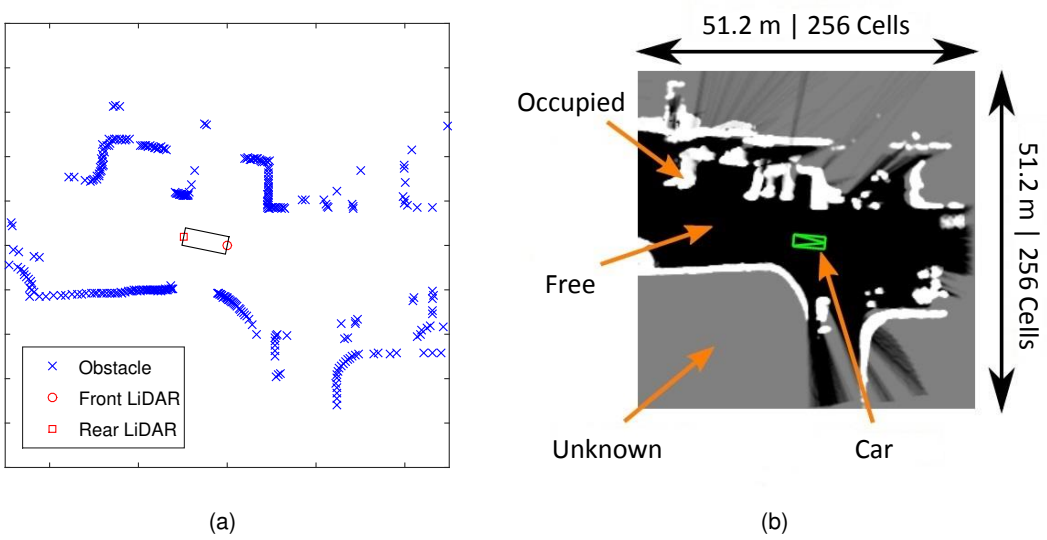

Figure 4.8 : (a) Raw LiDAR data in an example scene and (b) the corresponding occupancy grid

Figure 4.9(a) depicts a camera image of a narrow passage, in which the operator cannot easily determine the lateral distance of the remote car from the obstacles located on both sides. Figure 4.9(b) illustrates the occupancy grid of the same scene created by the remote car's two LiDAR sensors, which displays a 360° top view of the vehicle's surroundings.

4.3.3 Creation of the Mixed Reality Environment

To combine reality with virtuality and create a mixed reality environment, a HMD that enables the creation of a virtual environment is required.
In this work, an Oculus Rift development kit 2 (DK2) is used, which is equipped with an internal gyroscope, magnetometer and accelerometer. Each eye of this HMD has a resolution of 960 x 1080 pixels and an external infrared CMOS sensor tracks the head motion of the user.
As the images received from the remote car's three cameras provide the most important

(a) (b)

Figure 4.9 : (a) A narrow passage captured by the front camera of the remote car and (b) its corresponding 360° occupancy grid map created by two LiDAR sensors [144]

information about the vehicle's surroundings, they should be included within the virtual environment displayed by the head-mounted display.
In order to increase the human operator's awareness while engaged in teleoperation of a vehicle, he should know the exact position of the borders of the car as well as the orientation of its wheels. This information can be added as a form of augmented reality to the virtual environment displayed by the head-mounted display.
Such visualization of the images provided by cameras and the border of the remote car is illustrated in Figure 4.10. As can be seen in this image, the current orientation of the vehicle's wheels are visualized by means of the steering wheel's angle at the operator's workstation.
In order to give the human operator a realistic sensation of being in car, the position and the height of the visualized camera images should be adjusted to match the normal distance and height of the cars' windshield to a driver sitting in car.
As indicated previously, the transmitted camera images cover only a fraction of the vehicle's surroundings, which is not enough to precisely control the vehicle within narrow passages. To solve this problem, the missing parts of the environment can be reconstructed in the virtual environment using the occupancy grid.
The occupied cells of the occupancy grid represent the obstacles detected by the LiDAR sensors. These obstacles can be reconstructed as virtual obstacles in the virtual environment created by the HMD. Figure 4.11 illustrates an example of these virtual obstacles.
Through a combination of the camera images that represent reality and the reconstructed

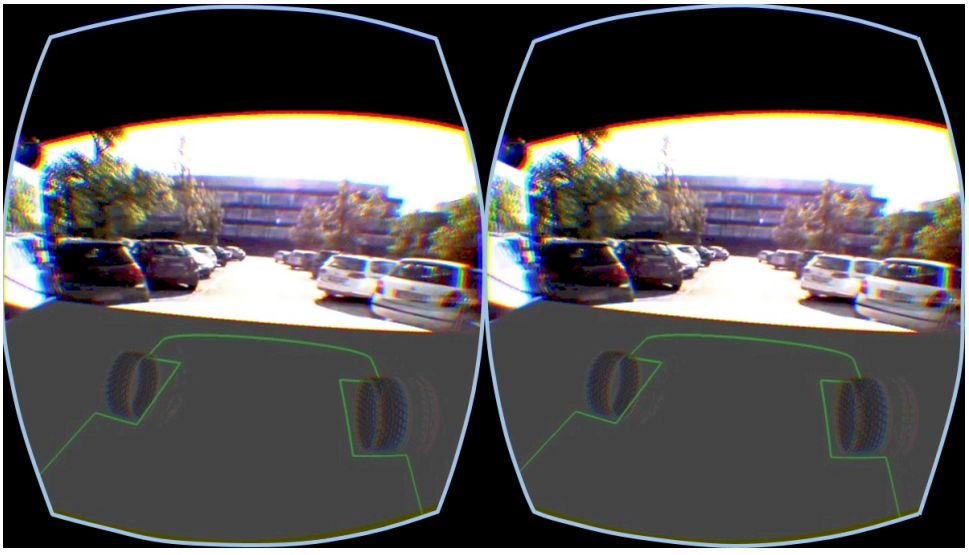

Figure 4.10 : Teleoperated driving within a narrow passage using a head-mounted display. The borders of the remote car as well as the orientation of its wheels are illustrated as augmented reality within the created virtual environment [144].

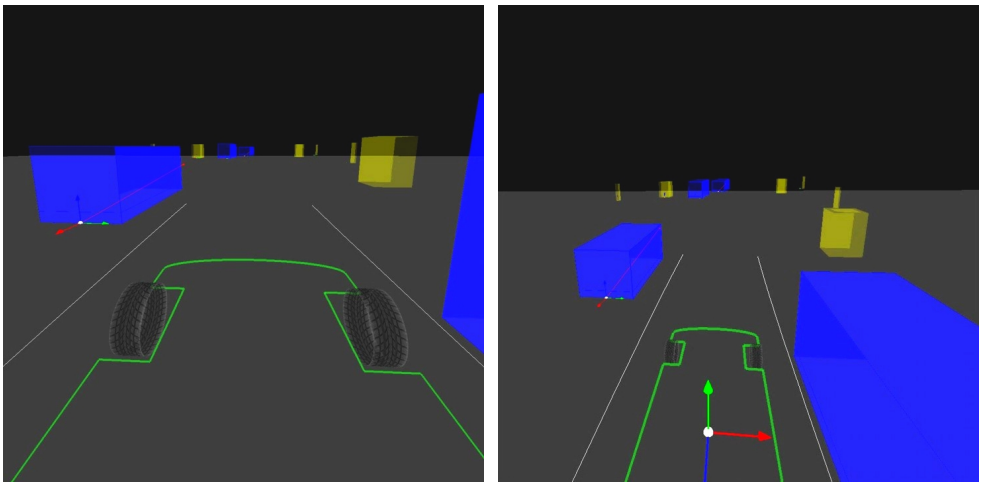

(a) (b)

Figure 4.11 : The virtual vehicle surroundings reconstructed using the transmitted occupancy grid map, seen within HMD from (a) operator's point of view and (b) perspective view [144]

parts of the environment functioning as a form of virtuality, a mixed reality environment can be realized. For this purpose, the camera and LiDAR sensors need to be calibrated with reference to a unified coordinate system. This can be done using a calibration wall positioned at a known distance in front of the test vehicle. As illustrated in Figure 4.12, the measurements provided by each sensor are based on its own local coordinate system. For the joint calibration of multiple sensors, a unified coordinate system needs to be determined. Thereafter, the local coordinate system of each sensor should be synchronized with this unified coordinate system. A description of this process being used for a similar application can be found in [142].

In this work, the projection of the center of the car's front axle onto the floor was chosen as the point of origin for the unified Cartesian coordinate system. Thus, the exact distance of this point to the calibration wall can be measured manually.

After an orthogonal positioning of the calibration wall in front of the car, its distance and orientation in relation to the LiDAR sensor was calculated. Through comparing these values to the known distance and orientation of the calibration wall with reference to the unified coordinate system, the extrinsic parameters of the LiDAR sensor were calculated.

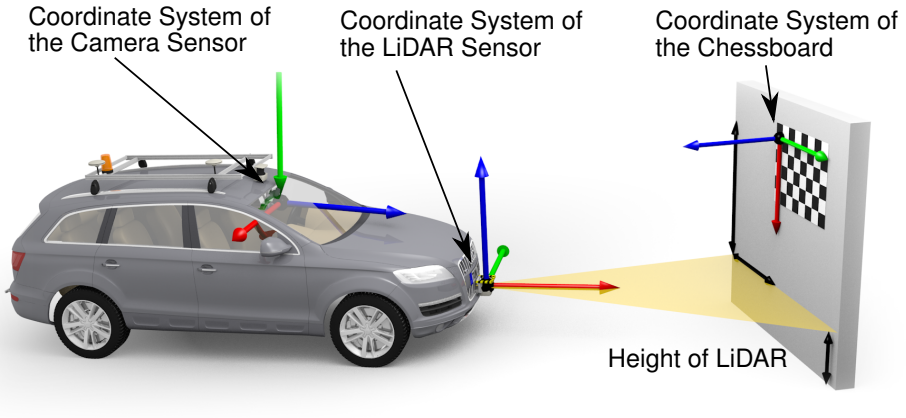

Figure 4.12 : Joint calibration of the camera and LiDAR sensors of the test vehicle to create the mixed reality environment

To determine the extrinsic parameters of the camera sensor with regard to the unified coordinate system, a chessboard with the known dimensions was hung on the calibration wall. Through several measurements of this chessboard at different positions on the calibration wall, the translation and orientation of the camera sensor with regard to the unified coordinate system could be measured.
After calculation of the extrinsic parameters of all of the used sensors, their measured data could be transformed from their local coordinate systems to the unified coordinate system. As a result, fusion of the data captured by different sensors became possible. This fusion enabled the combined visualization of the camera images and the virtually reconstructed environment using the data obtained by the LiDAR sensors. Figure 4.13 illustrates a top view of this mixed environment.

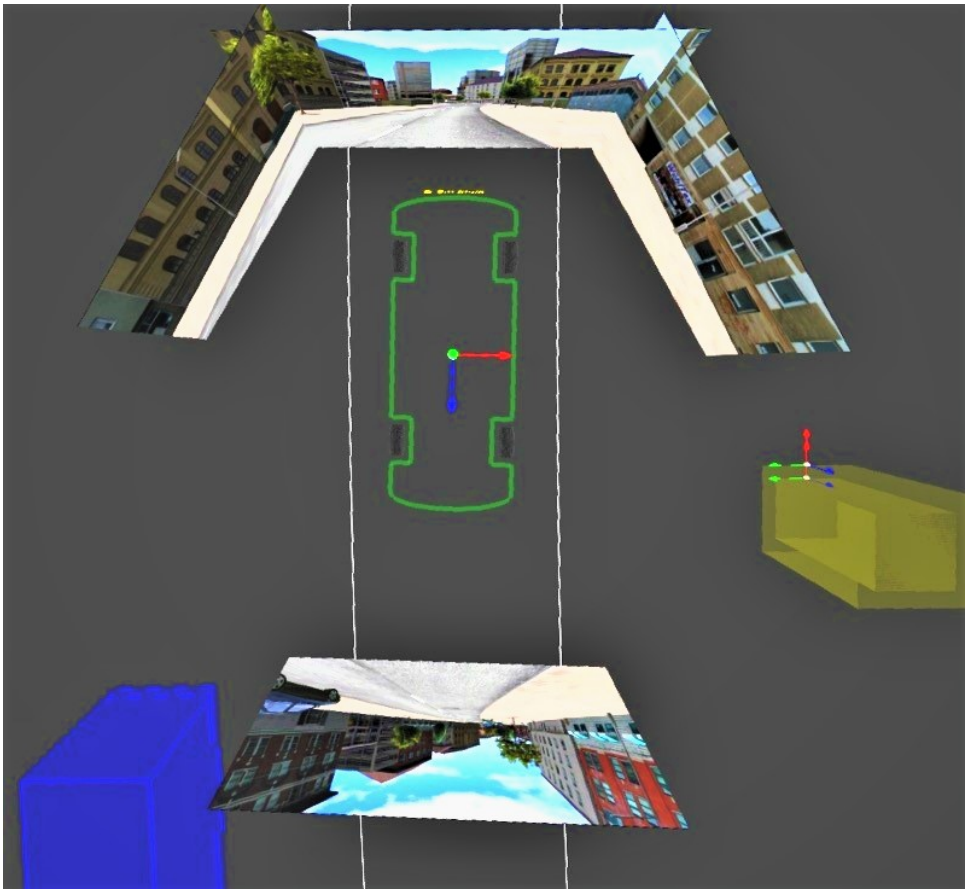

Figure 4.13 : Top view of the developed mixed reality environment for vehicle teleoperation [144]

As can be seen, the images captured by the rear camera sensor are visualized behind the human operator. Thus, the human operator would need to turn and look behind him- or herself when he wants to drive in reverse gear, which further promotes the impression of being in a real car.
Since the camera sensors used do not completely capture the lateral sides of the remote car, an existing object on the right-hand side of the car is illustrated by means of virtual reality.
Figure 4.14 illustrates a perspective view of the mixed reality environment created using this approach. As can be seen, the virtual obstacles appear to the human operator as soon as they are not within the field of view of the cameras.
Using this approach, the number of camera sensors required on the car can be reduced. Since the transmission of each camera image requires a percentage of the communication bandwidth, the images from the side camera can be replaced using virtual reality. Figure 4.15 illustrates a screenshot of the developed mixed reality environment during a test drive using the Audi Q7 experimental vehicle, in which only one camera image was used for representa-

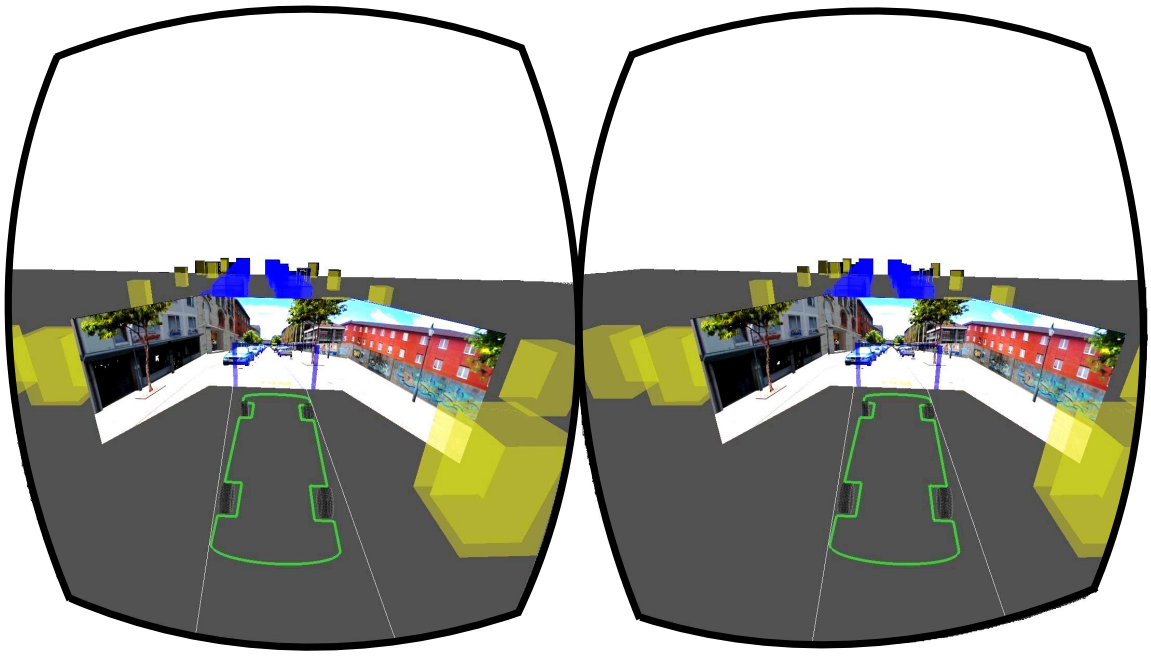

Figure 4.14 : Perspective view of the mixed reality environment shown within HMD to the human operator [144]

tion of the environment. As can be seen, the obstacles detected by the LiDAR sensors of the remote car are presented to the human operator using virtual reality.
The possibility of omitting all camera images and significantly reducing the communication load is discussed in Chapter 7.2.2.

4.4 Evaluation and Results

4.4.1 Test Design

The proposed HMI concept was evaluated using a variety of test scenarios. The test procedure and results are described below.

4.4.1.1 **Test Environment**

For evaluation, a human-in-the-loop test environment using the simulation tool SILAB [43] was developed. This simulation tool makes it possible to design urban environments with different types of traffic participants such as vehicles, pedestrians and bicycles as well as different kinds of streets and infrastructure. Using the existing single-track and two-track

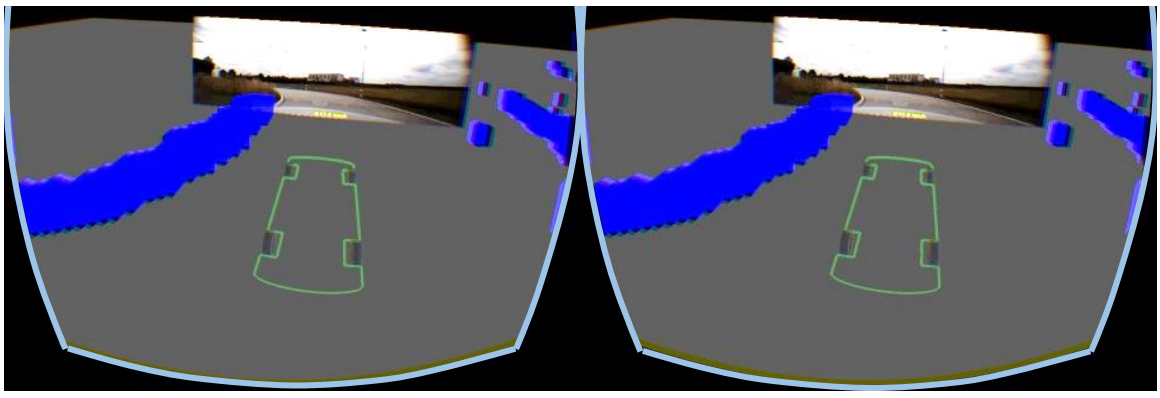

Figure 4.15 : Perspective view of the developed mixed reality environment using the received LiDAR measurement data from the remote car

vehicle dynamics models provided by this tool, the dynamics model of the ego-vehicle can be simulated.
The operator workstation used for this test is presented in Figure 2.9(a). The same operator's interface used for the teleoperated driving of a real experimental vehicle was used in this human-in-the-loop test environment. The connection between the operator's interface and the SILAB simulation tool was established via UDP, which corresponds to the connection used between the operator's interface and the real experimental vehicle.
The connections between different components of the test setup are depicted in Figure 4.16. The operator's interface ran on a computing unit of the operator's workstation. The SILAB simulation software ran on a separate computation unit, from which the encoded images of test environment, information from the remote vehicle and information about other traffic participants were transmitted to the operator's interface. The control commands, including steering angle and the states of the gas and brake pedals, were sent in the opposite direction from the operator's interface to SILAB.

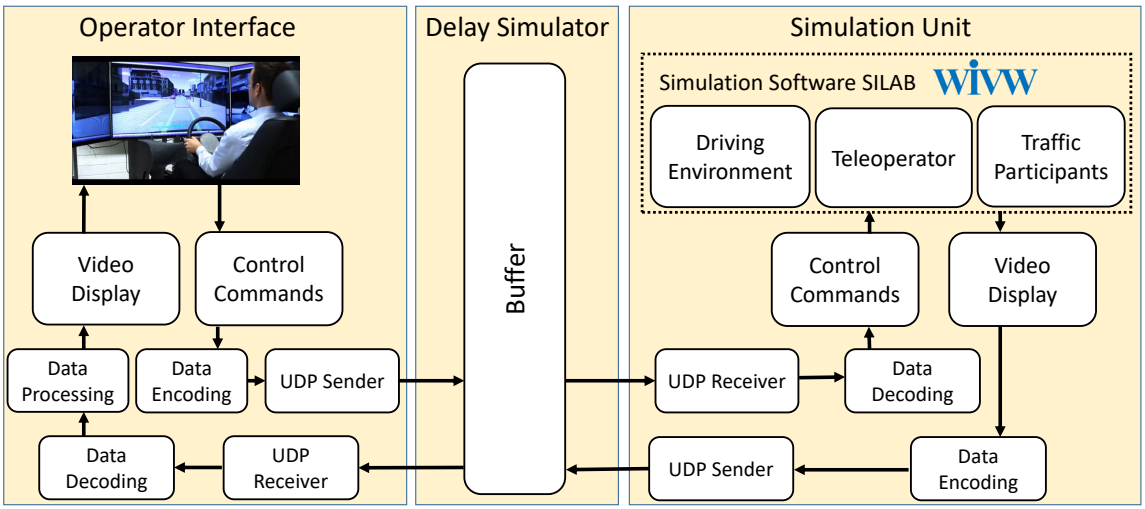

Figure 4.16 : The connections between several software modules of the test setup. To simulate the real condition of teleoperated driving, an artificial time delay is created between the operator's interface and SILAB.

To simulate the time delay that exists in teleoperated driving, communication between the operator's workstation and the simulated remote vehicle was artificially delayed. Similarly to the determined constant time delay encountered while operating a remote vehicle using LTE, the video received from SILAB was delayed by 500 ms at the operator's workstation.
To compare the proposed and the conventional HMI concepts using the same operator's workstation, the workstation was equipped with an Oculus Rift using development kit 2 which visualizes the test environment at the same time as the monitors of the operator's workstation. This is shown in Figure 4.17, in which a test person drives the simulated remote car using HMD and the corresponding video is shown simultaneously on the monitors of the operator's workstation.

4.4.1.2 **Test Scenarios**

To investigate the different performance aspects of the developed HMI concept, three different test scenarios were designed. These test scenarios are described below.

4.4.1.2.1 **Test scenario I: Precise Control**

The first test scenario was designed to investigate the ability of the human operator to precisely control the remote vehicle. The bird's-eye view of the test scenario is shown in Figure 4.18. This scenario consisted of two phases: in the first phase, the test persons were asked to drive parallel, as closely as possible, to a parked truck.
In the second phase, the operators were asked to drive in reverse gear, as closely as possible, to the same parked truck. In both phases, the test persons were asked to prevent a collision

Figure 4.17 : The used operator's workstation for evaluation, equipped with three monitors and a head-mounted display to compare both visualization possibilities [144]

with the parked truck.

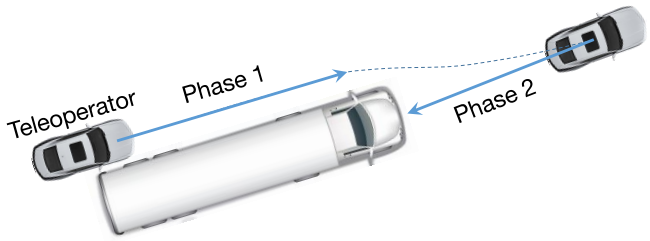

Figure 4.18 : Test scenario "precise control": The operator is asked to drive as close as possible from different directions to a parked truck.

4.4.1.2.2 **Test scenario II: Backing into a Parking Space**

The second test scenario focused on investigating the ability of the human operator to guide a remote vehicle, backward into a parking space. Figure 4.19 shows the different steps in this test scenario. The red located rectangles on both sides of the parking space represent the parked cars.

Compared to the first test scenario, this test scenario required the test subjects to focus more particularly on lateral control of the vehicle while backing up. The remote vehicle had a length of 5 m, while the parking space had a length of 6.8 m. The test persons were asked to park the remote vehicle in the middle of the parking space, meaning that the remote vehicle should ideally have a distance of 90 cm from the obstacles located on either side of the parking space.

Similarly to the first test scenario, the test persons were asked to prevent a collision with the parked cars located on either side of the parking space.

4.4.1.2.3 **Test scenario III: Urban Driving**

The third test scenario investigated the impact of using the proposed HMI concept while driving at speeds of up to $50\ \frac{km}{h}$ in a variety of urban environments. For this purpose, a test track with a length of approximately 20 km was simulated in SILAB. This test track was designed to include different types of streets and traffic conditions such as intersections, roundabouts, traffic lights and crosswalks.

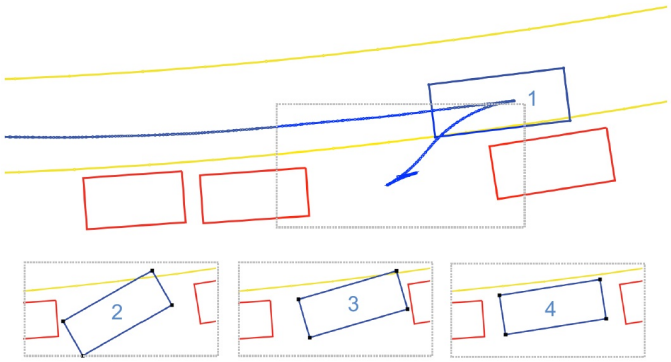

Figure 4.19 : Four steps of the test scenario "backing into a parking space". The test persons are asked to park the remote car as centric as possible within the parking space.

To investigate the performance of the test persons in narrow passages, the test track was narrowed at several locations using static obstacles such as parked cars or traffic cones.

4.4.1.3 **Test Persons and Test Procedure**

As described in Chapter 3.2, experienced operators are required for teleoperated driving. Hence, four trained test persons were used to evaluate the developed HMI concept. Through training, these test persons became accustomed to driving with a round-trip communication time delay of 500 ms.
Each test was conducted by each test person three times using the conventional HMI concept and three times using the developed HMD-based HMI concept. To minimize the learning effect while evaluating the developed HMI concept, the test drives using the monitors and HMD were conducted in a mixed order.

4.4.1.4 **Measured Parameters**

To evaluate the performance of the test persons during the test drives, several objective and subjective parameters were measured. These parameters were chosen with regard to the scope of and the given tasks in each test scenario.

4.4.1.4.1 **Objective Parameters**

To measure the ability of the test persons to precisely control the remote vehicle using both of the HMI concepts studied, the distance of the remote vehicle to each of the obstacles located in the scenario was measured.
In the first test scenario, the test persons were asked to drive the remote vehicle as closely as possible to a parked truck. Thus, the average lateral and longitudinal distances of the remote vehicle to the parked truck during the defined test phases were captured.
In the second test scenario, the test persons were asked to park the remote car in the middle of the parking space. Thus, the distance of the remote vehicle to the vehicle nearest to the parking space was measured.
To gauge steering performance using the proposed HMI concept at speeds of up to $50\ \frac{km}{h}$, the directional stability and the steering wheel reversal rate (SRR) were captured as the two main parameters for steering assessment. The directional stability parameter represents that percentage of the test course during which the vehicle was within the traffic lanes.
The steering wheel reversal rate (SRR) is defined as follows:

$$SRR = \frac{n_{gap}}{t_{driven}}, \tag{4.3}$$

where n_{gap} represents the absolute number of reversals within a driven track and t_{driven} is the time required to drive [74]. To determine the reversals, the local optimum values have to get extracted from the captured signal angle of the steering wheel. A reversal occurs when the following two local optimum values exceed a defined value: $\Delta\alpha_{gap}$. Figure 4.20 illustrates

the counting of reversals during an example signal of steering wheel angle. In this work, the value of 5° is determined as $\Delta\alpha_{gap}$.

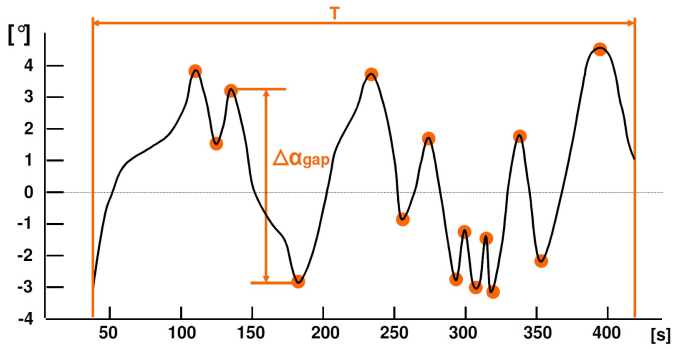

Figure 4.20 : Calculation of reversals in the captured signal of steering wheel angle [75]

In all three test scenarios, the test persons were asked to avoid collision with other obstacles. Hence, the number of collisions that occurred during each test was captured. This number serves as a sign of the safety while using each HMI concept within each test scenario.

4.4.1.4.2 Subjective Parameters

In addition to capturing the number of collisions that occurred, the test persons were asked about the number of collisions that occurred during each test scenario that they identified. Comparison of these values to the actual number of collisions would result in a parameter for measuring their situational awareness.
To measure the workload using both HMI concepts in each test scenario, the test persons were asked to fill in the NASA task load Index [76]. Using this assessment tool, an overall workload score can be derived, based on the weighted averages of the ratings of the six following subscales: mental demand, physical demand, temporal demand, performance, effort and frustration.
Finally, the test persons were asked to fill in a questionnaire after finishing each test scenario. This questionnaire assessed several subjective parameters, such as the test person's impression of the improvements in safety, situation awareness and telepresence that result from the use of the developed HMI concept.

4.4.2 Test Results

4.4.2.1 Results of the Test Scenario: Precise Control

Figure 4.21 illustrates some scenes from the "precise control" test scenario when using both the conventional and the proposed HMI concepts. As can be seen, using the mixed reality HMI the test person can perceive the exact longitudinal and lateral distances of the remote car to the parked truck, which would normally be impossible when using the conventional HMI.
Table 4 illustrates the average results as well as the maximum captured deviations from them within the first phase of the "precise control" test scenario. The illustrated values include the maximum deviation from the average results of three conducted test drives. As can be seen, using the mixed reality HMI all test persons were able to demonstrate finer control when operating the remote car closer to the parked truck.
Table 5 depicts the same results for the second phase of the "precise control" test scenario. As can be seen, using the mixed reality HMI all test persons could longitudinally control the remote car closer to the parked truck. These results illustrate the improvement in their ability to precisely control the remote car using the proposed HMI concept.
Table 6 shows the average number of collisions that occurred with the parked truck as well as their recognition rate by the test persons during both phases of the "precise control" test scenario. As can be seen, the average number of collisions was reduced when using the mixed reality HMI. This indicates that using this HMI provided more safety within this test

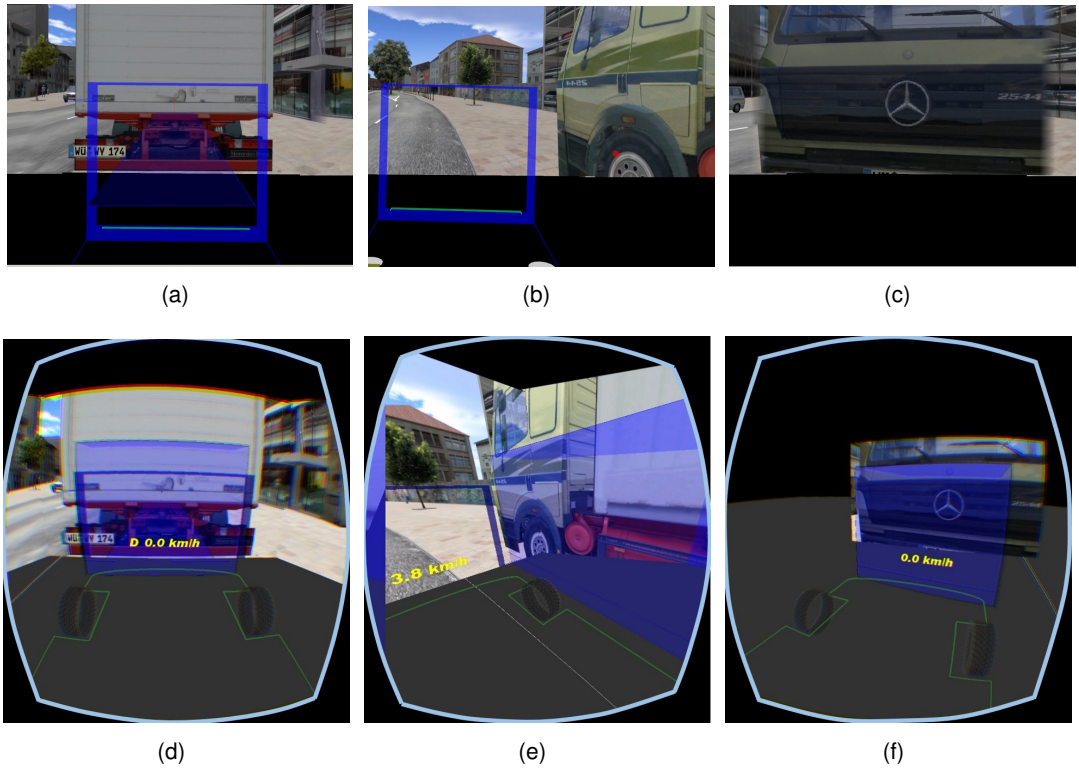

Figure 4.21 : (a-c) Some scenes of the test scenario "precise control" using the conventional operator's workstation and (d-f) the same scenes within the mixed reality environment [144]

Table 4 Average lateral distance of the remote vehicle to the parked truck during the first test phase of the scenario "precise control" [144]

Experienced Operator	Conventional HMI	Proposed HMI
Nr. 1	0.41 ± 0.37 m	0.20 ± 0.05 m
Nr. 2	0.34 ± 0.09 m	0.18 ± 0.09 m
Nr. 3	0.69 ± 0.05 m	0.25 ± 0.14 m
Nr. 4	0.67 ± 0.19 m	0.21 ± 0.02 m
Total Average	**0.53 ± 0.24 m**	**0.21 ± 0.08 m**

Table 5 Average longitudinal distance of the remote vehicle to the parked truck at the end of the second test phase of the scenario "precise control" [144]

Experienced Operator	Conventional HMI	Proposed HMI
Nr. 1	0.42 ± 0.03 m	0.13 ± 0.04 m
Nr. 2	0.34 ± 0.09 m	0.06 ± 0.00 m
Nr. 3	0.46 ± 0.08 m	0.13 ± 0.12 m
Nr. 4	0.63 ± 0.10 m	0.13 ± 0.03 m
Total Average	**0.48 ± 0.12 m**	**0.12 ± 0.06 m**

scenario.
In addition, the rate at which occurred collisions were recognized was significantly higher when comparing the use of the mixed reality HMI to that of conventional HMI. This indicates the greater situation awareness of the test persons when using the mixed reality HMI within this test scenario.

Table 6 Number of occurred collisions by each test person and the rate of collision recognition by him within the test scenario "precise control" [144]

Experienced Operator	Using the Conventional HMI		Using the Proposed HMI	
	Number of Collisions	Recognition Rate	Number of Collisions	Recognition Rate
Nr. 1	2	0 %	0	0 %
Nr. 2	3	0 %	4	75 %
Nr. 3	3	33 %	2	50 %
Nr. 4	2	50 %	0	0 %
Total Average	**2.5**	**20 %**	**1.5**	**66.6 %**

Table 7 shows the results of the NASA task load index. As can be seen, the total average of the workload when using the mixed reality HMI was lower than the corresponding value when using the conventional HMI. However, this comparison does not correspond with the values captured by one of the test persons.

Table 7 Workload of participants during the test scenario "precise control" assessed by NASA Task Load Index [144]

Experienced Operator	Conventional HMI	Proposed HMI
Nr. 1	31 %	31 %
Nr. 2	43 %	27 %
Nr. 3	27 %	38 %
Nr. 4	52 %	37 %
Total Average	**38.25 $\pm$ 11.41**	**33.25 $\pm$ 5.19**

4.4.2.2 **Results of the Test scenario: Backing into a Parking Space**

Figure 4.22 illustrates some scenes from the "backing into a parking space" test scenario when using the conventional and the proposed HMI concepts. Figure 4.22(e) shows the scene displayed to the test person when he turned to look behind from his right-hand side in order to reverse into the parking space. As can be seen, the exact position of the aside parked car was illustrated using virtual reality, and the rear camera feed was shown behind the car.
Table 8 shows the average results as well as the maximum captured deviations from them by three attempts at parking within the "backing into a parking space" test scenario. As can be seen, using the mixed reality HMI, all of the final distances to the nearest obstacle were closer than the desired distance of 90 cm. These results show that using the mixed reality HMI all test persons could park the remote vehicle more precisely than when using the conventional

HMI.

Table 8 Distance of the remote vehicle to the nearest parked vehicle in the parking space

Experienced Operator	Conventional HMI	Proposed HMI
Nr. 1	0.45 ± 0.35 m	0.82 ± 0.13 m
Nr. 2	0.54 ± 0.04 m	0.79 ± 0.05 m
Nr. 3	0.41 ± 0.40 m	0.71 ± 0.03 m
Nr. 4	0.27 ± 0.31 m	0.75 ± 0.07 m
Total Average	**0.42 ± 0.28 m**	**0.77 ± 0.08 m**

Table 9 shows the number of collisions that occurred and the rate at which test persons recognized during the "backing into a parking space" test scenario. As can be seen, when using the mixed reality HMI, the overall number of collisions that occurred was lower than the corresponding value when using the conventional HMI. In addition, the recognition rate of these collisions was higher using the proposed HMI. This indicates that using the proposed HMI concept results in greater safety and higher situation awareness while backing into a parking space.
The values obtained concerning the workload using the NASA task load index are illustrated in Table 10. As can be seen, the measured values show an absolute decrease in workload for all test persons when using the mixed reality HMI within the "backing into a parking space" test scenario. Comparing these values to the illustrated values in Table 7 reflects the subjective superior performance of the mixed reality HMI when negotiating narrow passages.

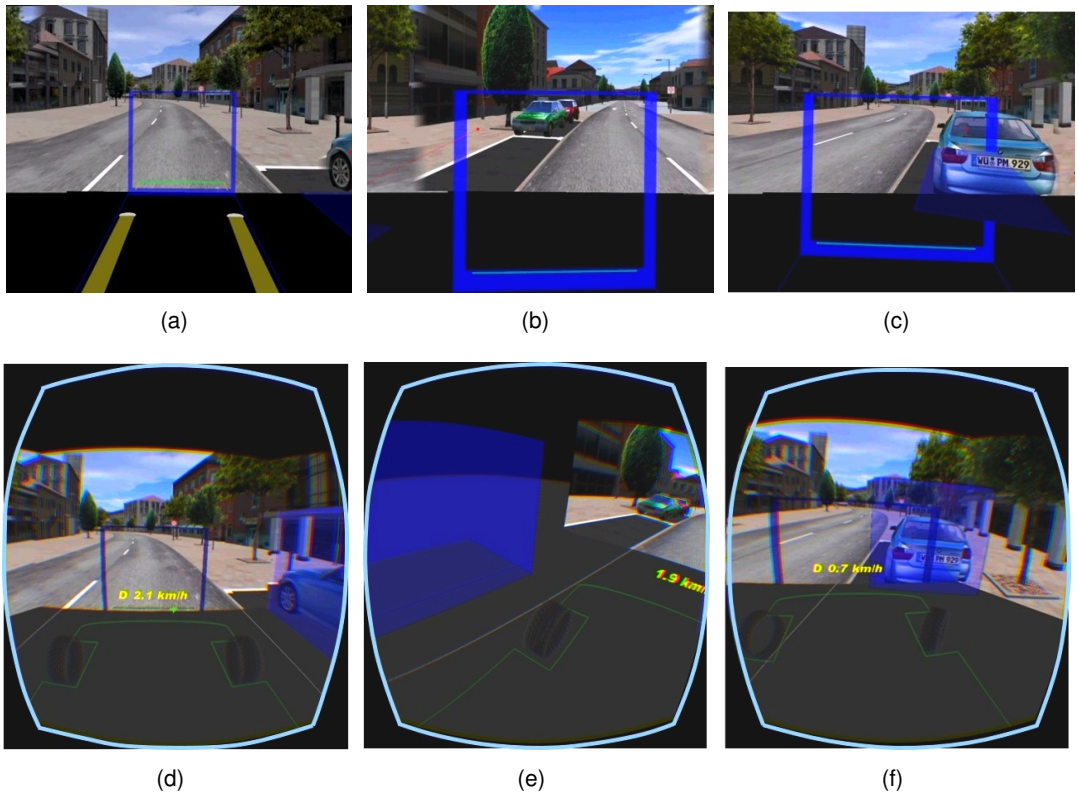

Figure 4.22 : Some scenes of the test scenario "backing into a parking space" (a-c) using the conventional operator's workstation and (d-f) the same scenes within the mixed reality environment

Table 9 Number of collisions by each operator and the rate of collision recognition by him in the scenario "backing into a parking space"

Experienced Operator	Using the Conventional HMI		Using the Proposed HMI	
	Number of Collisions	Recognition Rate	Number of Collisions	Recognition Rate
Nr. 1	1	0 %	1	0 %
Nr. 2	2	0 %	2	50 %
Nr. 3	3	33 %	3	33 %
Nr. 4	4	10 %	0	0 %
Total Average	**2.5**	**10 %**	**1.5**	**33 %**

Table 10 Workload of participants during the test scenario "backing into a parking space" assessed by NASA Task Load Index

Experienced Operator	Conventional HMI	Proposed HMI
Nr. 1	46 %	36 %
Nr. 2	41 %	27 %
Nr. 3	59 %	41 %
Nr. 4	60 %	39 %
Total Average	**51.5 $\pm$ 9.47 %**	**35.75 $\pm$ 6.18 %**

4.4.2.3 **Results of the Test Scenario: Urban Driving**

Figure 4.23 depicts some scenes from the "urban driving" scenario using both HMI concepts. As can be seen, the test track was similar to urban environments and included different types of streets.

The average directional stability as well as the maximum captured deviations demonstrated by the test persons during the three test drives within the entirety of the test track, using each HMI concept, is illustrated in Table 11. As can be seen, no significant difference in the measured values of directional stability can be detected when using either HMI concept. These results indicate that wearing a HMD does not increase the number of lane departures by the test persons.

Table 11 Comparison of directional stability in the whole test scenario "urban driving" using both HMI concepts [144]

Experienced Operator	Conventional HMI	Proposed HMI
Nr. 1	94 $\pm$ 3 %	86 $\pm$ 6 %
Nr. 2	85 $\pm$ 5 %	85 $\pm$ 4 %
Nr. 3	94 $\pm$ 1 %	93 $\pm$ 4 %
Nr. 4	77 $\pm$ 4 %	77 $\pm$ 3 %
Total Average	**88 $\pm$ 8 %**	**86 $\pm$ 7 %**

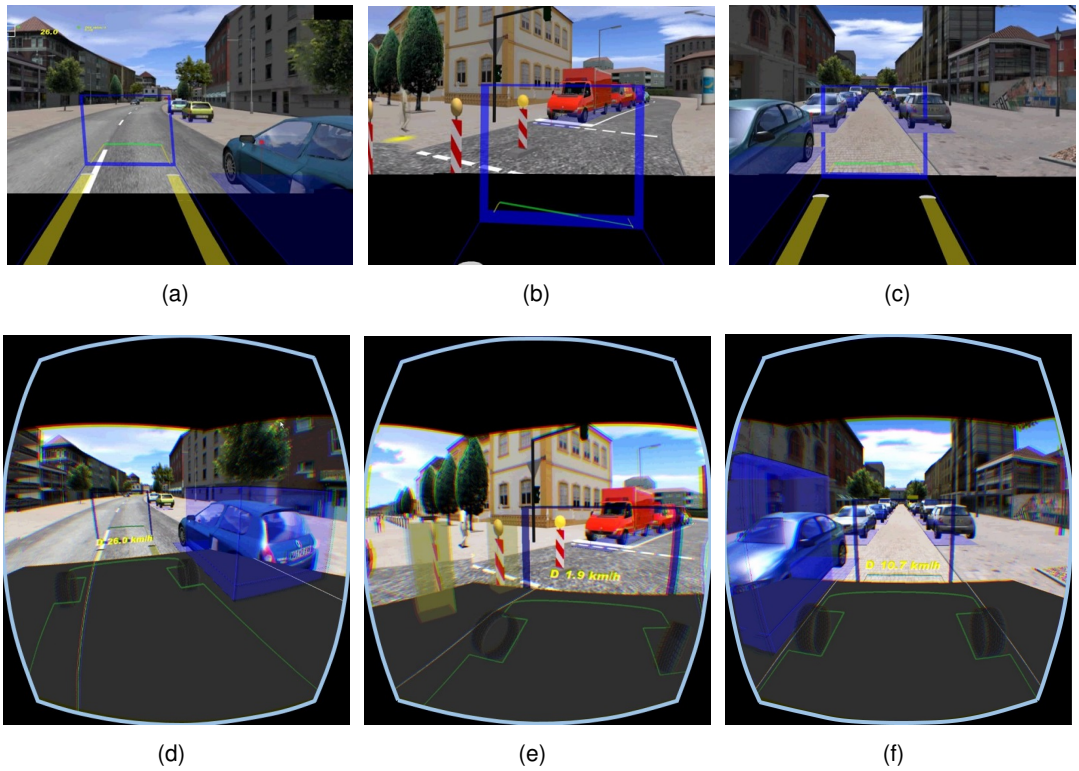

Figure 4.23 : (a-c) Some scenes from the test scenario "urban driving" using the conventional operator's workstation and (d-f) the same scenes within the mixed reality environment

The average SRR values are listed in Table 12. As can be seen, the SRR values increased for most of the test persons when using the mixed reality HMI. This may result from wearing the HMD while driving, which results in operators' hands as well as the steering wheel of the operator's workstation not being visible. This can result in test person exerting greater effort when steering the remote car. This challenge and its possible solution concepts are discussed further in Chapter 4.5.

Table 12 Comparison of the steering wheel reversal rate (SRR) within the test scenario "urban driving" using both HMI concepts [144]

Experienced Operator	Conventional HMI	Proposed HMI
Nr. 1	0.23 ± 0.05 [1/s]	0.23 ± 0.07 [1/s]
Nr. 2	0.19 ± 0.03 [1/s]	0.30 ± 0.04 [1/s]
Nr. 3	0.21 ± 0.02 [1/s]	0.25 ± 0.02 [1/s]
Nr. 4	0.26 ± 0.01 [1/s]	0.45 ± 0.10 [1/s]
Total Average	**0.22 ± 0.02 [1/s]**	**0.31 ± 0.05 [1/s]**

The values concerning the workload obtained through the use of the NASA task load index are illustrated in Table 13. As can be seen, there is no obvious difference in the total average of perceived workload when using either HMI concept, as some test persons gave a lower and others a higher workload rating when using the mixed reality HMI. The partial increase in the reported workload when using the mixed reality HMI could be a result of wearing the HMD and the lack of availability of some indicated information, such as the exact position of the steering wheel and the pedals of the operator's workstation.

Table 13 Workload of the participants during the test scenario "urban driving" assessed by NASA Task Load Index [144]

Experienced Operator	Conventional HMI	Proposed HMI
Nr. 1	30 %	39 %
Nr. 2	59 %	53 %
Nr. 3	37 %	41 %
Nr. 4	50 %	36 %
Total Average	**44 $\pm$ 13 %**	**42 $\pm$ 7 %**

4.4.3 Subjective Impression of the Test Persons

To measure the subjective impressions of the test persons with regard to improvements in precision, they were asked whether they felt that, through the use of the mixed reality HMI their ability to precisely control the remote car increased. The test persons' responses are illustrated in Figure 4.24.

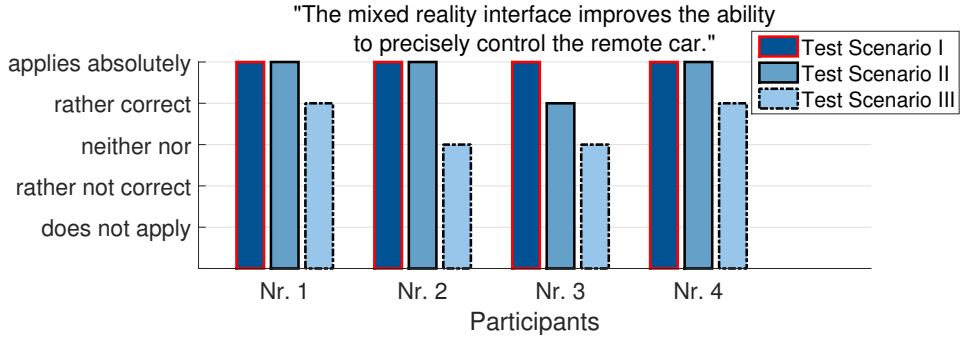

Figure 4.24 : Impressions of the test persons about "improving of precision"

As can be seen, in the first two test driving scenarios, namely "precise control" and "backing into a parking space", the test persons absolutely believed that using the mixed reality HMI improved their ability to precisely control the remote car. The main reason of this subjective result is that, using the mixed reality HMI the test persons could better perceive the distance of the remote vehicle to the obstacles located in the environment than when using the conventional HMI. Hence, they could perform their driving tasks with higher levels of trust.
These results show less improvement in the impressions of the test persons about the improvement of precision within the "urban driving" scenario. This is a result of the fact that, in this test scenario the test persons were confronted with proportionally fewer challenges regarding the precise control of the car when compared to two first test scenarios. Hence, an improvement in precision as a result of using the mixed reality HMI could not be obviously perceived.
Although the main intention of the developed HMI concept is the improvement of telepresence and task performance, its usage may affect safety while teleoperated driving. Hence, the test persons were asked about their "impression of safety" while engaged in teleoperated driving using the developed HMI concept. Figure 4.25 illustrates the answers of the test persons to the question of whether using the mixed reality HMI improved their safety while teleoperated driving.
As can be seen, particularly in the first two scenarios, the test persons believed that using the mixed reality HMI improved their safety while driving. This can be interpreted as representing a direct relationship between providing missing information concerning vehicle control and an improved feeling of safety.

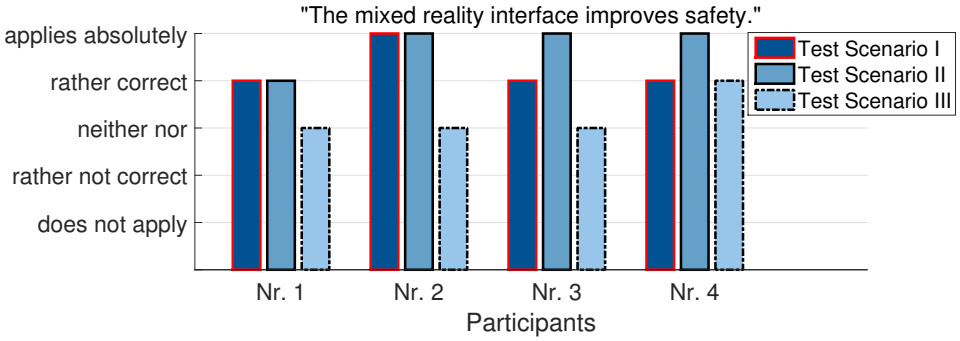

Figure 4.25 : Impressions of the test persons about "improving of safety"

As the next important subjective parameter, the test persons were asked whether using the mixed reality HMI improved their situation awareness. The responses of the test persons to this question are illustrated in Figure 4.26. As can be seen, the average answer given to the above question was positive.

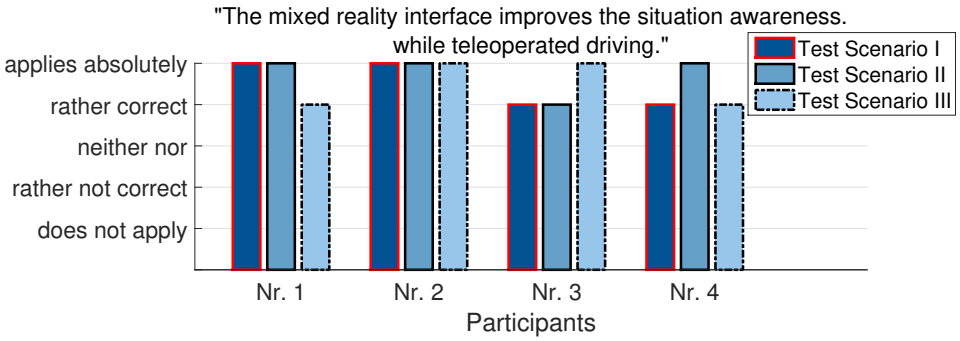

Figure 4.26 : Impressions of the test persons about "improving of situation awareness"

To measure the impression of the test persons concerning the improvement of telepresence, they were asked whether using the mixed reality HMI felt more realistic for them than using the conventional HMI. Their answers to this question are illustrated in Figure 4.27.

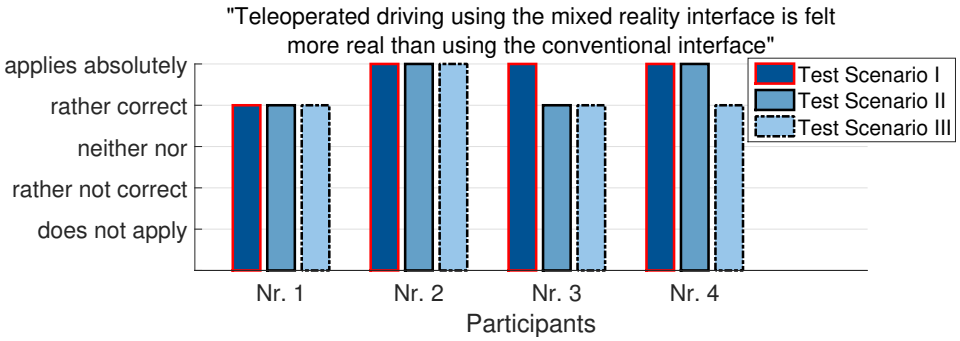

Figure 4.27 : Impressions of the test persons about "increasing the sense of reality"

As can be seen, the test persons on average believed that teleoperated driving felt a little more realistic when using the mixed reality HMI as opposed to the conventional HMI.

4.5 Conclusion and Discussion

The novel mixed reality HMI concept discussed in this chapter is intended to improve telepresence and task performance while a user is engaged in teleoperated driving. The variety

of objective and subjective parameters gained from the different test scenarios indicate that the desired goals are fully achieved.
The mixed reality HMI improves situation awareness and consequently the telepresence of the human operator. This is achieved through his decoupling from the real environment and the visualization of the missing information about the vehicle's surroundings. This enhancing of telepresence leads to improvement of the performance of the human operator when precisely controlling the remote car.
Besides the above-mentioned advantages of using this novel HMI, it also reduces the size and cost of building an operator's workstation for teleoperated driving. Through the ability provided by this HMI, some of the required information regarding the vehicle's surroundings can be replaced by means of virtuality. This enables a significant reduction of the communication load required for teleoperated driving.
The proposed HMI concept is applicable to both the control concepts of teleoperated driving, which have been introduced in Chapter 2.3.2. Although, in this work the proposed HMI is investigated in combination with the "direct control" concept, a similar application in combination with the "shared control" concept is conceivable.
To further improve task performance and telepresence while using this concept, the exact position of the steering wheel as well as the pedals of the operator's workstation could be added to the mixed reality environment. Two possibilities developed for this purpose are illustrated in Figure 4.28. As can be seen, this additional information could be visualized by means of virtuality or reality.

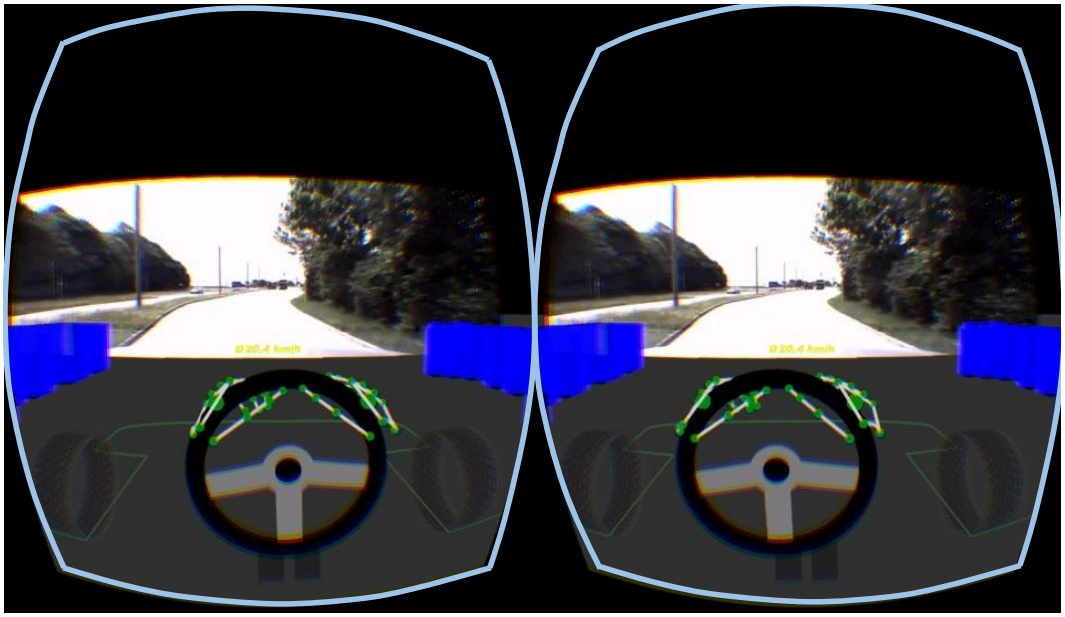

(a)

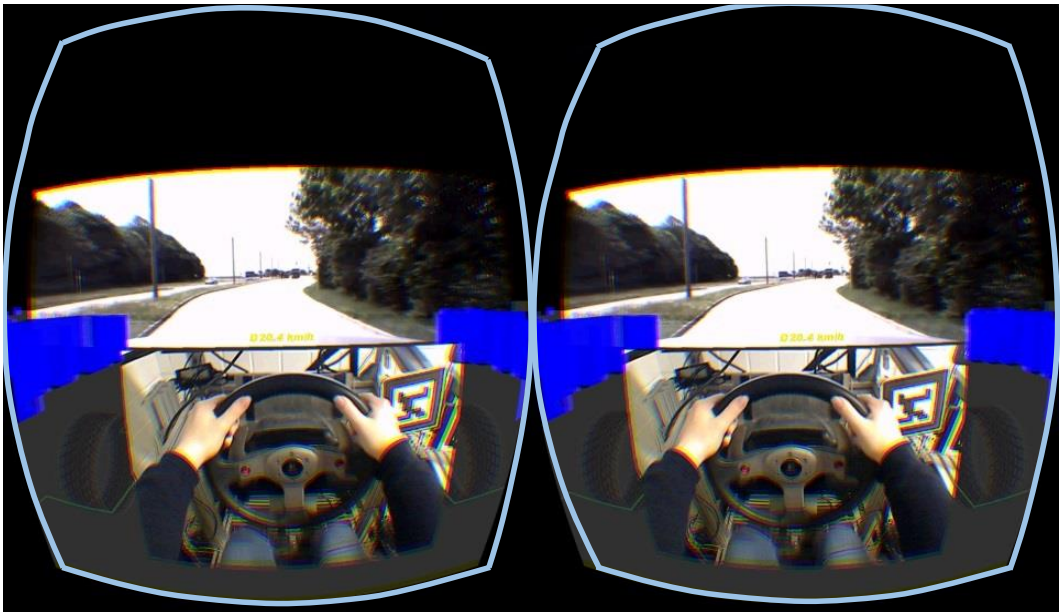

(b)

Figure 4.28 : Two possibilities to illustrate the operator's hands as weel as the actuators of the operator's workstation within the mixed reality environment: (a) as virtuality and (b) as reality

5 Predictive Brake Assistance for Enhancing Frontal Safety

The main content of the concept introduced in this chapter was previously presented in [146] and [145]. This chapter provides a description of this concept.

5.1 Problem Description

Interaction with other traffic participants despite communication time delay presents a considerable challenge. This challenge becomes more obvious when several dynamic obstacles exist in a driving scenario and the human operator perceives their movements with a delay.
As described in [5], a possible solution to this challenge would be using predictive display to represent the current positions of other traffic participants. However, as indicated in Chapter 3.1.2, simultaneous visualization of the predictive display for all of the dynamic objects in a driving scenario could result in ergonomic inconvenience for the human operator.
In addition, to visualize the predictive display of a dynamic obstacle, its current position is calculated based on the sensor data received at the operator's workstation. Since the sensor data received at the operator's workstation is delayed, this concept cannot immediately visualize the position of an obstacle that has newly entered into the scene.
This weakness of the predictive display concept poses a safety challenge in those scenarios in which a new dynamic obstacle enters suddenly the scene. Figure 5.1 illustrates this problem in an example scenario of teleoperated driving in an urban environment.
As can be seen, the human operator perceives the environment from the delayed position of the teleoperator, which is illustrated as shadowed behind its current position.

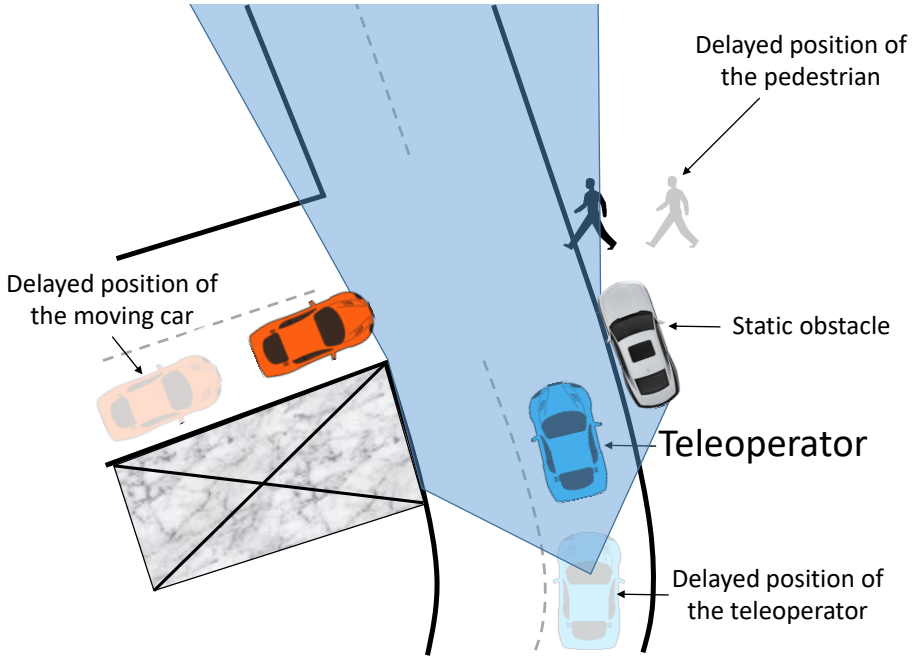

Figure 5.1 : Delayed Perception of the environment by the human operator

In this scenario, the current position of the teleoperator can be illustrated using a predictive display on the operator's interface. From the delayed point of view of the teleoperator, two of the dynamic obstacles in the scene (the pedestrian and the red car) are covered by a static obstacle or infrastructure. Hence, the operator cannot be aware of their existence in the scene.

Such a lack of knowledge about the dynamic environment while a human operator engages in teleoperated driving leads to a delayed reaction on his part to hazards. This illustrates the need for a specific active safety system for teleoperated vehicles, which is proposed in this chapter.

5.2 State of the Art: Frontal Collision Avoidance Systems

Research on frontal collision avoidance systems has a long history. As an example, a 1950s prototype by General Motors can be mentioned. This prototype measured the relative velocity of and the distance to the vehicle ahead using a radar sensor and displayed this information on the car's instrument cluster [77].
It took approximately four decades to mass produce the radar sensor for automotive applications. With the mass production of this sensor, as well as the development of an electronic stability program (ESP) in 1990s, the main elements required for environment perception and controlling of a car's actuators were provided.
The development of these technological innovations enabled the mass production of adaptive cruise control (ACC) in 1990s as an advanced driver assistance system that is intended to improve driving comfort. Based on this technology, the first generation of forward collision protection systems were later introduced to the market.
Generally, the forward collision protection systems of a car include the systems that warn of a frontal collision, mitigate or avoid it. One of the main criteria when choosing between the collision mitigation and avoidance system modes is the CU criterion (CU: collision unavoidable), which represents a situation in which a collision cannot be avoided, even by the best drivers imaginable [77].
Based on this criterion, emergency braking with the maximum possible deceleration becomes necessary only after collision avoidance is no longer possible through steering. This decision depends on the relative speed of the car compared to that of the vehicle ahead as well as the required lateral shift for evasive steering.
Figure 5.2 illustrates the distance required to avoid a collision with a stationary obstacle through braking or steering, under the assumption that both vehicles are undergoing the same longitudinal and lateral deceleration of $D = 8\ \frac{m}{s^2}$. As can be seen, with an increase in the lateral shift required to evade the obstacle, w, the required longitudinal distance to the obstacle, increases.

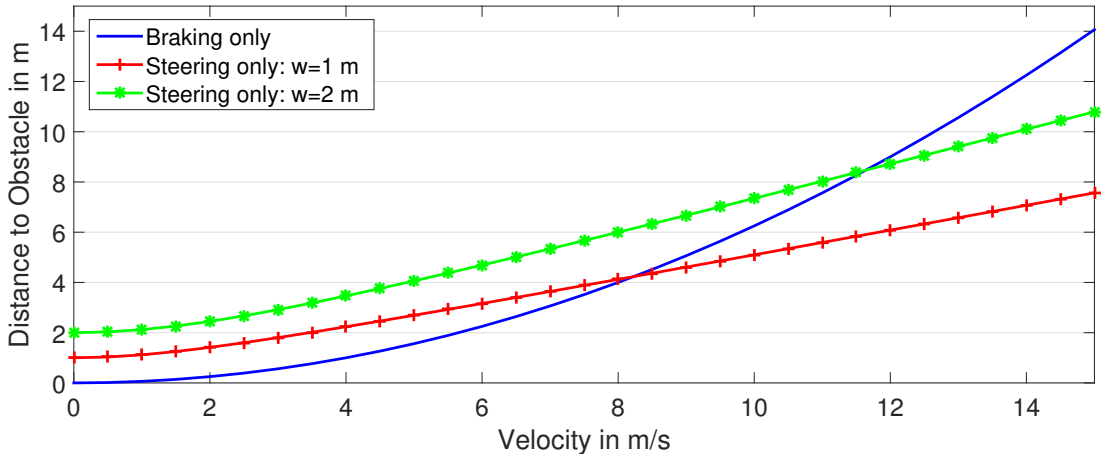

Figure 5.2 : The required distance to avoid a collision through braking or steering. w represents the required lateral shift to evade the obstacle through steering [78].

Based on this diagram, at velocities lower than the corresponding velocity of the collision point of the braking and steering curves, braking is safer than steering when attempting to avoid

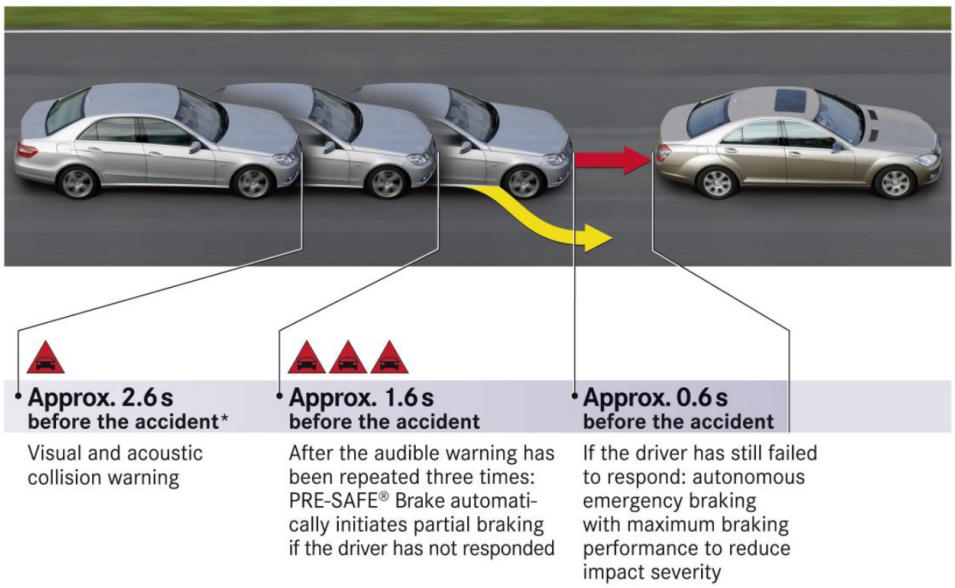

Figure 5.3 : Different intervention steps of an example autonomous emergency braking (AEB) [79]

a collision. For example, in the case of $w = 2\ m$, with a relative velocity of less than 11.5 $\frac{\text{m}}{\text{s}}$ (equivalent to 41.4 $\frac{\text{km}}{\text{h}}$) braking can avoid a collision over a shorter distance than steering. This illustrates the importance of braking assistance system when avoiding collision.
Different types of collision avoidance systems are available on the market. The current systems perceive the environment using a variety of different sensors, such as radar, LiDAR and/or cameras. In order to reduce the number of possible false interventions, these systems exclusively take into account the obstacles that exist on the car's driving path.
To assist the driver when attempting to avoid a forward collision, these systems generally employ several steps. An example is illustrated in Figure 5.3, which shows that, after collision with a hazard is predicted, the driver is informed by means of acoustic or optical feedback. Thereafter, partial braking is triggered. As the final step full braking is triggered, which is aimed at avoiding the forward collision.
Each of these steps is normally triggered at a certain time-to-collision (TTC). Figure 5.4 illustrates the intervention strategy of a two-stage braking system, the first step of which is partially braking with a deceleration of $D = 4\ \frac{m}{s^2}$, which is triggered at $t_{TC,1} = 1.6\ s$. At the second step, full braking, with a deceleration of $D = 10\ \frac{m}{s^2}$, is triggered at $t_{TC,2} = 0.6\ s$. The collision warning is given before $t_{TC,1} = 1.6\ s$.

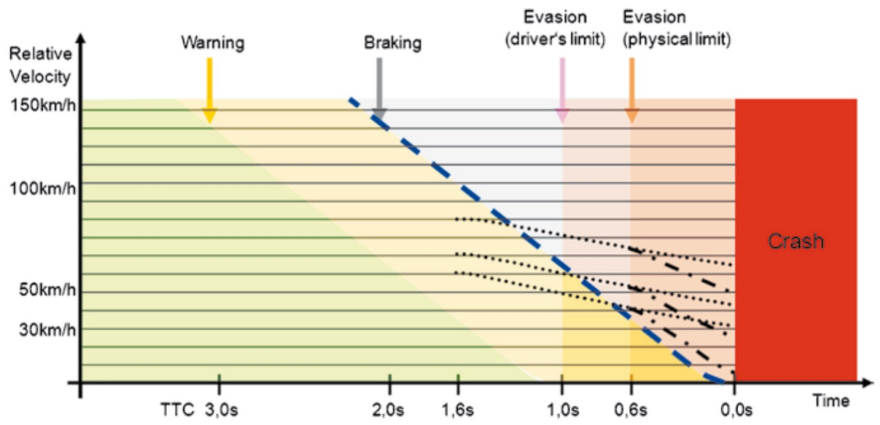

Figure 5.4 : The intervention strategy of a two-stage braking system for three different realtive velocities $v = 60, 70, 90\ \frac{km}{h}$ [77]

5.3 Approach

To ensure the safety of a remote car during teleoperated driving, a predictive brake assistance system is required. This assistance system must compensate for the delayed perception of the environment by the human operator using a local intelligence in the remote car. In addition, it should offer the possibility of appropriate collaboration between the human operator and the remote car. The components of this driver assistance system are described below.

5.3.1 Autonomous Intervention

The total reaction and stopping distances while teleoperated driving are longer than the corresponding distances while driving a manned car. As shown in Figure 5.5, this is a result of the time delays involved in transmitting the video images from the teleoperator to the operator's workstation and in transmitting the control signals in the opposite direction.

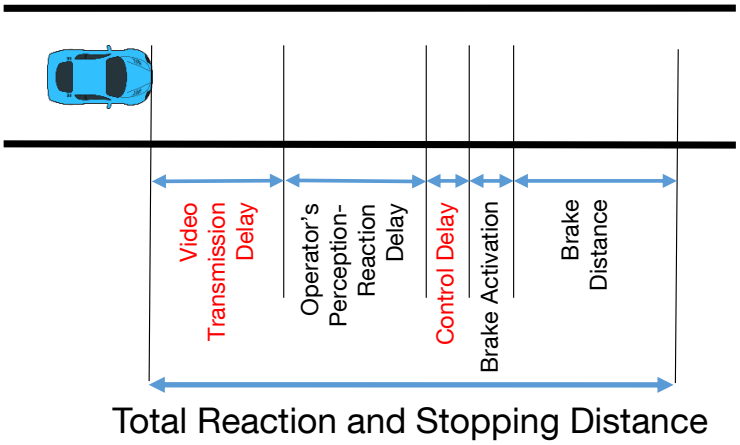

Figure 5.5 : Total reaction and stopping distance while teleoperated driving [146]

The total reaction time during teleoperated driving can be formulated as follows:

$$t_{Total} = t_{Video} + t_{P-R} + t_{Control} + t_{BrakeActivation}, \tag{5.1}$$

where t_{Video} is the transmission time of the video images from the teleoperator to the operator's workstation, and $t_{Control}$ is the transmission time of the control signals in the opposite direction. t_{P-R} stands for the perception-reaction time of the human operator and $t_{BrakeActivation}$ represents the activation time of the brake actuator.
When using a commercial LTE network, these measurements show a maximum ping time of 70 ms and an average time of 47 ms [141]. In order to address the possible communication issues, a constant time delay of 100 ms can be assumed as representing the transmission time of the control signals from the operator's workstation to the teleoperator, including the steering angle and the states of the brake and gas pedals.
As described in Chapter 1.3, the communication time delay is not constant and sometimes a jitter greater than 400 ms can postpone the delivery of camera images. Hence, the camera images received at the operator's workstation are buffered by 500 ms in order to provide fluid video streaming to the human operator.
To have realistic values for the perception-reaction time of the human operator and the activation time of the brake actuator, the following time values can be assumed: $t_{BrakeActivation} = 150\ ms$, $t_{P-R} = 1\ s$ [80]. With the assumed $t_{Video} = 500\ ms$ and $t_{Control} = 100\ ms$, a total reaction time of $t_{Total} = 1.75\ s$ results.
To increase the safety of the vehicle, these reaction and stopping times need to be reduced. This can be achieved through the use of predictive braking in hazardous scenarios. The core idea behind predictive safety while operating a teleoperated vehicle relies on scene prediction

and autonomous intervention in the braking system of the remote car. By predicting the motion trajectories of dynamic obstacles and the remote car, a collision can be predicted and consequently the speed of the remote vehicle can be adjusted.
Figure 5.6 illustrates collision prediction in an example driving scenario, which was previously depicted in Figure 5.1. As soon as an overlap between the predicted motion trajectory of the remote car and the predicted motion trajectory of at least one dynamic obstacles is determined, the autonomous braking system intervenes. Depending on the situation, this autonomous intervention can take the form of either partial or full braking.

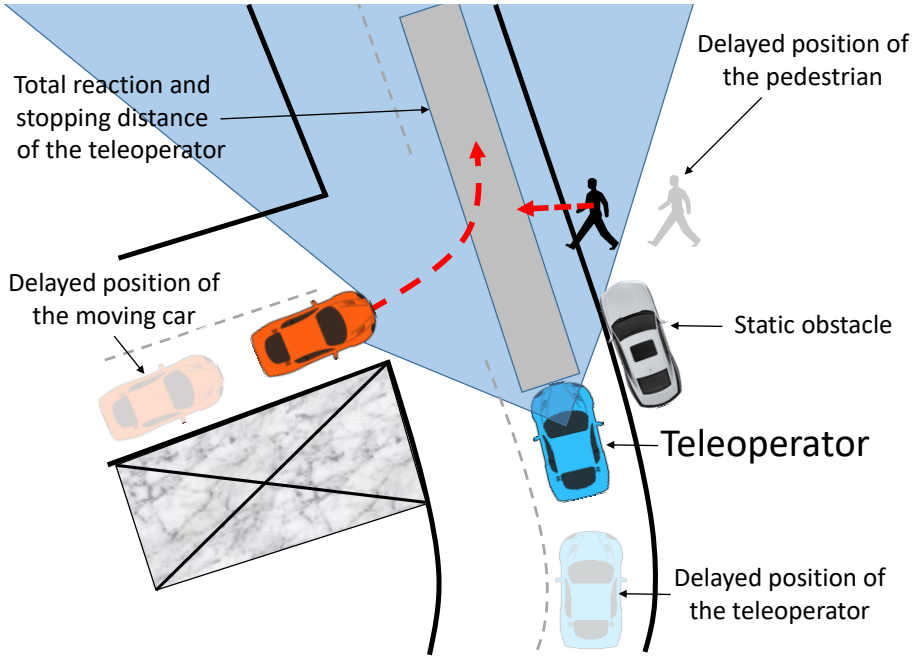

Figure 5.6 : Collision prediction by overlapping of the predicted trajectories of moving obstacles with the total braking distance of teleoperator. The delayed positions of the teleoperator as well as other dynamic objects are illustrated shadowed [146].

After an obstacle entered into the total reaction and stopping distance of the remote car, a human operator will not be able to avoid the collision by braking. Hence, this distance must be observed by the vehicle's sensors.
The total reaction and stopping distance, $d_{Reaction-Stopping}$, can be approximated as follows:

$$d_{Reaction-Stopping} = v_{diff} t_{Total} + \frac{v_{diff}^2}{2D}, \tag{5.2}$$

in which v_{diff} stands for the relative speed of the teleoperator to the obstacle and D represents the vehicle's deceleration [77]. Through insertion of the calculated total reaction time during teleoperated driving by means of the equation 5.1 as well as the maximum relative speed of $v_{diff} = 50\ \frac{km}{h}$ as an example of the desired speed limit for teleoperated driving in urban environments and the longitudinal deceleration of $D = 8\ \frac{m}{s^2}$ in equation (5.2) a total braking distance of $d_{Reaction-Stopping} = 36.36\ m$ is resulted.
To avoid an unnecessary intervention by the braking system, the prediction horizon of the dynamic environment should not be longer than the sum of the reaction time of the human operator and the communication time delay. Otherwise, the braking system will intervene in situations that have already been perceived by the operator. Such interventions may result in frustration of the operator, as the intended main decision-maker in the control loop.
As indicated in Chapter 1.4, the proposed ADAS package in this work intends to raise the limits on teleoperated driving to such a level that they are equivalent to those encountered while driving a manned vehicle. Hence, the prediction horizon of the dynamic environment is set as equal to the constant communication time delay. Adding the driver's reaction time

to this prediction horizon may increase the number of unnecessary interventions parallel to increasing the level of safety. Hence, this option is omitted.
Because of the delayed interaction between the teleoperator and the human operator, direct control of the remote car should be managed using cruise control. For this purpose, the operator should set the driving speed using the gas and brake pedals of the operator's workstation, and the remote vehicle should match its speed to the desired speed using its cruise control system.
After prediction of a collision within the indicated prediction horizon, the braking system gets activated. The type of braking intervention applied depends on the distance of the predicted collision point to the remote vehicle. If this distance is equal to or shorter than the braking distance of the car with its highest possible deceleration, D_{max}, full braking is unavoidable. This distance $d_{FullBraking}$ can be formulated as follows:

$$d_{FullBraking} = v_{diff} t_{BrakeActivation} + \frac{v_{diff}^2}{2D_{max}}. \tag{5.3}$$

If the distance of the remote vehicle to the predicted collision point, $d_{PredictedDistance}$, is greater than $d_{FullBraking}$, partial braking is triggered. The required deceleration for such a partial braking, $D_{PartialBraking}$, for a dynamic obstacle with a constant speed can be calculated as follows:

$$D_{PartialBraking} = \frac{v_{diff}^2}{2d_{PredictedDistance}}. \tag{5.4}$$

Using this partial braking, even without the intervention of the human operator, the predicted collision can be avoided and the safety of the vehicle is guaranteed. In addition, through avoiding full braking a smooth braking behavior is ensured.

5.3.2 Motion Prediction using a Stereo Vision System

Generally, there are two main approaches to predicting the motion trajectories of dynamic objects. The recognition category includes approaches that recognize objects using *pattern recognition* techniques during a first step and track them in a following step.
The category *track-before-detect* includes approaches that track dynamic objects without using pattern recognition techniques. These approaches rely on motion estimation through comparing a series of measurements.
Although there has been considerable progress in the field of pattern recognition, its current state is still not comparable to the human ability to recognize patterns. Hence, the above-mentioned approaches do not demonstrate robust performance in all complex urban environments.
The track-before-detect approaches are generally faster and more accurate than recognition approaches when it comes to motion estimation [81]. However, these approaches cannot distinguish between hazardous and nonhazardous dynamic objects.
To benefit from the advantages of both of these approaches, detected dynamic objects using a track-before-detect approach can be examined by means of a recognition approach. However, this combination decreases the speed of motion estimation. An example in [81] shows that the fusion of a track-before-detect system and a recognition-based approach requires more than 15 image frames in order to correctly estimate the speed of a pedestrian, while the track-before-detect system can estimate this speed using only three image frames.
Since, for the autonomous intervention system described in section 5.3.1, potential hazards need to be detected as rapidly as possible, motion estimation through the track-before-detect approach is more suitable than the other possibilities discussed.

5.3.2.1 **Fusion of Stereo Vision and Optical Flow**

The track-before-detect approaches for motion estimation can be realized using different sensors, such as radar, LiDAR or camera sensors. In [82], this technique is realized using airborne radars. The main advantage of using vision systems to realize this technique is that

vision sensors deliver features from the environment, which can be used to estimate the motion of various kinds of dynamic obstacles.
A motion in a series of images can be estimated using optical flow approaches. These approaches are mainly based on the "constant brightness assumption" [83], which states that the intensity of a projected point from the world's coordinates onto an image, $I(x, y, t)$, does not change within short periods of time:

$$\frac{d}{dt} I\left(x\left(t\right), y\left(t\right), t\right) = 0. \tag{5.5}$$

Derivation and expansion of this equation using Taylor series results in the "optical flow constraint equation" [84]:

$$\nabla I \cdot \mathbf{u} + \frac{\partial}{\partial t} I = 0, \tag{5.6}$$

in which $\mathbf{u}$ is defined as $u(x, y) = (u_1(x, y), u_2(x, y))$ and represents the two-dimensional displacement field of each image point. This equation is the basis for estimating the two-dimensional motion vector of each image point in a series of successively captured images.
Using a stereo vision system, the depth information of a scene can be extracted. This information can enhance the estimated motion of image point by optical flow. For this purpose, a stereo vision system is developed. The mounting position of this stereo vision system in the teleoperator and its coordinate system are illustrated in Figure 5.7.

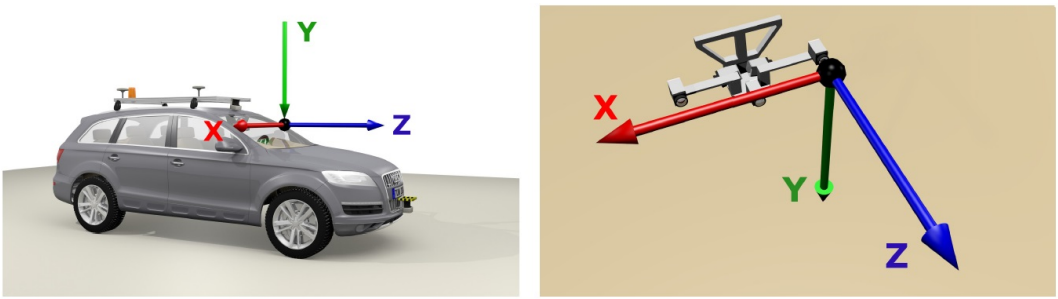

Figure 5.7 : (a) The developed stereo vision system with the baseline of 50 cm in the experimental vehicle; (b) The camera platform and the defined Cartesian coordinates of the stereo vision system

Using depth information, the optical flow approach makes it possible to estimate the three-dimensional motion vector of each image point. This technique, referred to as 6D vision [85], is not restricted to particular algorithms when calculating depth and optical flow information.
An approach for achieving high performance in motion estimation would be using dense approaches to calculate both stereo map and optical flow. Although this approach, referred to as Dense6D, demonstrates a reasonable performance in terms of estimation, the calculation time it requires makes it inappropriate for real-time applications [86].
Rabe [85] proposed the fusion of the Kanade-Lucas-Tomasi tracker (KLT) with the semi-global stereo matching approach, which shows high performance in motion estimation. However, the approach applied to estimate optical flow in this fusion selects features only in those specific regions of an image that have rich textures. This region-based preselection of features may result in the loss of some critical image information.
To avoid the preselection of features in the images the TV-L1 algorithm can be used, which calculates optical flow through minimizing the following cost function:

$$E\left(\mathbf{u}\right) = \int_{\Omega} \underbrace{\left|\nabla u_1\right| + \left|\nabla u_2\right|}_{\mathrm{TV}} + \underbrace{\lambda \left|\rho\left(\mathbf{u}\right)\right|}_{\mathrm{L}^1} \, \mathrm{d}\Omega. \tag{5.7}$$

This cost function consists of a regularization term using the total variation (TV) of the flow and a data term using the L^1 norm [87] [84].
To calculate the stereo disparity map, the semi-global matching algorithm can be used, which

is known to represent a tradeoff between run-time and accuracy [88]. This approach minimizes the following cost function in order to determine stereo disparity:

$$E(D) = \sum_{\boldsymbol{p}} \left[C\left(\boldsymbol{p}, D_{\boldsymbol{p}}\right) + \sum_{\boldsymbol{q} \in N_{\boldsymbol{p}}} P_1 \cdot T\left[\left|D_{\boldsymbol{p}} - D_{\boldsymbol{q}}\right| = 1\right] + \sum_{\boldsymbol{q} \in N_{\boldsymbol{p}}} P_2 \cdot T\left[\left|D_{\boldsymbol{p}} - D_{\boldsymbol{q}}\right| > 1\right] \right]. \tag{5.8}$$

In this cost function, the first term represents the stereo matching costs, the second term represents a penalty for all pixels q in the neighborhood N_p of p for which the disparity changes one pixel, and the third term represents a larger penalty for all larger disparity changes [88].
To calculate the ego-motion of the teleoperator, the algorithm of Geiger *et al.* [89] can be used, as it demonstrates robust performance in real-time calculation. With the fusion of data using an extended Kalman filter (EKF), the three-dimensional position of the moving object as well as its three-dimensional motion vector can be calculated. The structure of this fusion is illustrated in Figure 5.8. The extended Kalman filter applied in this architecture has the following state vector:

$$\boldsymbol{X}_k = (x, y, z, \dot{x}, \dot{y}, \dot{z})^T, \tag{5.9}$$

in which x, y and z stand for the position in the Cartesian coordinate system.

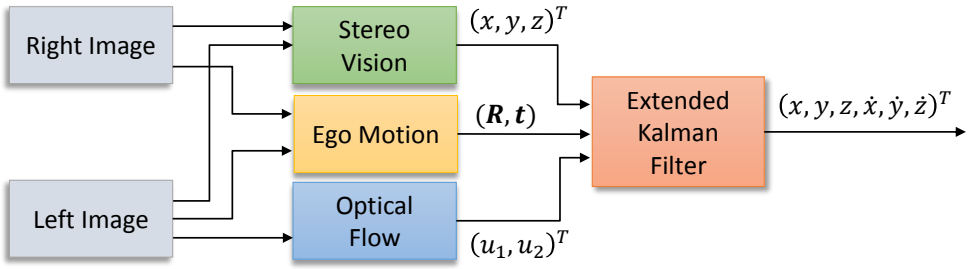

Figure 5.8 : Fusion of the stereo disparity and optical flow maps using an extended Kalman filter [146]

Devoting a tracker to each pixel in order to fuse the stereo and flow data leads to a high computing cost. To avoid this problem, the image can be divided into a grid of cells of the same size. Using this approach one tracker can be employed to track the motion in each cell, which leads to acceleration of the fusion step. A schematic illustration of this approach is shown in Figure 5.9(a), in which each cell has a size of 25x25 pixels.
The starting value of each Kalman filter is the central pixel of each cell. These positions are marked green in Figure 5.9(a). The position states of the state vector of the extended Kalman filter, $\boldsymbol{X}_k$, are initialized based on the three-dimensional coordinates of the corresponding pixel. The speed states of this state vector are set to zero in the initial step.
In the following time steps, the state vector is updated using the data provided by stereo disparity and optical flow. The updated positions of the trackers are marked red in Figure 5.9(b). If there is no valid stereo value on the position newly determined by the optical flow of the image point, this tracker is deleted. These trackers are marked yellow in Figure 5.9(b). After a tracker is deleted, its cell receives a new initialized tracker.
With filtering and clustering of the resulted motion vectors, the motion vectors of dynamic objects are estimated.

5.3.2.2 **Parallel processing using a graphics processing unit (GPU)**

For the real-time computation of the proposed approach to motion prediction, a specific hardware with parallel-processing ability is required.
This can be realized using a graphics processing unit (GPU). Using the compute unified

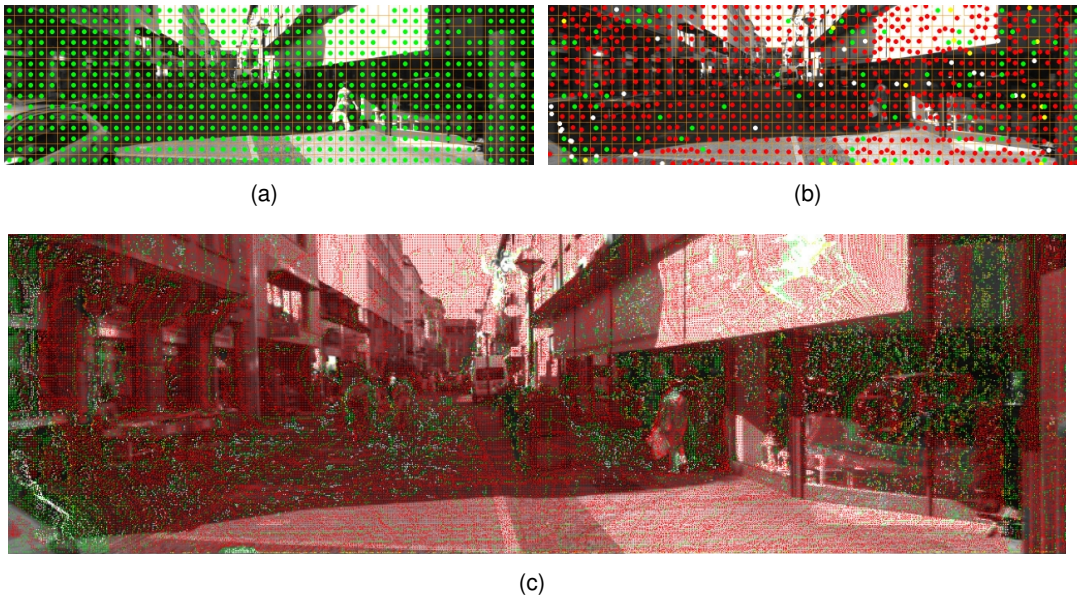

Figure 5.9 : Grid-based distribution of an image to accelerate the fusion step: (a) schematic visualization of the initializing step of the Kalman filter in each cell, (b) schematic visualization of the update step of the Kalman filter in each cell, (c) update step of the Kalman filter, with a cell size of 3x3 pixels. The raw image is from the KITTI Dataset [146].

device architecture (CUDA) of a GPU, it is possible to define several parallel streams for the synchronizing and parallel performance of the computing tasks.
Figure 5.10 illustrates the sequence diagram of the entire computing process. As can be seen, the computing process of the GPU is divided into four streams. The first stream (marked in orange) is dedicated to synchronizing the tasks. The other streams (1, 2 and 3) are responsible for parallel computing.
Among the three streams dedicated to parallel computing, the first GPU stream computes the stereo disparity map, while the second stream calculates the optical flow. Parallel to these

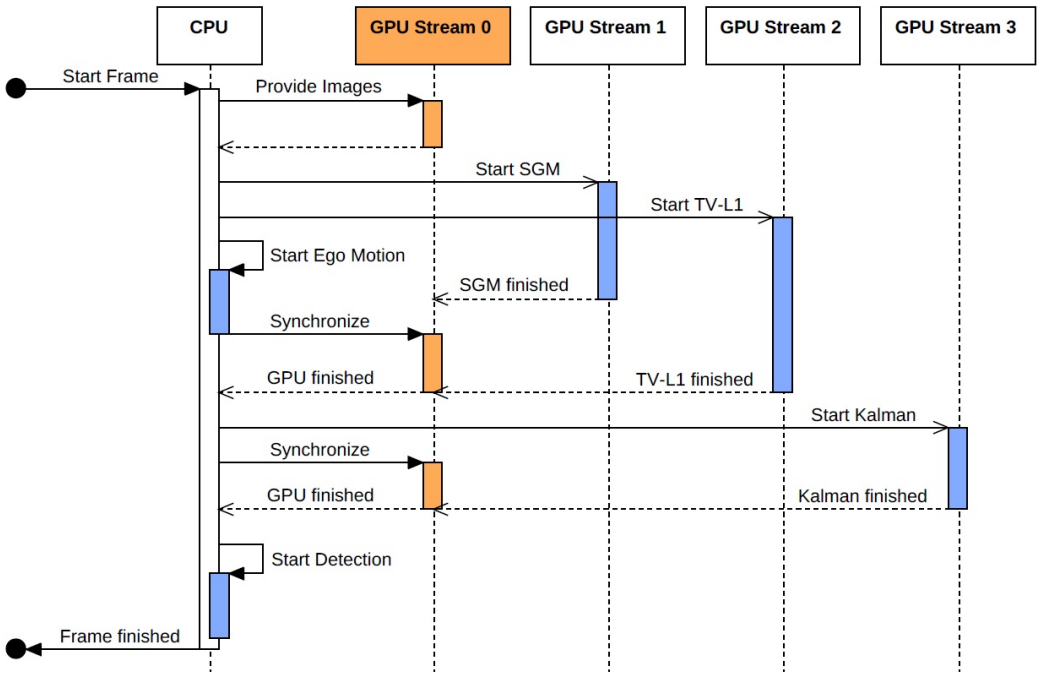

Figure 5.10 : Parallel computing process to predict the motion using the graphics processing unit

two GPU streams, ego motion is calculated by the CPU. After completing all of these steps on the GPU and CPU, data fusion using the extended Kalman filter is performed on the third GPU stream. After this step is completed, the results are sent to the CPU and the processing of the next image starts.

5.3.3 Interaction with the Human Operator and Overrideability

After an autonomous intervention occurs in the braking system, the human operator should be informed of it. This can be realized by means of giving acoustic, visual or haptic feedback to him or her at the operator's workstation.
For visual feedback, transparent augmented reality can be used. However, since the "direct control" concept is mostly based on augmented reality, adding new visual information may lead to the human operator becoming overburdened.
An appropriate solution for informing the human operator of an autonomous intervention in the braking system would be blinking and the changing of the color of the predictive display to red. An example of this kind of warning is illustrated in Figure 5.11, in which the human operator is made aware of an autonomous partial braking at an intersection.

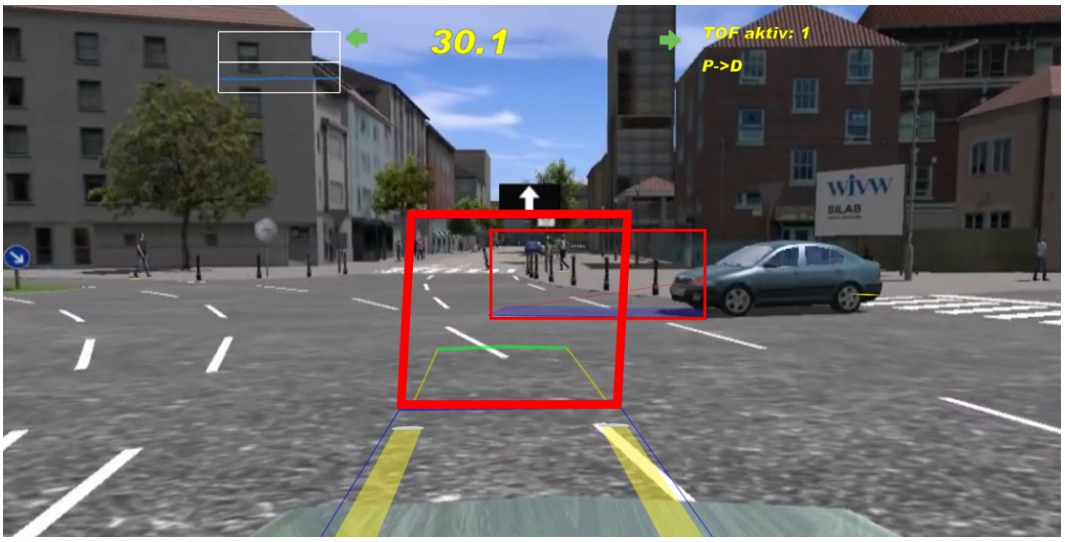

Figure 5.11 : Informing the human operator about an autonomous intervention by means of see-through augmented reality [146]

One of the most important topics in the development of driver assistance systems is their overrideability. The Vienna Convention on Road Traffic, agreed to at the United Nations Economic and Social Council conference on the 8th of November 1968, states that "every driver shall at all times be able to control his vehicle or to guide his animals" [90].
The March 2014 update of this convention includes a justification provided by the governments of Austria, Belgium, France, Germany and Italy, which states that "keeping the driver in a superior role is a guiding principle of road traffic regulations. Therefore, overrideability as well as the possibility for the driver to switch systems off ensure that the driver's will is put forth" [91].
To satisfy this requirement in the developed brake assistance system, overrideability is provided through the possibility of pressing a specific button on the steering wheel of the operator's workstation or by depressing the brake pedal. Thereby, the human operator sends a message to the teleoperator that he has the situation under control and does not require further autonomous intervention in this specific situation.
This option would be particularly helpful when the human operator identifies a false positive detection by the system or when he prefers to perform an evasive maneuver in a hazardous scenario instead of letting the machine brake autonomously.

5.4 Evaluation and Results

5.4.1 Evaluation of the Trajectory Prediction System

The proposed system for motion prediction is evaluated in different scenarios. Figure 5.12 illustrates the results of different applied computing steps for an example scene captured by the stereo vision system of the experimental Audi Q7 vehicle. The specifications of the camera sensors used are described in Chapter 2.3.

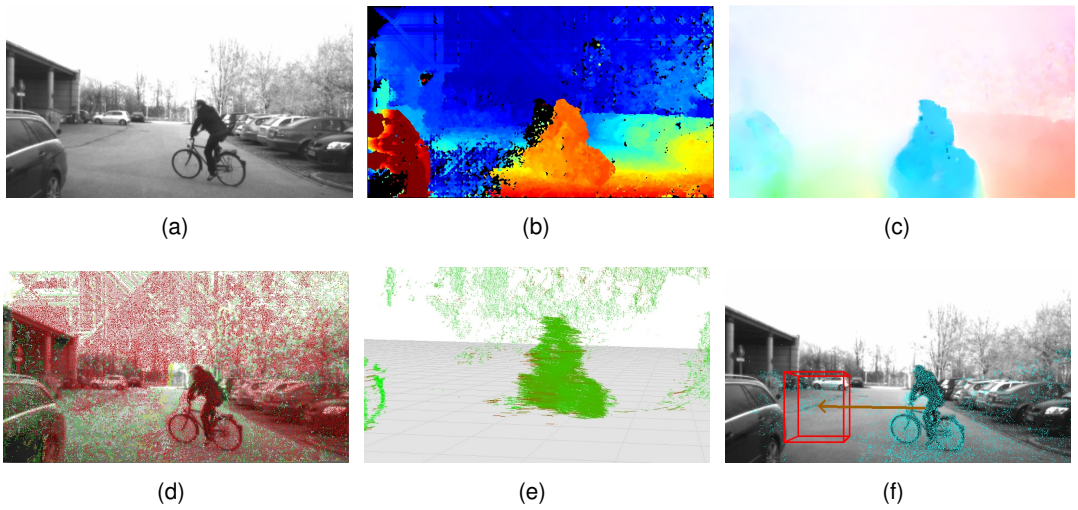

Figure 5.12 : (a) Raw left image, (b) stereo disparity map by semi-global-matching (SGM) (c) optical flow by TV-L1 algorithm, (d) grid-based fusion by EKF, (e) 3D-visualization of the predicted motion and (f) trajectory prediction and visualization over 1 s [146]

As can be seen in Figure 5.12(d), the stereo disparity map is noisy. This lies on the intense background noise of raw images which may cause initialization of new Kalman filters on some static objects.
As illustrated in Figure 5.12(f), the estimated motion of the cut-in obstacle is used to predict its motion trajectory. This trajectory can be used to predict colliding of the teleoperator with an obstacle.
For the parallel processing of the algorithms developed for motion estimation, a GPU of the NVIDIA GeForce GTX 780 Ti [92] type is employed. The architecture of the implementation corresponds with the the process illustrated in Figure 5.10. The entire time required to process an image with a resolution of 640x355 pixels by this GPU is about 36.4 ms. The required time for each calculation step is ilustrated in Table 14. The overall time enables a processing speed of 25 image frames per second.

Table 14 Required runtime for parallel processing of stereo images with the resolution of 640x355 using a GPU of the NVIDIA GeForce GTX 780 Ti

Calculation Step	Required Time
Stereo Disparity, Optical Flow and Ego Motion	26.5 ms
Kalman Filter	5.6 ms
Object Detection	4.3 ms
Total	36.4 ms

To compare the performance of the developed algorithms with a ground truth, the KITTI vision benchmark [93] as well as synthetic images are used. The gained results are briefly described

below.

5.4.1.1 **Evaluation Using the KITTI Vision Benchmark**

The KITTI vision benchmark [93] includes captured measurement data by two high-resolution color and grayscale video cameras with a low background noise. Accurate ground truth is provided by a Velodyne LiDAR sensor and a GPS localization system. The captured measurement data are open-access and can be used by developers to compare the perfromance of algorithms for environment perception on a common basis.
Table 15 provides a brief description of the test sequences of the "City" category of the KITTI benchmark, which have been used in this work. As can be seen, the most used test sequences include several crossing pedestrians, cyclists and cars with different motion velocities.

Table 15 Description of the used test sequences of the KITTI vision benchmark

Sequence	**Ego Velocity**	**Description and Duration**
2011_09_26_drive_0113	$8 - 12\frac{\text{km}}{\text{h}}$	Cyclist on collision course (00:08min)
2011_09_28_drive_0016	0	Crossing pedestrian (00:18min)
2011_09_28_drive_0034	$0 - 1.4\frac{\text{km}}{\text{h}}$	Cut-in cyclist (00:04min)
2011_09_28_drive_0037	$0 - 16\frac{\text{km}}{\text{h}}$	Turning scenario with pedestrians (00:08min)
2011_09_28_drive_0038	$4.5 - 16\frac{\text{km}}{\text{h}}$	Passage with pedestrians (00:11min)
2011_09_28_drive_0066	0	Pedestrian runs in front of the vehicle (00:02min)
2011_09_29_drive_0071	$0 - 13\frac{\text{km}}{\text{h}}$	Pedestrians with changing brightness (01:45min)

Table 16 illustrates the detection rate of the developed approach when applied to the above mentioned test sequences. To have a realistic evaluation, only the dynamic objects are considered, which intervene in the traffic.

Table 16 Evaluation of the developed track-before-detect approach using raw data from KITTI vision benchmark [146]

Raw Data	**Detection rate of moving objects**			**False**
	Pedestrian	Bicyclist	Car	**Postive**
2011_09_26_drive_0113	0 / 0	1 / 1	0 / 0	1
2011_09_28_drive_0016	3 / 3	2 / 2	2 / 2	0
2011_09_28_drive_0034	0 / 0	1 / 1	0 / 0	0
2011_09_28_drive_0037	2 / 3	3 / 5	0 / 0	0
2011_09_28_drive_0038	5 / 6	2 / 2	1 / 1	0
2011_09_28_drive_0066	1 / 1	0 / 0	0 / 0	0
2011_09_29_drive_0071	47 / 50	7 / 7	3 / 4	6

Among these scenarios, the greatest number of false positive detections was found for the KITTI test sequence 2011_09_29_drive_0071, as a result of its high complexity and longer

duration. Figure 5.13 illustrates the prediction results in two example scenes from this test sequence.

(a)

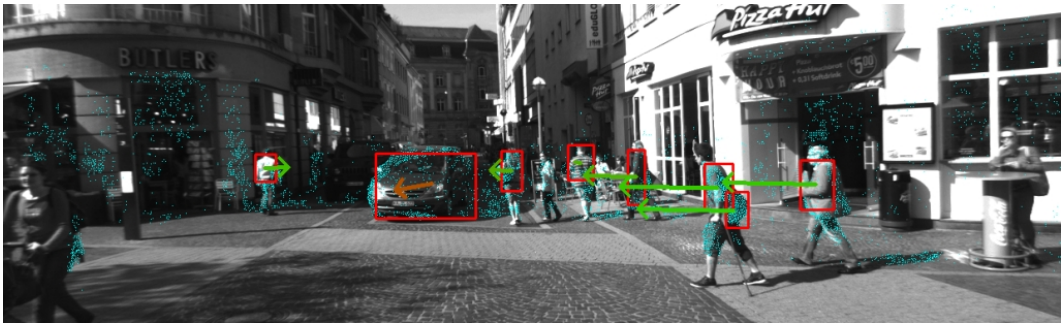

(b)

Figure 5.13 : Trajectory prediction of the moving objects by the proposed track-before-detect approach in two example scenes of the KITTI test sequence 2011-09-29-drive-0071 [146]

The pedestrians in the Figure 5.13(a) walked in the last time stamps parallel to the roadway and crossing now the ego lane. Although the pedestrians are partially covered by each other and moving with a similar velocity, each single pedestrian is detected.
Table 17 illustrates the required runtime for parallel processing of KITTI stereo images using a GPU of the NVIDIA GeForce GTX 780 Ti. The architecture of the implementation corresponds with the the process illustrated in Figure 5.10.
Compared to Table 14, the KITTI images need a longer processing runtime. This lies on the higher resolution of these images compared to the images captured by the stereo vision system of the experimental vehicle.

Table 17 Required runtime for parallel processing of KITTI stereo images with the resolution of 1242x375 using a GPU of the NVIDIA GeForce GTX 780 Ti

Calculation Step	Required Time
Stereo Disparity, Optical Flow and Ego Motion	49.1 ms
Kalman Filter	9.5 ms
Object Detection	13.0 ms
Total	71.6 ms

5.4.1.2 **Evaluation Using the Synthetic Images**

In addition to KITTI benchmark, synthetic images have been used to evaluate the detection performance. The synthetic images are generated by computer graphic techniques and enable the evaluation of the developed approach without existing of any background noise. In

addition, in contrast to real camera images, it can be ensured that the extrinsic calibration does not change during the generation of images.
The applied synthetic test sequence is an intersection scenario with two moving cars from both sides and the ego velocity is $75\frac{km}{h}$.
Figures 5.14(a) and 5.14(b) show the detection performance on two different timestamps with the time difference of 0.24s and the prediction time of 1s. As can be seen in Figure 5.14(c), the corresponding stereo disparity image shows a high quality. This lies on the lack of background noise in the synthetic images.

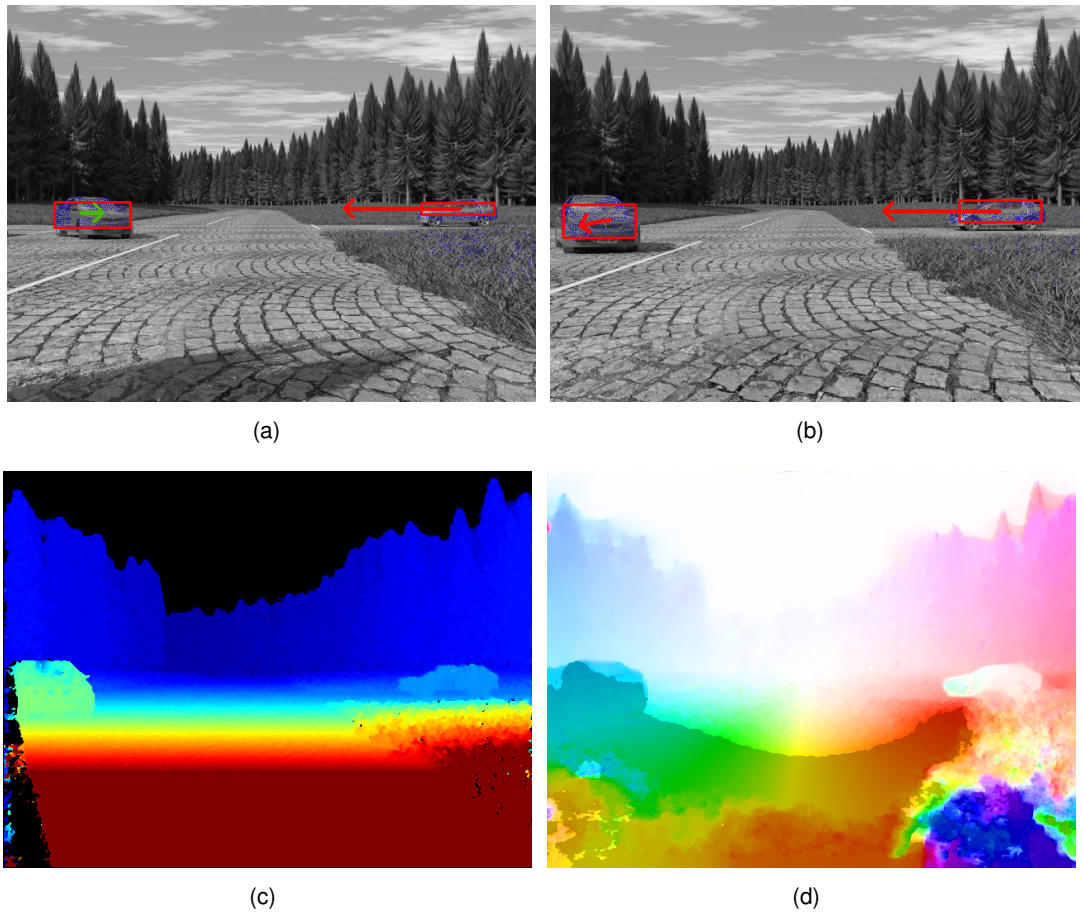

(a) (b)

(c) (d)

Figure 5.14 : Motion prediction in the synthetic images at two different timestamps (a,b) as well as the corresponding stereo disparity (c) and optical flow (d) of the image (a). The raw images are from [94].

Table 18 illustrates the evaluation of object detection based on the synthetic images. As can be seen, both moving cars in the scene have been detected and no false positive detection was available.

Table 18 Evaluation of synthetic test sequences

Detection of dynamic objects			**False positive detection**
Pedestrian	Cyclist	Car	
0 / 0	0 / 0	2 / 2	0

5.4.2 Evaluation of the Autonomous Intervention System

5.4.2.1 Test Design

The proposed assistance system is evaluated in different test scenarios. The test procedure and its results are described below.

5.4.2.1.1 **Test Environment**

Similarly to Chapter 4.4, the developed brake assistance system was evaluated in a human-in-the-loop test environment. The same test setup described in Chapter 4.4.1.1 was used to connect the operator's workstation with the SILAB simulation software over UDP. To simulate the time delay that exists in teleoperated driving, a constant round-trip communication time delay of 500 ms was created between the operator's workstation and the remote vehicle. The operator's workstation used for this test is presented in Figure 2.9(b).
Figure 5.15 depicts a test person while driving within the test scenario developed by SILAB. Since the visualized images had an artificial delay of 500 ms, the test person used a predictive display in order to control the remote car.

Figure 5.15 : A hazardous scenario while teleoperated driving with the time delay of 500 ms. The screen behind the operator shows the environment without time delay.

The monitor behind the test person displays the images sent from the simulated car in SILAB without any time delay. As can be seen on this monitor, the purple car started to cut into the front of the remote car. Because of the time delay, this hazard could still not be seen in the displays of the operator's workstation. This scenario depicts one of the use cases of the developed brake assistance system.

5.4.2.1.2 **Test Scenarios**

The test track developed using SILAB simulates an urban environment with a length of approximately 20 km. This test track was designed to include different types of streets and traffic conditions such as intersections, roundabouts, traffic lights and crosswalks.
The test track includes six critical crash scenarios taken from the category "cross-traffic" as the main source of hazards while driving under time delay. To realize these scenarios, various obstacles such as moving or parked cars, pedestrians or bicycle drivers cross the path of the teleoperator suddenly. Figure 5.16 illustrates three examples of these test scenarios.

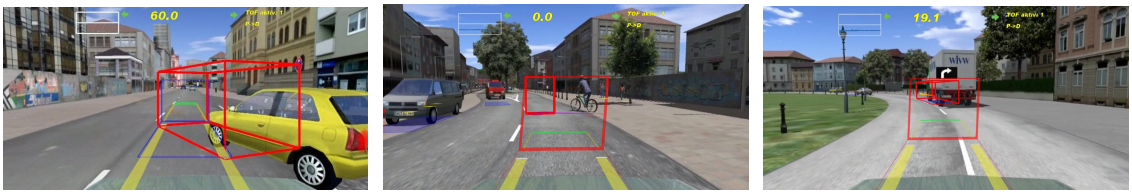

(a) (b) (c)

Figure 5.16 : Examples of the category "cross-traffic" as the main collision potential during teleoperated driving

In addition to the scenarios from the "cross-traffic" category, possible hazards from the following categories were studied: crashes with static obstacles, crashes with oncoming traffic

and crashes with front vehicles.

5.4.2.1.3 **Test Persons and Test Procedure**

Similarly to Chapter 4.4, four experienced operators were used to evaluate the developed assistance system. All test persons had received driving training using the operator's workstation and had become accustomed to the communication time delay and driving with the direct control concept.
The entire test track was driven by each test person twice without and twice with the developed brake assistance system. To simulate real driving conditions, no specific driving speed was given to the test persons. As an upper limit, the speed of $50\ \frac{km}{h}$ was allowed.
To reduce the possible learning effect, all of the designed scenarios were distributed among the entire test track and their order was changed in each driving test. To realize the same hazard conditions for all test persons, each test scenario was triggered at the same time before arrival of the remote car at the expected collision location.

5.4.2.1.4 **Measured Parameters**

To evaluate the conducted test drives, several objective and subjective parameters were used, which are described below.

Objective Parameters

The most obvious objective parameter for evaluating the developed brake assistance system is the number of collisions that occur throughout the entire test track.
Another important parameter when assessing this active safety system is the resulting time-to-collision (TTC) in hazardous scenarios. This parameter is defined as follows:

$$TTC = \frac{d}{v_{rel}}, \tag{5.10}$$

in which d and v_{rel} represent the distance and the relative speed to the target object, respectively.
In addition to TTC, the time-integrated time-to-collision (TIT) indicator can be used to express the level of safety. This indicator calculates the integral of the difference of the resulting TTC values and a specific threshold, TTC^*, and is described as follows:

$$\begin{gathered} TIT^* = \int_o^T [TTC^* - TTC(t)]dt. \\ \forall\ 0 \leq TTC(t) \leq TTC^* \end{gathered} \tag{5.11}$$

Contrary to TTC, TIT does not measure the hazard at only one point in time but can instead be used to assess the degree of hazard throughout the length of each test scenario. The greater the TIT in a scenario, the more hazardous the scenario is. Figure 5.17 depicts the calculation of the TIT indicator based on the threshold value, TTC^*. To calculate the TIT indicator in this example scenario, the shaded area should be subtracted from the area below the threshold value. The TIT indicator calculates the time integral of the area that remains below the defined threshold value, which is illustrated as a dark surface.
In addition to the parameters identified above for safety assessment, the average deceleration applied by triggered brakes throughout the entire test track would be a sign of braking behavior. A lower average deceleration of triggered brakes throughout the entire test track would indicate smoother braking behavior.

Subjective Parameters

The test persons were asked to fill out a questionnaire after finishing the test drives. This questionnaire assessed several subjective parameters, such as the test persons' impressions regarding improvements in safety and comfort, the level of assistance offered and whether or not they felt overburdened while using the developed brake assistance system.

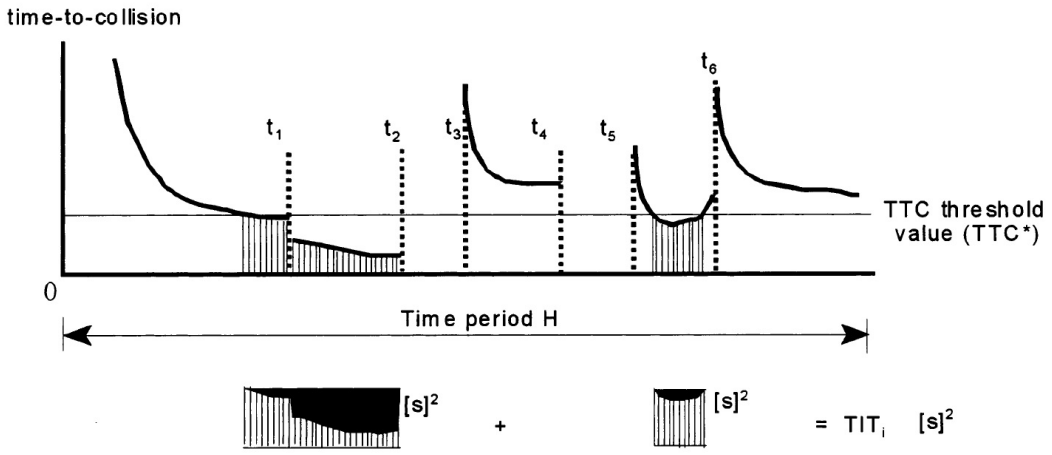

Figure 5.17 : Calculation of the TIT indicator as an integral of the difference of the resulted TTC values and a specific threshold [95]

5.4.2.2 **Test Results**

5.4.2.2.1 **Objective Results**

The overall number of collisions that occurred during both test drives without using the active safety system is illustrated in Table 19. Using the proposed active safety system, no collision occurred in the other two test drives.

Table 19 Overall number of occurred collisions within the whole test drives without using an active safety system

	Nr. 1	Nr. 2	Nr. 3	Nr. 4
Number of occurred collisions	4	4	2	2

Ten of these twelve collisions occurred in "cross-traffic" scenarios, which cannot be handled by the active safety systems that currently exist on the market. This scenarios include crossing of a bicycle, a car or a truck into the driving path of the teleoperator. To avoid possible false positive interventions, the currently existing AEBs on the market brake only if they detect an obstacle on the driving path of the car. As discussed before, such a reaction cannot ensure a collision avoidance while teleoperated driving. Two further collisions occurred with oncoming traffic, which could have been avoided using conventional active safety systems.
For this reason, some objective results of the occurred collisions in the "cross-traffic" category are investigated below. Figure 5.18 depicts the results of one of the test persons while driving using the developed brake assistance system in the scenario illustrated in Figure 5.16(a). In this scenario, a parked car suddenly cuts into the path of the teleoperator and drives along the street.
The x-axes of the plots illustrated in Figure 5.18 represent the longitudinal distance of the remote car from the starting point of this specific scenario within the entire test track. As can be seen in Figure 5.18(a), in both of the conducted test drives, the proposed assistance system predicted the hazard at approximately $X = 90\ m$ and intervened in the longitudinal control of the remote car. This intervention can obviously be seen in Figure 5.18(d), in which the acceleration of the remote car is illustrated.
After the autonomous intervention by the brake assistance system, the operator was informed of it through the HMI system and decided to manually control the situation. To do so, he pushed the brake pedal at approximately $X = 95\ m$, thereby aborting the autonomous intervention of the brake assistance system in the longitudinal control of the remote car. This can be seen in Figure 5.18(b), in which the state of the brake pedal is illustrated.
Figure 5.19 illustrates the TTC profiles of all of the test persons within this scenario. The profiles with the same color in the upper and lower images represent the TTC profile produced

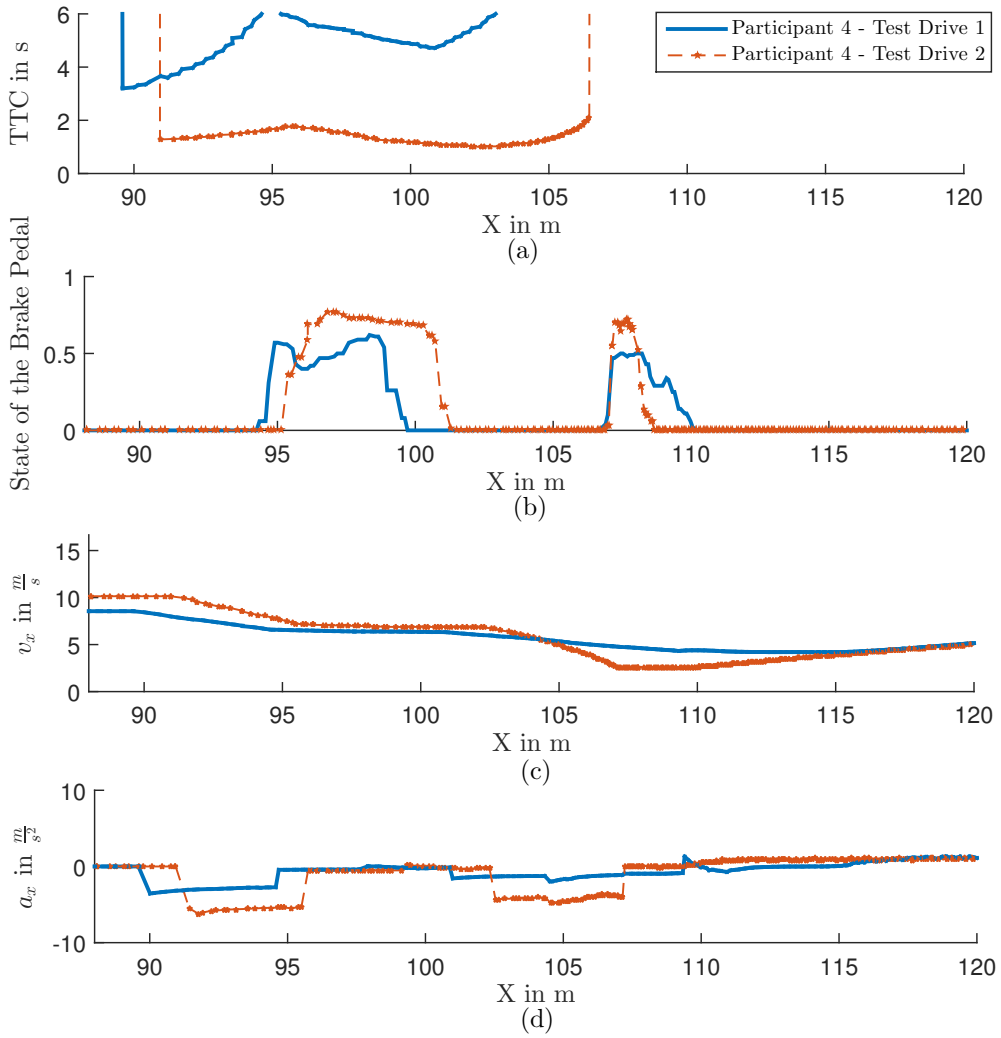

Figure 5.18 : System performance during teleoperated driving within the "cross-traffic" scenario illustrated in Figure 5.16(a). (a) TTC to the obstacle, (b) state of the brake pedal of the operator's workstation, (c) velocity curve of the teleoperator and (d) acceleration curve of the teleoperator [146]

by the same person following the same order of the test. As can be seen, without the use of the proposed brake assistance system, two collisions occurred. Using the system, these collisions were avoided and the overall TTC increased. These results indicate that safety with regard to the "cross-traffic" category was increased within this scenario as a result of using the proposed brake assistance system.

Similar behavior can be identified in other scenarios from the "cross-traffic" category. Figure 5.20 compares the TTC in a similar scenario, shown in Figure 5.15, with and without the use of the proposed brake assistance system. The profiles with the same color in the upper and lower images represent the TTC profile produced by the same person following the same test order. As can be seen, similarly to the results illustrated in Figure 5.19, using the proposed assistance system increased the overall TTC.

Figure 5.21 compares the TIT indicators of the conducted test drives during teleoperated driving within the "cross-traffic" scenario shown in Figure 5.16(a). The TTC profiles of this driving scenario were previously shown in Figure 5.19. The threshold value used to calculate the TIT indicator, TTC^*, was set as $5\ s$. As can be seen, using the proposed brake assistance system, this indicator decreased for all test persons. This result indicates an overall increase in safety during teleoperated driving in this "cross-traffic" scenario when using the developed brake assistance system.

In addition to increasing safety, the improving of braking behavior while controlling a teleoperated vehicle is one of the main goals of the proposed brake assistance system. Figure 5.22

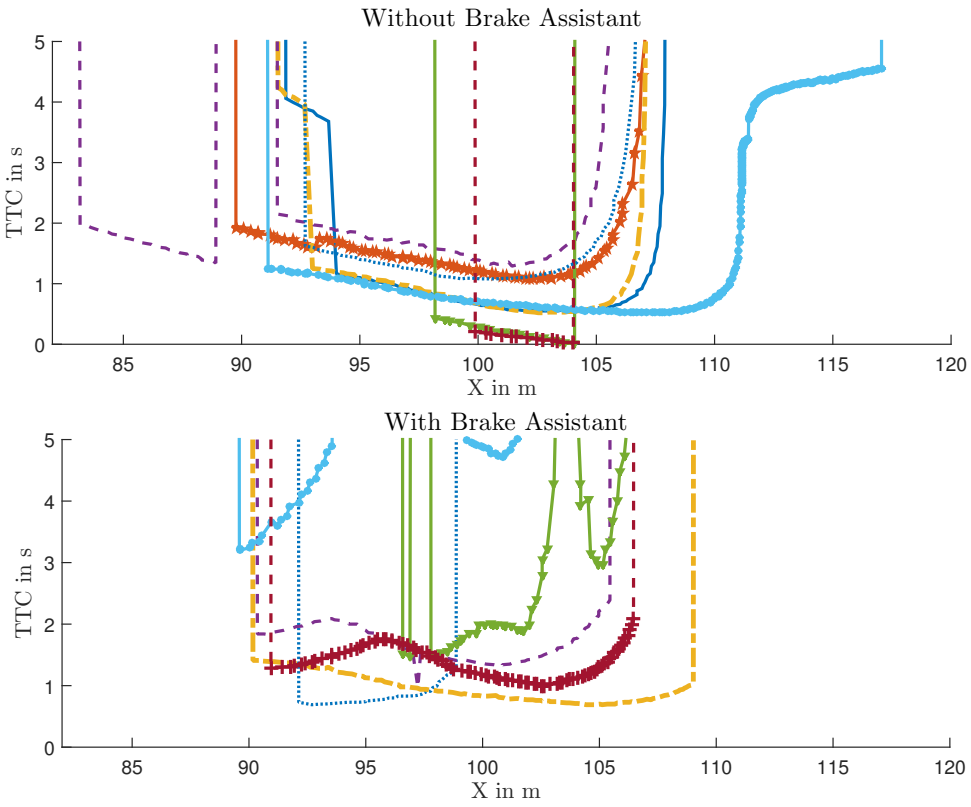

Figure 5.19 : The overall TTC of all trained test persons during teleoperated driving within the "cross-traffic" scenario shown in Figure 5.16(a): (a) without and (b) with the proposed brake assistance system [146]

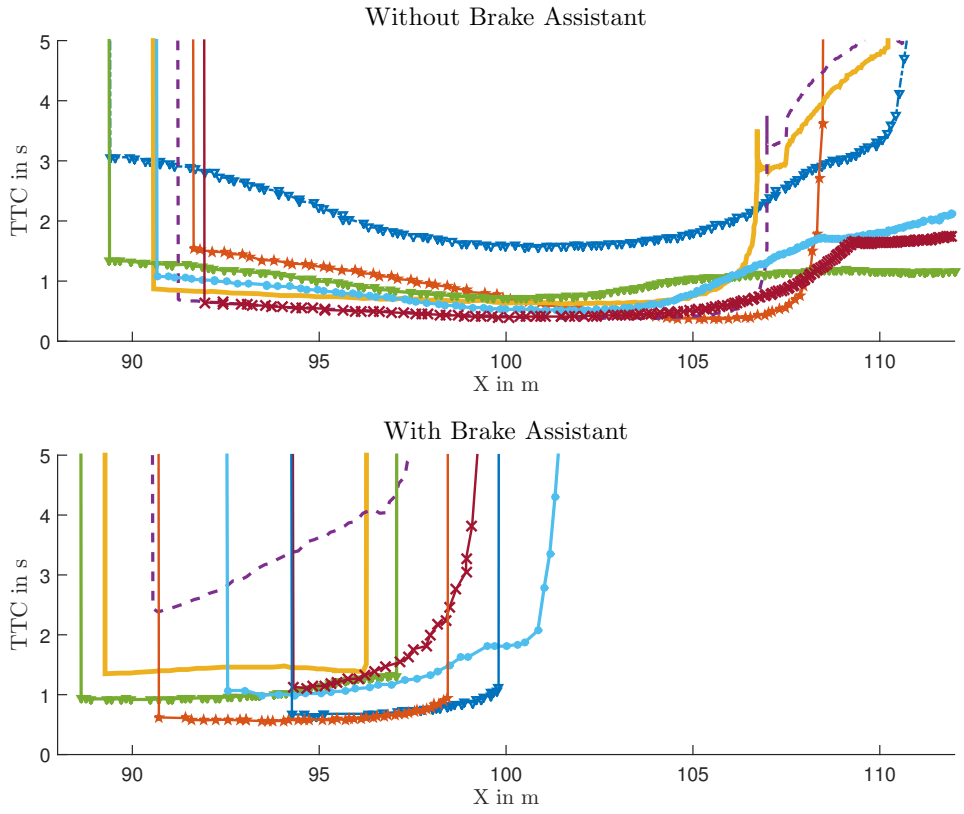

Figure 5.20 : The overall TTC of all trained test persons during teleoperated driving within a "cross-traffic" scenario shown in Figure 5.15: (a) without and (b) with the proposed brake assistance system

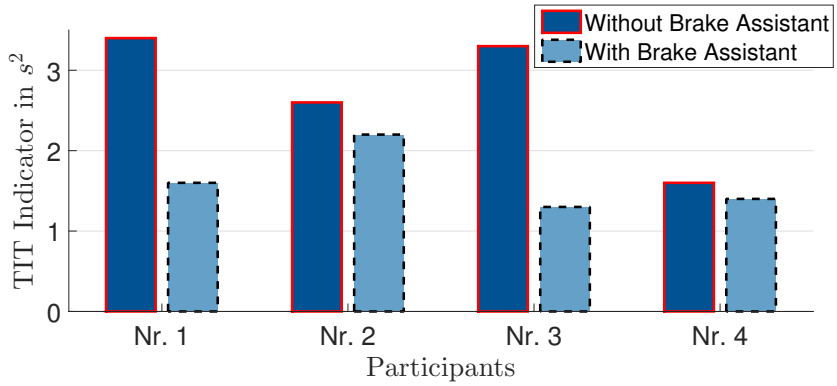

Figure 5.21 : TIT values of the conducted test drives during teleoperated driving within the "cross-traffic" scenario shown in Figure 5.16(a)

illustrates the average triggered brakes by the test persons throughout the entire test track. As can be seen, this value decreased when the proposed brake assistance system was used. This indicates an overall smoother use of brakes to avoid hazards when using the proposed brake assistance system.

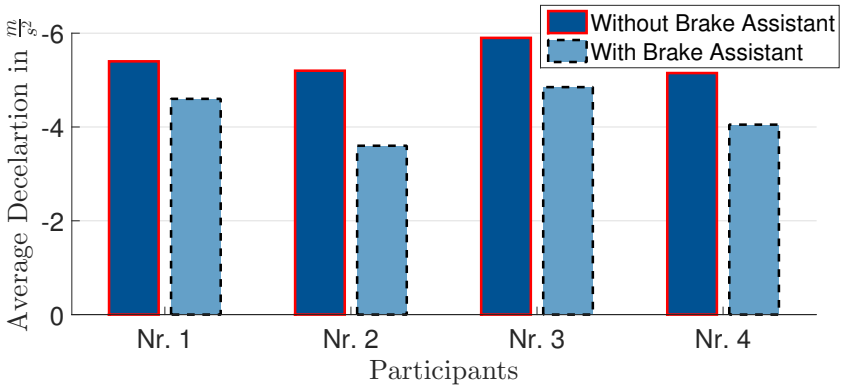

Figure 5.22 : Average of the triggered brakes within the whole test track including all critical test scenarios [146]

5.4.2.2.2 **Subjective Results**

In order to evaluate the "impression of safety" as an important subjective parameter, the test persons were asked whether the use of the brake assistance system increased their sensation of safety while engaged in teleoperated driving. Figure 5.23 illustrates their answers to this question. As can be seen, all of the test persons absolutely believed that the use of the predictive assistance system increased safety while they were engaged in teleoperated driving.

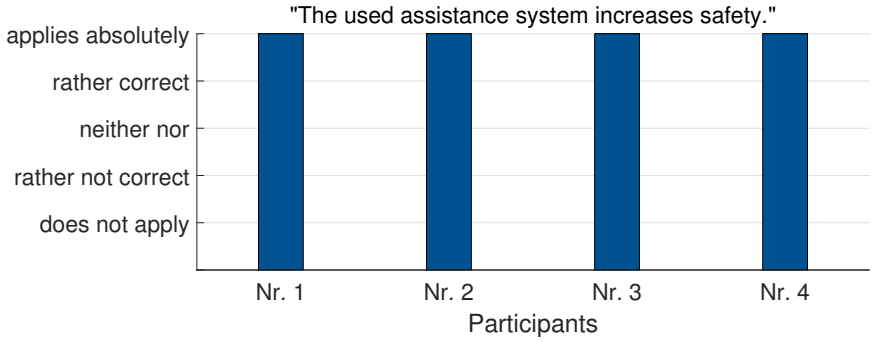

Figure 5.23 : Impressions of the test persons about "improving of safety"

To evaluate the "impression of comfort" as another important subjective parameter, the test persons were asked whether the use of the brake assistance system increased their comfort while engaged in teleoperated driving. The answers of the test persons to this question are illustrated in Figure 5.24. As can be seen, the responses varied, but on average the test persons believed that the predictive brake assistance system increased driving comfort while they drove the teleoperated vehicle.

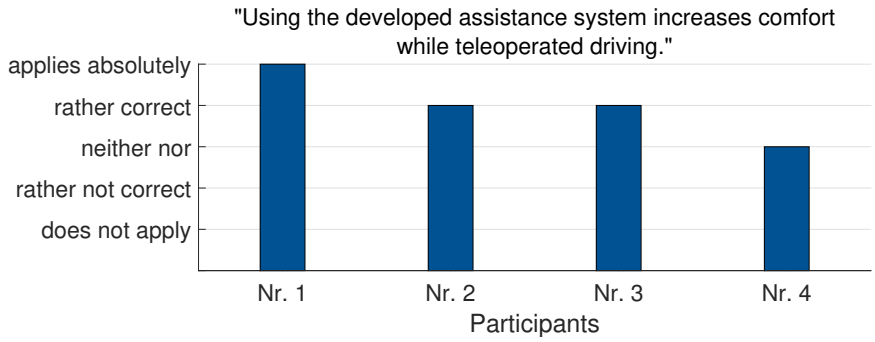

Figure 5.24 : Impressions of the test persons about "improving of comfort"

One of the main factors that may affect operator's comfort while using the proposed brake assistance system is the possibility of false positive interventions. This may happen in highly dynamic scenarios, in which the motion behavior of a dynamic object can change rapidly. A predictive intervention by the brake assistance system in such situations may be interpreted by the human operator as inappropriate, even if at an earlier point in time this intervention was appropriate.
To evaluate the impressions of the test persons regarding whether or not the brake assistance system made an excessive number of interventions, they were asked whether they found the degree of intervention to be excessive. Figure 5.25 illustrates their answers to this question. As can be seen, the perceptions of the test persons varied, and no definite statement about this subjective parameter can be made. However, it can be seen that two test persons believed that the system intervened excessively in some scenarios.

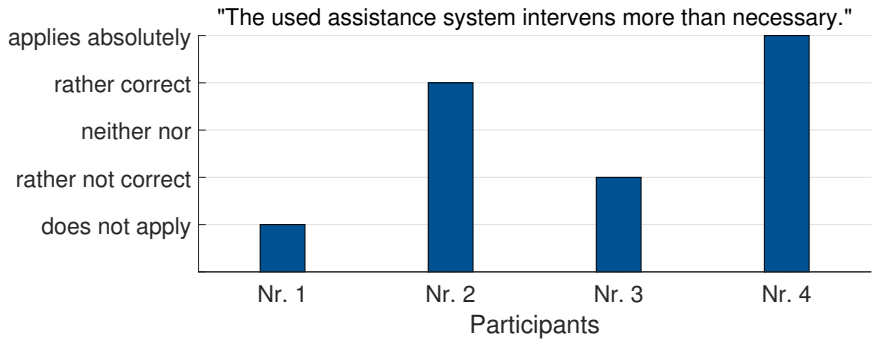

Figure 5.25 : Impressions of the test persons about the intervention level of the proposed brake assistance system

At the end, the test persons were asked whether they felt overburdened while using the proposed brake assistance system. Figure 5.26 illustrates their answers to this question. As can be seen, for the most part the test persons did not feel overburdened while using the proposed brake assistance system. These results correspond with the subjective parameter measured concerning increased comfort while using the proposed brake assistance system, which is illustrated in Figure 5.24.

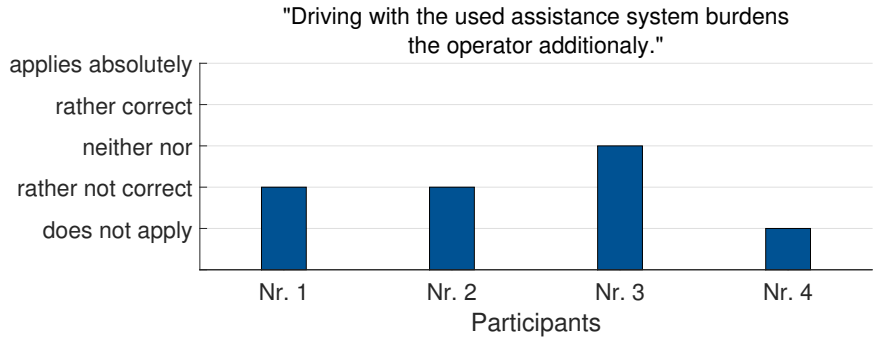

Figure 5.26 : Impressions of the test persons about a possible overburdening using the proposed brake assistance system

5.5 Conclusion and Discussion

The proposed active safety system is intended to intervene in the longitudinal control of the remote car in order to compensate for the communication time delay that exists in teleoperated driving.
The parameters investigated within the conducted human-in-the-loop test drives show an obvious increase in safety as a result of using the proposed active safety system. These results illustrate that the core goal of the proposed driver assistance system has been satisfied.
In addition to improving safety, the test results show an improvement in braking behavior as a result of using the proposed brake assistance system. This is the result of predictive autonomous intervention on the part of the remote car, which decreased the average deceleration required to avoid hazards.
Besides the objective parameters, the subjective parameters analyzed indicated an overall improvement of the test persons' feelings regarding increased safety and comfort while engaging in teleoperated driving using the proposed driver assistance system.
To reduce the possibility of excessive interventions of this system, the proposed track-before-detect approach for this ADAS could be improved by a fusion of the stereo vision system with other sensors or by combination with pattern recognition approaches.
In addition, the intervention logic should be so parametrized that unnecessary interventions in the braking system are minimized.
Although, in this work the proposed brake assistance system was applied in combination with the direct control concept, it is also applicable to the trajectory-based control concept for teleoperated driving. For this purpose, the proposed intervention system of the remote car would need to autonomously modify the received driving trajectories from the human operator.

6 Predictive Haptic Assistance for Enhancing Lateral Safety

The main content of the concept introduced in this chapter was previously presented in [147] and [145]. This chapter provides a description of this concept.

6.1 Problem Description

As discussed in the previous chapter, communication time delay is one of the main challenges in teleoperated driving. This challenge significantly affects the ability of the human operator to laterally control a remote car. The reduction of driving performance due to time delay was discussed in Chapter 3.1.2. In addition, a number of other works in the field of teleoperated driving, such as [41], [96] and [97] have explored this topic.
While engaged in teleoperated driving, the human operator perceives the output of his steering command after a communication time delay. This problem can lead to instable steering when the communication time delay is greater than approximately $200\,\mathrm{ms}$. With a time delay greater than $500\,\mathrm{ms}$, the ability of the human operator to laterally control of the car is reduced by up to $50\,\%$ [41].
As indicated in Chapter 3, this problem can be partially smoothed by using a predictive display to provide visual feedback about the current position of the remote car [40]. However, it cannot completely solve this problem and make a stable lateral control of the car possible.
This problem is partially dependent on the driving skills of the human operator. The driving performance of 22 test persons with low levels of experience in teleoperated driving was analyzed in Chapter 3.1.2. As discussed in Chapter 3.2, human operators need to pass a specific training course in order to become accustomed to driving under time delay, with a specific HMI and the operator's workstation.
To provide an overview of the abilities of trained operators, a human-in-the-loop study was conducted. In this study, the DYNA4 [42] software was used to simulate both vehicle dynamics and a test track. Similarly to the test setups used in Chapters 5.4 and 4.4, a round-trip communication time delay of $500\,\mathrm{ms}$ was artificially created between the operator and the remote car. In order to evaluate their control performance under time delay, four trained operators were asked to drive at an arbitrary speed up to $50\,\frac{\mathrm{km}}{\mathrm{h}}$ on a sinuous handling course five times. Figure 6.1(a) shows a scene from this test while driving using the predictive display. The test track itself is shown in Figure 6.1(b).

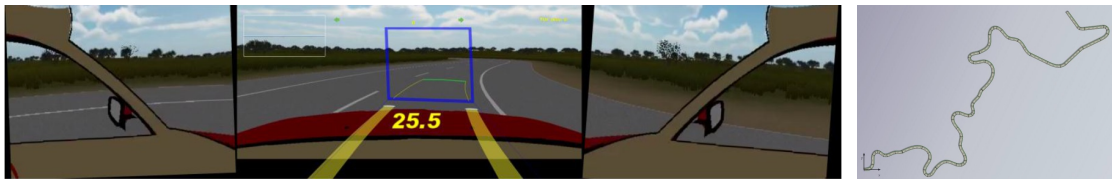

(a) (b)

Figure 6.1 : The human-in-the-loop handling course to evaluate the ability of four test persons in lateral control of the remote car using predictive display, (a) a scene of the test environment in DYNA4 (b) the top view of the sinuous test track

Among the several objectives and subjective results of this study, the objective parameter of directional stability can serve to illustrate the ability of these trained operators to maintain stable lateral control of the remote car.
Figure 6.2 shows the directional stability in all 20 of the conducted tests. In this figure, each circle represents the directional stability in one test drive.
These results indicate that even trained operators using a predictive display cannot guarantee

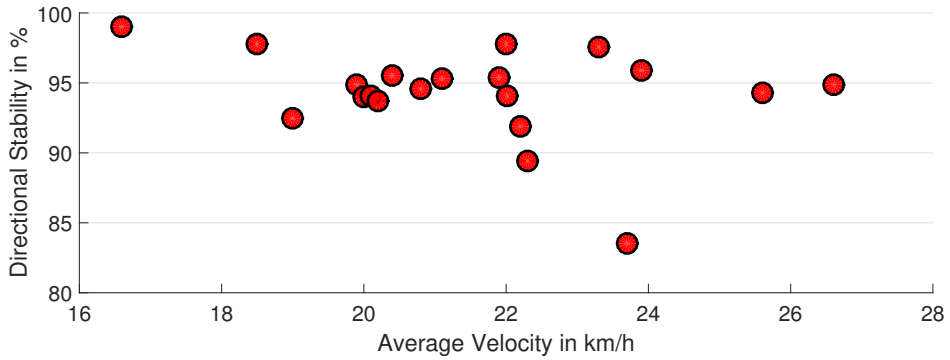

Figure 6.2 : The resulted directional stability in 20 test drives conducted by 4 experienced test persons using predictive display in the test track illustrated in Figure 6.1(b)

stable lateral control of the remote car under time delay.
With a constant time delay and an increase in vehicle speed, the distance between the predictive display and the delayed position of the remote car increases. In such cases, the human operator needs to control the car from a rather long distance behind its actual position, which leads to inconsistency while performing lateral maneuvers.
Such inconsistent lateral control of the car may lead to significant hazards while teleoperating a vehicle. Although the predictive display smooths the effect of communication lag between the human operator and the remote car, it cannot completely overcome the lack of situation awareness.
To address this problem associated with the direct control concept and to increase the safety of the car while performing lateral maneuvers, onboard autonomy intended to support the operator in the steering task is required. This topic is discussed in this chapter.

6.2 State of the Art: Haptic Assistance

6.2.1 Haptics as an Interaction Channel

In human-machine interaction, haptics refers to providing the feeling of force, motion and vibration and is divided into kinesthetic, proprioceptive, and tactile submodalities [98].
Through using haptic feedback in combination with other means of interaction, such as providing visual and auditory feedback, a multimodal human-machine interface for teleoperation can be created. This multimodal HMI could enhance the feeling that the human operator has of being in the remote environment and could consequently increase his task performance. An example of such multimodal interfaces being used for vehicular teleoperation can be found in [99].
Several studies in the field of haptics for teleoperation have focused on creating the "sense of touch" [98], which would be useful for various use cases, such as telesurgery or remote gripping. These applications focus mainly on the tactile submodality.
In automotive applications, haptics is mainly used for the generation of force feedback on the steering wheel or pedals. It is also used to generate vibration of the driver's seat in order to increase safety or comfort while driving. Since this work aims at improving lateral safety through steering assistance, it focuses mainly on the generation of the force feedback on the steering wheel.

6.2.2 Increasing Safety Using Haptics

One of the main applications of force feedback in teleoperation systems is increasing safety. The existing systems for increasing safety using haptics can broadly be divided into the two following approaches:
The first approach generates additional forces as virtual fixtures [100], which are aimed at

preventing the operator from approaching forbidden regions. Using this approach, the operator is *pulled* away from the defined boundaries [101]. Examples of this approach can be found in [102] and [103] for applications related to telesurgery and UAV control. Forsyth and MacLean [104] used this approach to develop look-ahead haptic guidance for automotive applications.
The second approach generates forces that guide the human along some sort of optimal trajectory. When compared to the first approach, a greater machine intelligence is required in order to realize this approach and to plan these optimal trajectories. Using this approach, the operator is *pushed* to the desired trajectory whenever he deviates from it [100]. Examples of this approach being used in automotive applications can be found in [105], [106] and [107].

6.2.3 Steering Assistance Systems

One of the main applications of haptics in the field of driver assistance is intervening in the steering system in order to increase comfort and promote lateral safety. Beginning with the lane-keeping and lane-departure warning system, this concept is further developed to narrow road passage assistance systems. A brief technical overview of these systems is provided below.

6.2.3.1 **Lane Departure Warning and Lane Keeping Assist**

The first generation of lateral assistance systems was introduced to the market in the 1990s. This generation included lane-departure warning (LDW) systems and lane-keeping assistance (LKA).
The lane-departure warning system informs the driver through haptic, optical or acoustical feedback when he makes an undesired departure from the traffic lane.
Lane-keeping assistance supports the driver in keeping the vehicle between traffic lanes through active intervention in the steering. A general system architecture of these assistance systems can be seen in Figure 6.3.

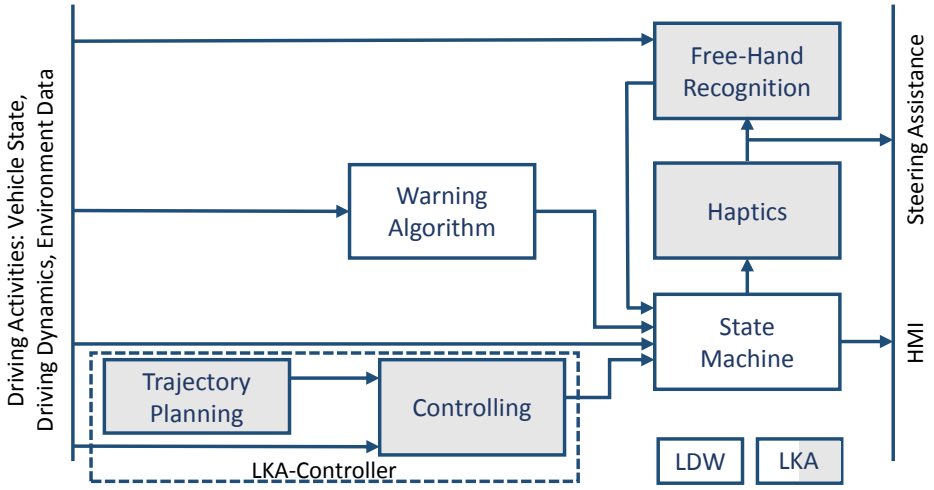

Figure 6.3 : System Architecture of the lane keeping assist (LKA) and the lane departure warning (LDW) systems [77]

Both of these systems mainly rely on the position of the lane marks for trajectory planning, which are normally by the camera sensors. Hence, these systems are only practical in situations in which lane marks can be robustly detected by the vehicle's sensors.
For the lane-departure warning system, time-to-line-crossing (TLC), t_{LC}, is the main criterion used when triggering a warning. This criterion shows the remaining time required to cross the traffic lane and is calculated as follows [77]:

$$t_{LC} = d_{LC}/vsin(\phi), \tag{6.1}$$

in which d_{LC} stands for the lateral distance of the vehicle to the lane mark, v stands for the

longitudinal velocity of the car and the ϕ represents the angle between the longitudinal axis of the vehicle and the traffic lanes.
Generally, two types of lane-keeping assistance systems exist [77]:
The first type of LKA systems focuses on safety and avoiding departure of the traffic lanes through active intervention in the steering system. The function used to generate the assistance torque in this type of LKA is depicted in Figure 6.4(a). As can be seen, the assistance torque is generated once the vehicle closes to the lane mark.
The second type of LKA systems considers comfort in addition to safety and uses a trajectory planning system that calculates a trajectory along the center of the detected lane marks as the desired trajectory of the vehicle. If the predicted trajectory of the car does not correspond to its desired trajectory, assistance torque is applied to the car's steering wheel. Thus, the assistance system guides the car onto the desired trajectory. The functions used to generate the assistance torque in this type of LKA are depicted in Figures 6.4(b) and 6.4(c).

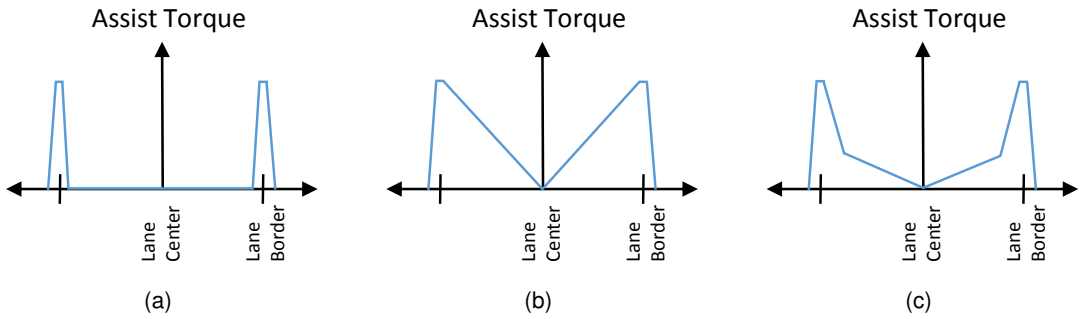

Figure 6.4 : Different strategies to generate an assistance torque on the steering wheel: (a) loos guidance, (b) tight guidance, (c) comfort guidance [77]

6.2.3.2 **Narrow Road Assistant**

The new generation of lateral assistance systems is aimed at supporting the driver while driving within narrow road passages. This generation is principally seen as an evolution of the lane-keeping assistance systems for inner-city situations.
Several developers have announced that they have begun work on these types of assistant systems. BMW [108] has announced that it has prepared its first research prototype of the "Narrow Passage Assistant", which is intended to help the driver while driving within narrow passages, such as the gap between a truck and a guardrail. This system measures the width of the gap between the obstacles using a LiDAR sensor and informs the driver whether driving through the gap is feasible. While driving within the gap, the vehicle measures its distance to the obstacles on both sides using ultrasonic sensors and displays this information using specific symbols on the head-up display. If the vehicle's distance to the barrier decreases below a predetermined value, the vehicle gives a brief steering pulse to the driver and, after receiving his confirmation, guides the vehicle to the optimal trajectory within the gap.
Volkswagen [109] announced that it has begun work on a similar system for assisting drivers while driving through building sites. The research prototype that the company presented uses a stereo-vision system that looks to the front of the car as well as four ultrasonic sensors on both sides of the vehicle in order to model the environment. Since this assistance system is seen as a further development of the lane-keeping assistance systems, its logic relies heavily on detecting lane marks by means of the vehicle's sensors.
Bosch [110] [111] recently presented its more advanced research prototype, called the "Narrow Road Assistant", which has been developed as part of the UR:BAN project [112]. The realization of this ADAS would require several sub-systems, such as those dedicated to self-localization in urban environments, path planning and recognition of the driver's intentions. Some of these sub-systems are known as current challenges in the field of automated driv-

ing in urban environments. Hence, it is unlikely that this system will soon be released to the market.

6.3 Approach

The most stable solution to the problems posed by lateral control of a remote car would be full automation of the steering task. Such a solution requires a robust environment perception, which is still not available in all urban environments.
Hence, an appropriate solution for addressing this safety problem associated with teleoperated driving would be assisting the operator through autonomous intervention in the steering task. As described in Chapter 6.2.2, this goal can be achieved through either *pulling* the remote vehicle away from defined boundaries or through *pushing* it onto an optimal trajectory.
Since path planning in unstructured urban environments without the use of an offline digital map still fails to demonstrate robust performance, this approach to guiding the human operator onto a desired path cannot be used in all scenarios. Even with stable path planning, it is possible that a planned path does not correspond to the operator's desired driving path. This may lead to the human operator becoming dissatisfied with the guidance system.
To increase lateral safety in teleoperated driving, pulling the remote vehicle away from defined boundaries seems to be a more appropriate solution. Thus, the driver-assistance system intervenes only in hazardous scenarios and permanent steering support is avoided. The system architecture of this driver assistance system is described below.

6.3.1 Human-Machine Cooperation in the Steering Task

The general system architecture of the proposed haptic assistance system is illustrated in Figure 6.5. As can be seen, depending on the driving situation, the haptic assistance system generates force feedback on the steering wheel in order to support the operator when attempting to avoid a lateral collision.

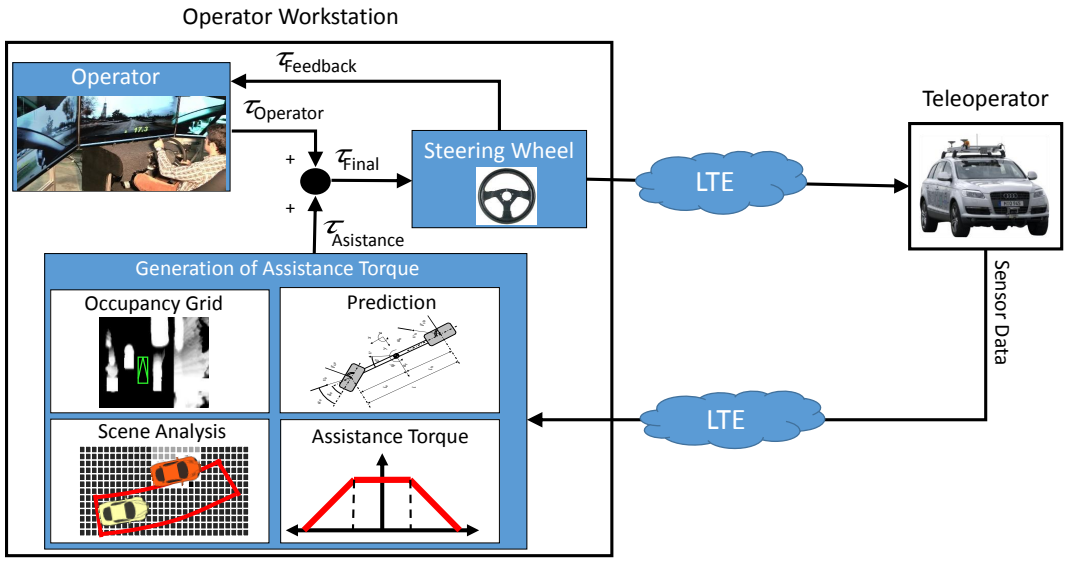

Figure 6.5 : General system architecture of the proposed haptic assistance system to increase the lateral safety while teleoperated driving [147]

Since this assistance system is aimed at enhancing the situation awareness of the human operator in order to improve safety, its intelligence unit needs to be located at the operator's workstation. Using this approach, the human operator is informed of the assistance system's decisions without any communication time delay.
One of the main factors in designing a steering assistance system is its level of automation. As indicated in Chapter 5.3.3, per the Vienna Convention on Road Traffic, the human operator

should have the superior role in the entire control loop of a teleoperated vehicle and should have the ability to override the machine's decisions at any time.
Hence, the final output of the steering system is the sum of the steering torques given by both the human operator and the machine. Since the maximum input of the machine is restricted to a small fraction of the maximum possible input that can be given by the human operator, the latter can override the machine's intervention at any time.
For situational analysis, the vehicle's surroundings need to be modeled using the vehicle's sensors. This can be achieved using the LiDAR sensor data from the vehicle. To create an environment model at the operator's workstation, the LiDAR sensor data should be sent to the operator's workstation together with the camera images. After the creation of a 360° environment model at the operator's workstation, the effect of communication time delay on the model must be eliminated. The creation of the predictive environment model as well the intervention logic of the assistance system is described below.

6.3.2 Predictive Environment Model

Similarly to some other driver-assistance systems and automated driving functions, a haptic assistance system requires a model of the vehicle's surroundings. This can be realized using a LiDAR-based occupancy grid, which was introduced in Chapter 4.3.2. Since the environment model created at the operator's workstation is delayed, its current state needs to be predicted. This procedure is illustrated in Figure 6.6.

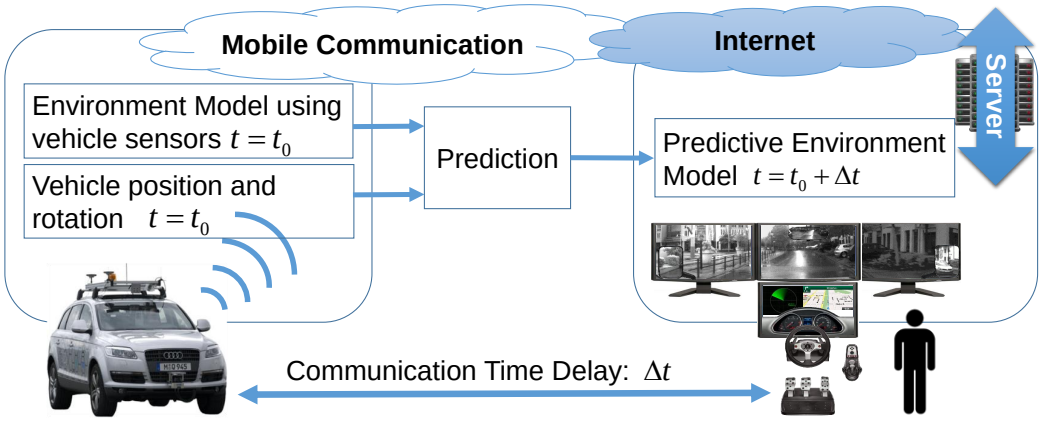

Figure 6.6 : Elimination of the effect of communication time delay in the received environment model at the operator's workstation [147]

The elimination of the effect of the communication time delay includes the prediction of the current positions of the teleoperator as well as the existing dynamic obstacles in the scene. These steps are described below.

6.3.2.1 Prediction of the States of the Remote Vehicle

The first step to eliminate the effect of time delay on the environment model is the prediction of the current position of the remote car on the map. This can be conducted using the same approach used to calculate the predictive display.
Using a non-linear single-track model, the states of the remote vehicle over the communication time delay can be estimated as follows [5]:

$$\psi(t) = \psi_0 + \int_0^t \dot{\psi}(\tau)\,\mathrm{d}\tau \tag{6.2}$$

$$x(t) = x_0 + \int_0^t \mathrm{v}(\tau).\cos(\psi(\tau) + \beta(\tau))\,\mathrm{d}\tau \tag{6.3}$$

$$y(t) = y_0 + \int_0^t \mathrm{v}(\tau).\sin(\psi(\tau) + \beta(\tau))\,\mathrm{d}\tau, \tag{6.4}$$

where $x(t)$ and $y(t)$ respectively stand for the longitudinal and lateral coordinates of the center of gravity of the vehicle, v represents its velocity and $\psi(t)$ and β represent its heading and the side slip angles.

6.3.2.2 **Prediction of the Dynamic Environment**

The second step involved in eliminating the effect of time delay on the environment model is the prediction of the current states of the dynamic obstacles on the map. The detection of dynamic obstacles using the occupancy grid requires parallel tracking of all cells, which may lead to a high computational load. Hence, in this work other traffic participants are recognized using the raw data obtained by the LiDAR sensors and the detection results are projected onto the occupancy grid.

To create a 360° dynamic environment map, the dynamic obstacles can be detected either through motion or through model-based recognition and tracking using the raw sensor data.

Since for the haptic assistance the sides of the car in addition to its front must be perceived, the approach for motion detection using a stereo-vision system proposed in Chapter 5.3.2 is insufficient to create a dynamic environment map.

The model-based approach for object detection using active sensors has been addressed in several previous works in the area of environment perception for ADAS and automated driving. Some related works can be found in [113] and [114]. Table 20 illustrates the procedure for object detection using LiDAR sensors applied in this work.

Table 20 The applied steps to detect obstacles and predict their future states using LiDAR sensors.

1. Segmentation of Raw Data
2. Feature Extraction
3. Classification
4. Tracking and Data Association
5. Prediction

To detect objects, it is first necessary to generate object hypotheses. For this purpose, the raw LiDAR data should be segmented. This can be achieved by using different distance-based approaches, such as the region-growing algorithm, OPTICS algorithm [115] or the iterative end-point-fitting approach [116]. Among these approaches, the OPTICS algorithm demonstrates the best segmentation performance, which is a consequence of its ability to sort the measurement data based on their densities.

In the next step, the existing features in each segment need to be extracted. For this purpose, the measurement data should be fitted to lines. Using this fitting, several geometrical characteristics of each segment can be defined, which are used later for classification. The length and the width of each segment, the angles between its vertices, the number and distribution of the measurement samples in each segment and the surface of the segment are some of the geometrical features that can be extracted from each segment.

These features are then proved and allocated to shape-based classes such as I-shaped, L-shaped, U-shaped and point-shaped, which represent the observed shapes of traffic participants including cars, bikes and pedestrians from different points of view. Different classifiers such as Bayesian classifiers, neural networks or support vector machines can be used for this purpose.

After classification of the segmented obstacles, their motion is tracked using a Bayesian filter, such as the extended Kalman filter. To reduce the uncertainty in data association, the probabilistic approaches can be used [117]. For this purpose, after using ellipsoidal gating around the extended measurement data, the JIPDA approach [118] is used, which allows for the possibility that multiple tracks interfere with each other, resulting in recursive expressions for

the probability of the target's existence. Figure 6.7 illustrates the visualization of recognized vehicles based on their geometrical features in two example scenes.

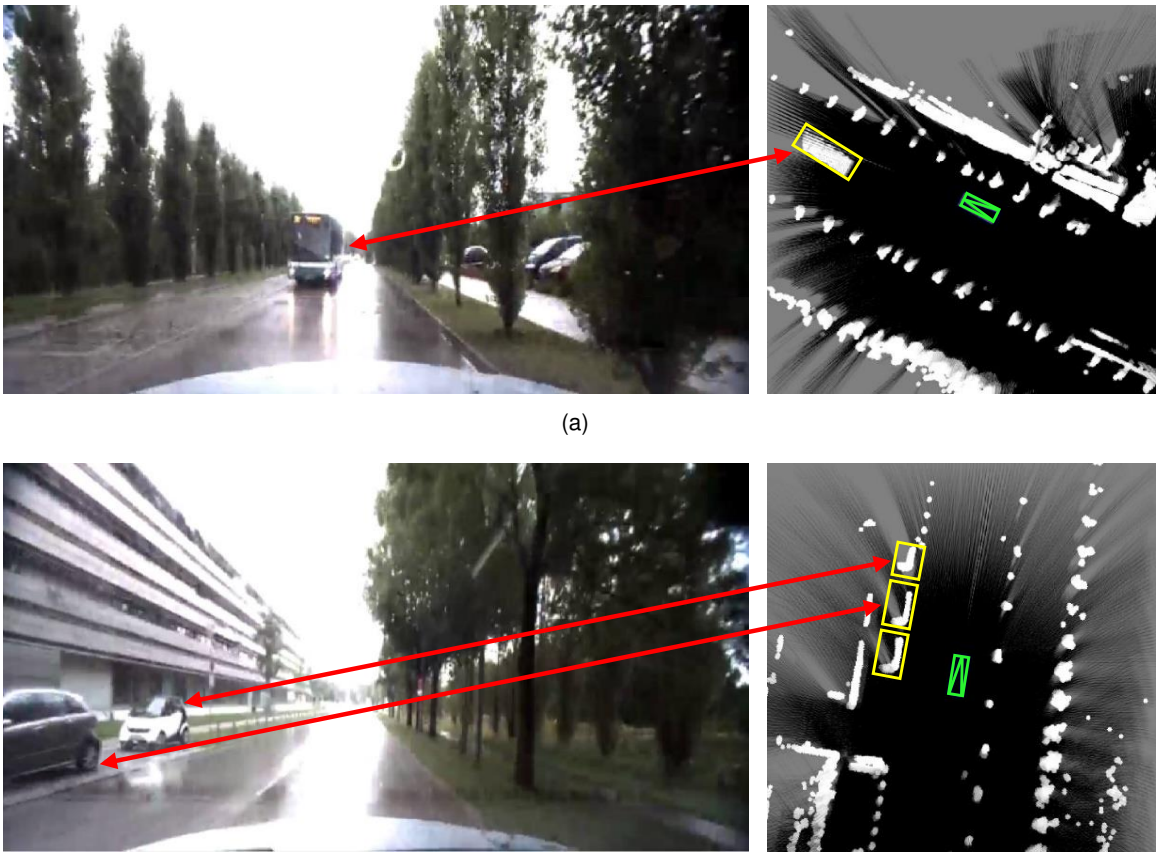

Figure 6.7 : Recognition of other vehicles using LiDAR measurement data based on their geometrical features: (left) camera image of the scene, (right) projection of the recognized vehicles on the LiDAR occupancy grid

Using the same approach employed in 6.3.2.1, the current states of the detected dynamic obstacles can be predicted over the communication time delay. This enables the elimination of the effect of time delay on the environment map.
This approach to creating a 360° dynamic occupancy grid demonstrates reasonable performance when detecting dynamic cars and bikes using LiDAR sensors. These obstacles are the main dynamic obstacles that should be considered by a haptic assistance system in urban environments.
However, this approach could be extended by a fusion of LiDAR sensor data with other sensors, such as radar and stereo vision. This would make the resulting 360° environment model more precise and robust.

6.3.3 Scene Analysis and Steering Intervention

In general urban environments, without depending on lane marks and digital maps, a steering assistance system can mainly support the human operator in avoiding lateral collisions, not permanently guide him or her to a reference driving path. For this purpose, the haptic assistance system needs to identify potential hazards that may lead to a lateral collision and generate an adequate assistance torque.
To predict potential hazards, a safety area needs to be defined around the remote vehicle. This area works much like a *virtual bumper*, causing the generation of an assistance torque on the steering wheel once it collides with an obstacle.
This safety area needs to predict the future states of the remote vehicle at a predefined prediction time, t_{LA}. This can be conducted using the same mathematical approach to estimating

the current position of the remote vehicle discussed in Chapter 6.3.2.1.
This approach to considering the future state of the vehicle for the purposes of haptic assistance is known as *look-ahead*. It compares the end point of the predicted trajectory to the current state of the vehicle [104]. However, in order to take into account all of the expected changes in the dynamic environment, the entire trajectory between the current position of the vehicle and its predicted position after the look-ahead time, t_{LA}, must be kept under control.
When setting a constant look-ahead time, the distance considered in front of the remote car depends on its velocity. This helps to reduce the possibility of unnecessary interventions by the assistance system in the steering task.
In addition to monitoring a certain distance in front of the remote car, the safety area also needs to consider the lateral sides of the vehicle. For this purpose, a certain boundary on both sides of the car needs to be defined, which is assumed to be the hazardous lateral distance of the car to obstacles.
Figure 6.8 displays a schematic of this safety concept, in which d stands for the observed distance on the lateral sides of the remote car and b represents the car's width.

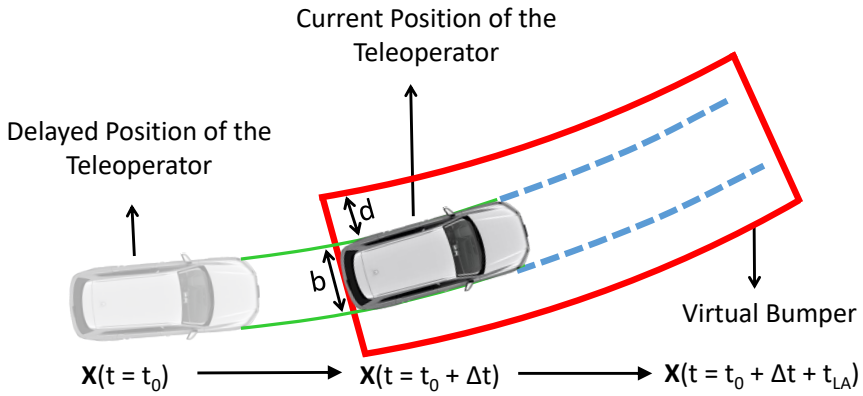

Figure 6.8 : The defined safety area around the remote vehicle on the created environment map at the operator's workstation [147]

An inappropriate look-ahead time could cause inconveniences while performing highly dynamic maneuvers [119]. In this work, the look-ahead time is set as $0.5\ s$, as suggested by the literature [119] [120]. In addition, in order to provide adequate haptic assistance in situations where it is necessary, and to prevent permanent intervention in the steering task, the considered lateral distance, d, on both sides of the car is set as $1\ m$.
Once a collision of this virtual bumper with a barrier is detected, the assistance torque on the steering wheel of the operator's workstation should resolve it. The kind of steering assistance required depends on the driving scenario. If only one side of the virtual bumper collides with an obstacle, the steering assistance system should assist the human operator to conduct an evasive maneuver. Thus, the risk of a lateral collision would be reduced.
If the virtual bumper collides with obstacles located on the both lateral sides of the remote car and there is enough place for the remote vehicle to drive through the obstacles, the assistance system should guide the operator onto the middle path of the passage between the obstacles. Thus, the risk of a lateral collision while driving through such a passage would be reduced.
In the case that there are obstacles on both lateral sides of the remote car and the passage between them is not drivable, the brake assistance system proposed in Chapter 5 intervenes. In such scenarios, the haptic assistance system does not need to intervene in the steering system.
Once the virtual bumper collides with an obstacle that is located on one side of the remote car, the human operator should be assisted in evading the collision. The assistance torque required can be calculated based on the lateral distance of the obstacle to the remote car.
As illustrated in Figure 6.9(b), the assistance torque generated on the steering wheel is raised

to its maximal value once the lateral distance of the obstacle from the remote car is reduced. This logic is similar to the logic used in LKA systems. However, the main difference is that LKA systems guide the driver to a reference trajectory, but the proposed system guides the operator in avoiding the predicted collision. Hence, the torque profile proposed in Figure 6.9(b) differs from the profiles used in LKA systems, which are illustrated in Figure 6.4. The maximal value for the generated assistance torque is set at $1.5\ Nm$, which is within the range of acceptable assistance torques given to a human driver. Applying higher levels of torque on the steering wheel may irritate the human operator.
In order to provide smooth steering assistance, the assistance torque should be linearly raised to the required value. As illustrated in Figure 6.9(c), the TTC can be used as the time horizon when raising the assistance torque.

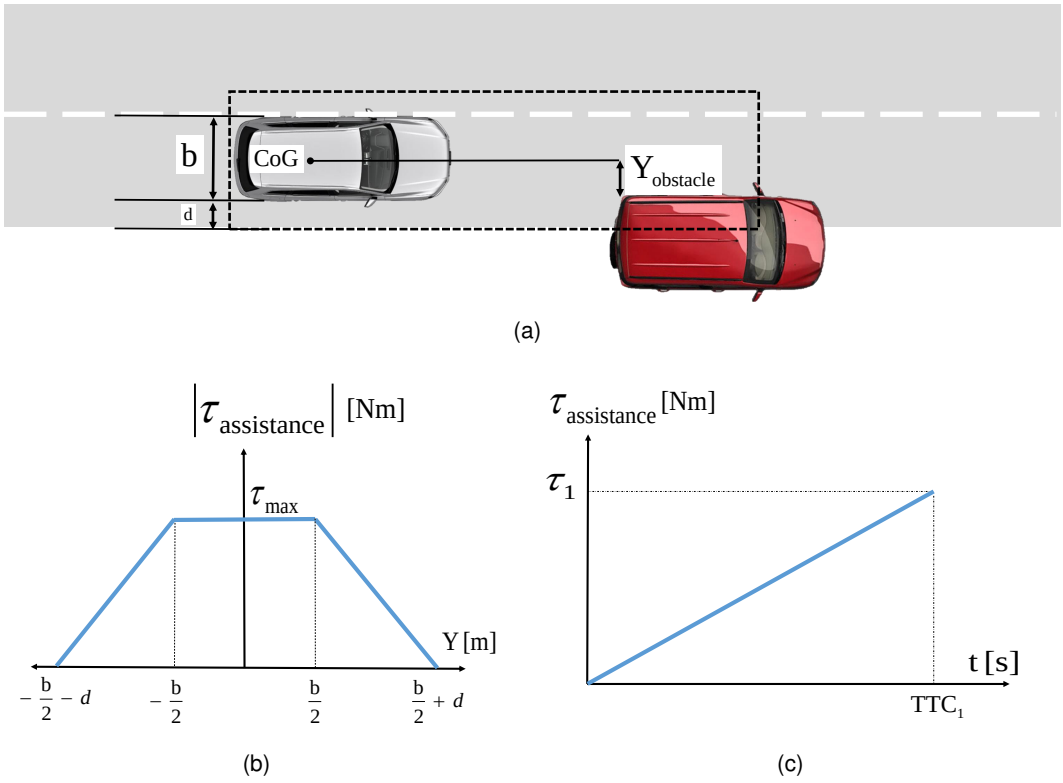

Figure 6.9 : (a) Collision of the virtual bumper with an obstacle from one lateral side; (b) Relation of the lateral distance of the obstacle and the assistance torque; (c) Linear raising of the currently supplied assistance torque to the newly calculated assistance torque

If several obstacles with different longitudinal distances to the remote car collide with one lateral side of the virtual bumper, the nearest of them is taken into account. After resolving the collision of the virtual bumper with the nearest obstacle, the next obstacle is handled. This successive handling of collision hazards provides smooth steering assistance to the human operator. A schematic handling of several obstacles is illustrated in Figure 6.10.
When the safety area collides with barriers on both lateral sides, the haptic assistance system behaves similarly to the narrow road assistance system. In such cases, the middle trajectory between the barriers needs to be planned based on the environment model. The generated assistance torque then guides the human operator along this reference trajectory.
Figure 6.11 illustrates an example scenario in which the human operator intends to drive through two other vehicles. As can be seen, the safety area collides on both lateral sides with the dynamic obstacles.
The intervention logic of the haptic assistance system in this scenario is similar to the logic of the first type of LKA systems (see Chapter 6.2.3.1). Longitudinal and lateral control of the remote car along the desired trajectory is addressed in [41].

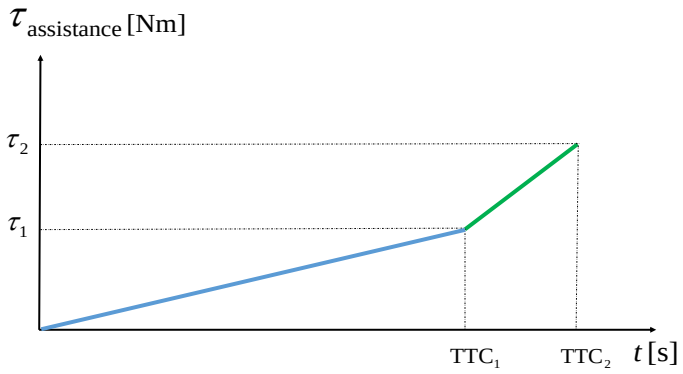

Figure 6.10 : Linear raising of the currently supplied assistance torque to the newly calculated assistance torque

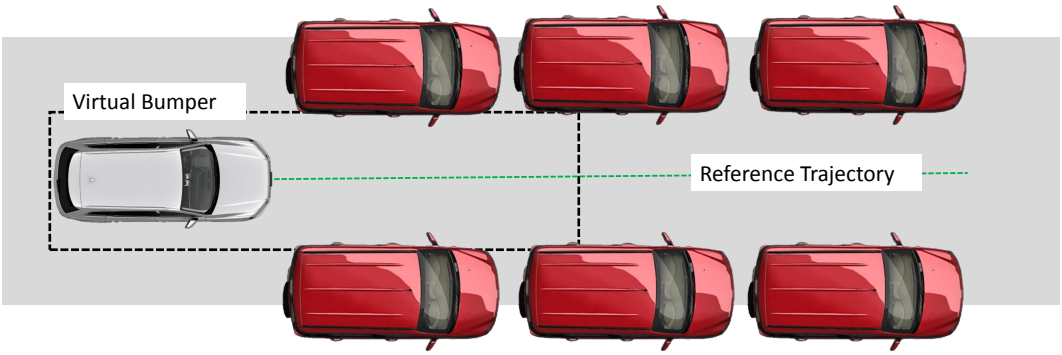

Figure 6.11 : Guiding the operator to the middle trajecory between obstacles, when the virtual bumper collides from both lateral sides with obstacles

6.4 Evaluation and Results

6.4.1 Test Design

The proposed assistance system was evaluated in several test scenarios. The test procedure and results are described below.

6.4.1.1 **Test Environment**

Similarly to Chapters 4.4 and 5.4, the developed haptic assistance system was evaluated using a human-in-the-loop test environment. The same test setup described in Chapters 4.4.1.1 and 5.4.2.1.1 was used to connect the operator's workstation with the SILAB simulation software over UDP. To simulate the time delay that exists in teleoperated driving, a constant round-trip communication time delay of 500 ms was created between the operator's workstation and the remote vehicle. Figure 6.12 shows a driving scene from within the test scenario developed in SILAB.

The operator's workstation used for this test is presented in Figure 2.9(b). The steering wheel of this operator's workstation cannot control itself to a specific steering angle, but it is able to generate a limited torque with a resolution of 0.3 Nm [37] in both steering directions.

The SILAB simulation software is equipped with a perfect sensor model, which in some cases does not correspond to the real levels of environment perception that a vehicle's sensors are capable of. In order to approximate a realistic environment model, SILAB's perfect sensor model was abstracted and only that part of the environment data that is robustly detectable by vehicle sensors in an urban environment was used.This part of the environment consists of vehicles' surroundings and static obstacles, which are available on the LiDAR occupancy grid described in Chapter 6.3.2. Since there are no lane markings in some urban areas

Figure 6.12 : Human-in-the loop test using the simulation software SILAB to evaluate the developed haptic assistance in simulated urban environments

and/or vehicle sensors are not always capable of robustly detecting them in all urban areas, the existing lane marks in SILAB's perfect sensor model were not used for the creation of the environment model.

6.4.1.2 **Test Persons**

Similarly to Chapters 4.4 and 5.4, four experienced operators were used to evaluate the developed assistance system. The level of experience with teleoperated driving and the personal driving capability of an individual operator have a significant influence on his ability to maintain lateral control of a remote car while engaged in teleoperated driving. Hence, some important information concerning driving experience of each test person was obtained. This information is provided in Table 21.

Table 21 Personal information and driving experience of the test persons

Experienced Operator	Nr. 1	Nr. 2	Nr. 3	Nr. 4
Sex	W	M	M	M
Age	25	27	31	26
Driven Distance (Kilometers/Year)	<5000	<5000	<5000	<5000
Driving Style	conservative	conservative	sportive	sportive
Experience with the Operator's Workstation	< 2 Weeks	> 5 Months	> 6 Months	> 2 Months
Experience in Computer Games	none	none	a little	very much

Among these test persons, test person Nr. 1 had the least experience of teleoperated driving. Her experience with the system included driving for approximately 20 minutes on several handling courses and in some urban environments.
Test person Nr. 2 had the most extensive experience of teleoperated driving. He executed several test drives over a period of several months in the simulation environment and was fully aware of the effect of time delay on teleoperated driving. Test person Nr. 3 had much experience with the system and its functionality but did not have extensive experience of teleoperated driving.
Test person Nr. 4 had a fair amount of experience of teleoperated driving: his experience with the test setup was greater than that of test person Nr. 1 and less than that of test person Nr. 2. However, a unique characteristic of this participant is his intensive experience of racing

games using a driving console at home.

6.4.1.3 **Test Scenarios and Test Procedure**

The developed assistance system was evaluated in different driving scenarios within a static or dynamic environment. Two of these test scenarios are described below.

6.4.1.3.1 **Test scenario I: Double Lane Change**

The double lane change test scenario involves a driving maneuver that is standardized under ISO/DIS 3888-1 [121]. As the name of this test indicates, it includes two successive lane changes within positioned pylons.
The main purpose of this standardized test is to subjectively determine the vehicle dynamics and road-holding ability of passenger cars within a closed loop test [121]. Hence, it would be an appropriate maneuver for examining the road-holding ability while laterally controlling a remote car. Figure 6.13(a) illustrates the specifications of this test scenario from a bird's-eye view. An operator's view of this scenario is illustrated in Figure 6.13(b).

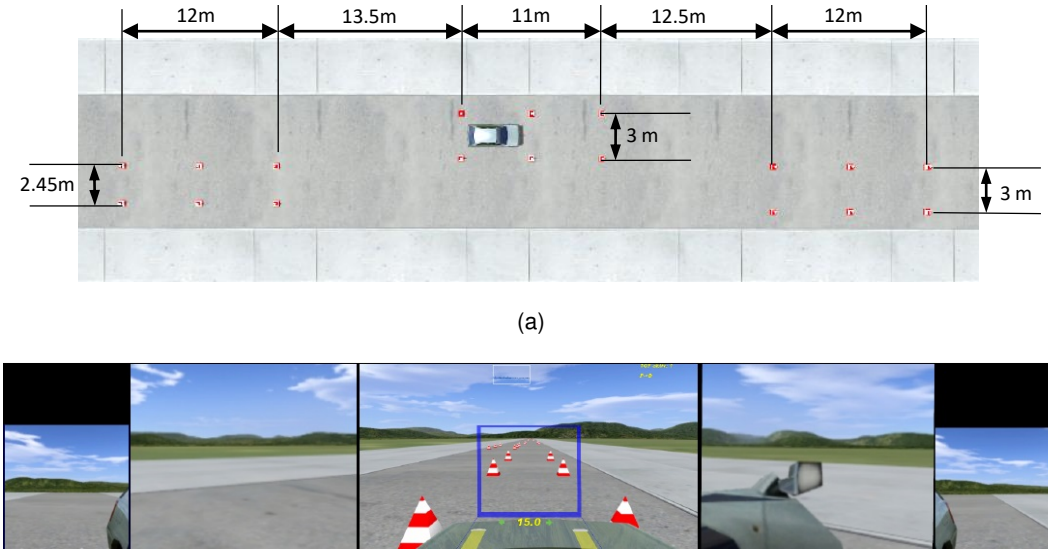

(a)

(b)

Figure 6.13 : (a) Specifications of the test scenario "Double Lane Change"; (b) A scene of this test scenario from operator's view

The entire test included 15 test drives with the following constellations:

- Five test drives without time delay and without haptic assistance;
- Five test drives with a constant time delay of 500 ms using the predictive display and without haptic assistance;
- Five test drives with a constant time delay of 500 ms using the predictive display and the developed haptic assistance system.

The test drives without time delay and without haptic assistance were considered as the basis for evaluating the driving performance of the test person using the operator's workstation.
To minimize the learning effect while evaluating the developed haptic assistance system, a mixed order of the test constellations, both those with and without using the haptic assistance system, were applied.
In the environment model of this test scenario, traffic cones are recognized as static obstacles and approaching them triggers an intervention by the haptic assistance system. The test persons were asked to drive as centrically as possible within the traffic cones without colliding with them.

The driving speed within the scenario has a direct influence on the results. Generally, drivers with greater driving abilities can perform this maneuver at higher speeds. Based on the results of the acclimatization test drives, a speed of 15 $\frac{km}{h}$ was chosen as a fair value for examining the driving limits of the test persons. With an upper velocity limit, some test persons still demonstrated acceptable driving performances, but others were not able to perform the maneuver. Since all of the test drives had to be conducted under the same conditions, the constant speed of 15 $\frac{km}{h}$ was determined for all test persons.

6.4.1.3.2 **Test scenario II: Collision Evasion**

This scenario evaluates the performance of the developed system within a dynamic environment. In this test scenario, the test persons are asked to drive within a narrow street, on both sides of which are parked several cars. The drivable area of the street between the parked cars was $4.2\ m$ wide.

During the test, one of the parked cars suddenly cuts into the middle of the street in front of the remote car. To avoid a collision, the human operator needs to evade this car. Figure 6.14(a) illustrates the specifications of this scenario. Figure 6.14(b) shows a scene from this scenario, in which one of the parked cars begins to suddenly cut into the middle of the street.

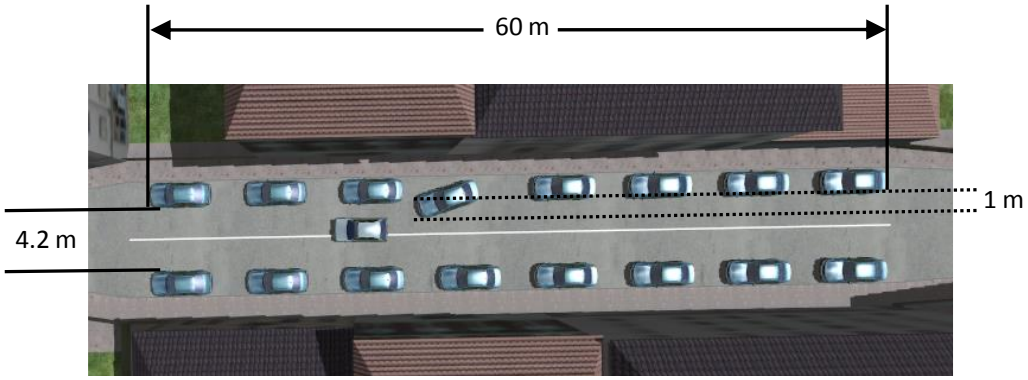

(a)

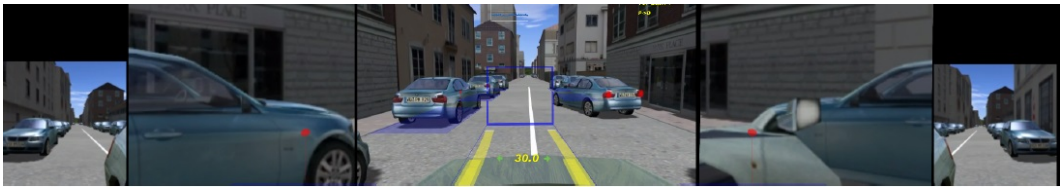

(b)

Figure 6.14 : (a) Specifications of the test scenario "Collision Evasion"; (b) A scene of this test scenario from operator's view, in which a parked car cuts suddenly into the middle of the street

Within this scenario, the test persons are made aware that one of the parked cars will cut into their path, but they do not know which vehicle will do so. The veering car is chosen randomly in each scenario and cuts in at a constant time before arriving in the path of the remote car. The test persons are asked to drive as centrically as possible without colliding with the static and dynamic obstacles or the veering car itself.

Similarly to the previous scenario, to minimize the learning effect the order of the test constellations, both those with and without the haptic assistance system, were mixed. The entire test included 15 test drives, using the same three constellations used in the double lane change test scenario.

Based on the results of the acclimatization test drives, a speed of 30 $\frac{km}{h}$ was determined as a fair limit for all test persons. Although some of the test persons could demonstrate a reasonable driving performance at higher speeds, others were not able to perform the maneuver at higher speeds. Hence, the constant speed of 30 $\frac{km}{h}$ was used in all test drives.

6.4.1.4 **Measured Parameters**

In order to evaluate the conducted test drives, several objective and subjective parameters were used, which are described below.

6.4.1.4.1 **Objective Parameters**

Since the main purpose of the developed assistance system is improving safety, appropriate objective parameters are required to evaluate whether or not this purpose was fulfilled.
As indicated in 5.4.2.1.1, the most obvious objective parameter for evaluating safety is the number of collisions that occurred.
Another important objective parameter for evaluating lateral safety is the severity of the lateral collisions that occurred during the test drives. The static obstacles in the simulated environment are not deformed after a collision. Hence, the entire overrun surface in a collision of the remote car with the static environment can be used as an objective parameter for measuring the severity of the collision. Figure 6.15 illustrates this parameter in an example collision.

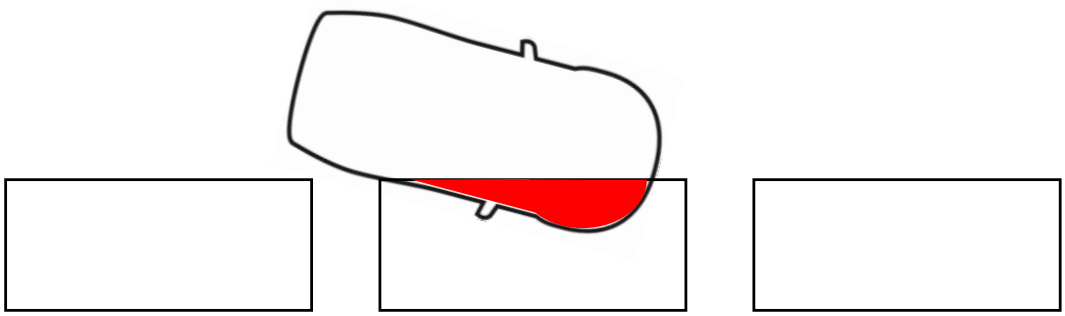

Figure 6.15 : The Overrun surface between the remote car and an obstacle, illustrated in red, as an objective parameter representing the severity of the occured collision

In addition to the parameters identified above, lateral deviation of the driven trajectories from the middle of the lane was measured. This parameter demonstrates the ability of a test person to control the car centrically, as requested in the test scenarios. In the double lane change test scenario, this parameter was measured only in areas that were surrounded by traffic cones.

6.4.1.4.2 **Subjective Parameters**

At the end of the test drives, the test persons were asked to fill out a questionnaire. This questionnaire assessed several subjective parameters, such as the impressions of the test persons concerning their perceptions of safety and comfort, as well as the level of assistance, while using the developed haptic assistance system.

6.4.2 Test Results

6.4.2.1 **Results of the Test Scenario: Double Lane Change**

Figure 6.16 shows the trajectories driven by one of the test persons within the double lane change test scenario. These trajectories represent the position of the center of gravity of the remote vehicle within the test track.
Figure 6.16(a) illustrates the driving performance of this test person while driving without any time delay. This result can be considered as representing a baseline for evaluating the performance of the developed assistance system under a time delay.
Figure 6.16(b) illustrates the trajectories driven by the same test person, with a time delay of 500 ms, using the predictive display. As can be seen, because of the time delay, the test person's ability to laterally control the remote car was significantly degraded. Several collisions with the traffic cones can be observed, particularly after the first lane change.
Figure 6.16(c) illustrates the trajectories driven by the same test person, with a time delay of 500 ms, using both the predictive display and the developed haptic assistance system. As can be seen, when compared to Figure 6.16(b), the ability of the test person to laterally control

the remote car improved significantly when using the haptic assistance.

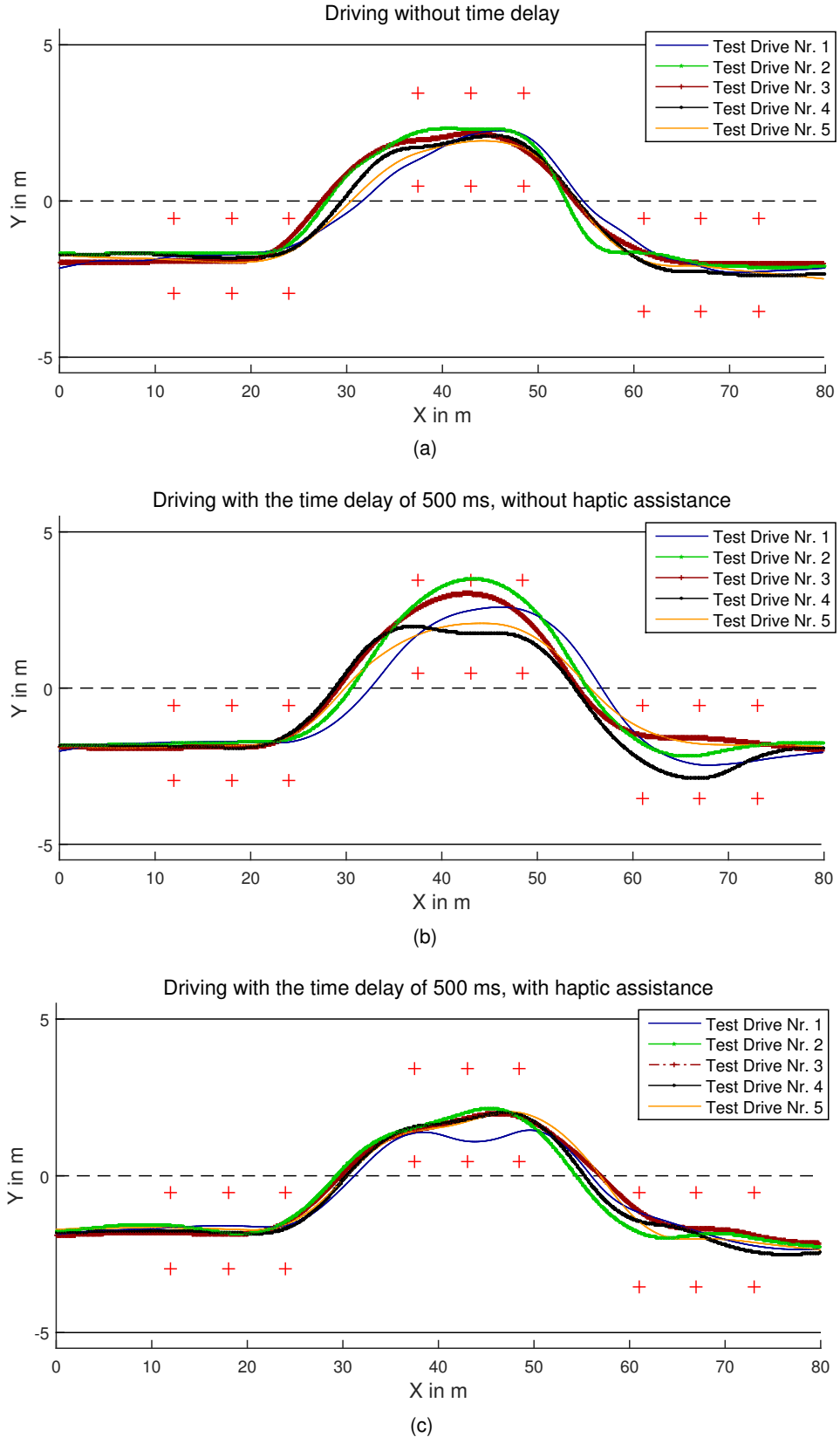

Figure 6.16 : Driving trajectory of the test person Nr. 4 within the test scenario "Double Lane Change": (a) Without time delay, (b) with the time delay of 500 ms and without haptic assistance, (c) with the time delay of 500 ms and using haptic assistance

Figure 6.17 provides an overview of the interventions of the haptic assistance system in the double lane change test scenario. As can be seen, after the virtual bumper collided with

the traffic cones, an assistance torque was applied to the steering wheel, which helped the operator to avoid a lateral collision.

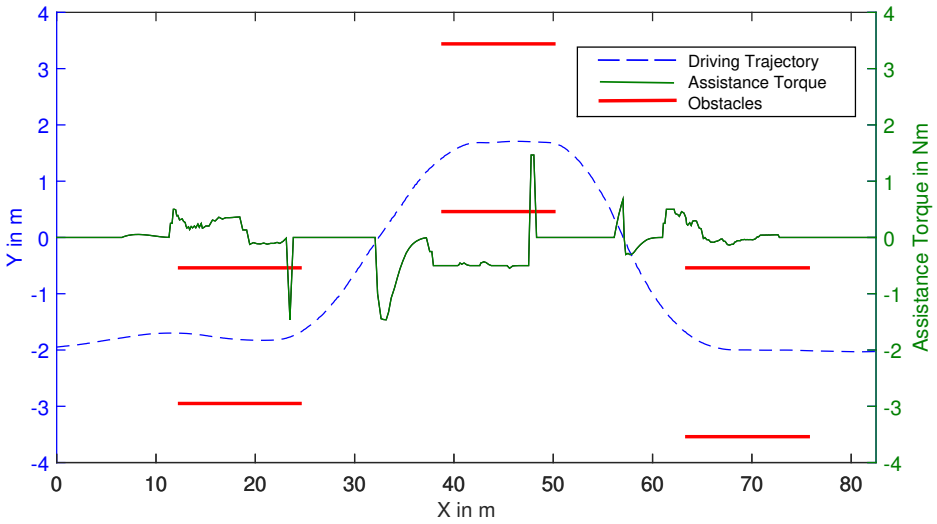

Figure 6.17 : Applied assistance torque in the test scenario "Double Lane Change" to avoid lateral collisions

The overall number of collisions that occurred for each test person, using each constellation, is illustrated in Figure 6.18. When comparing the two constellations that had a time delay, it can be seen that the use of the haptic assistance system reduced the total number of collisions of all test persons. This indicates an objective increase in lateral safety as a result of the use of the developed steering assistance system.

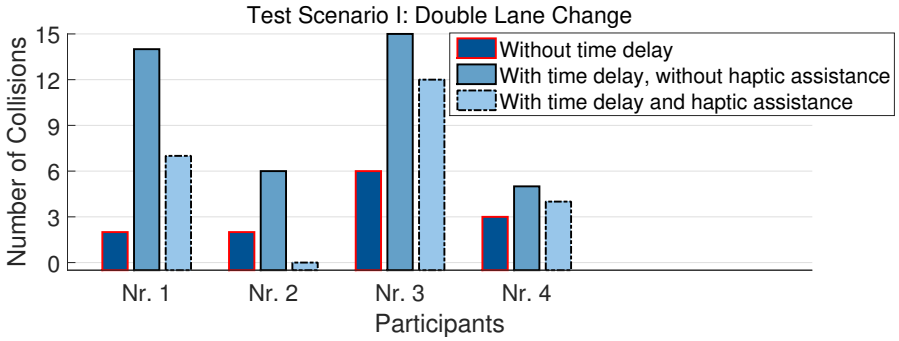

Figure 6.18 : The overall number of occurred collisions using three constellations in the test scenario "Double Lane Change"

In addition to tracking the number of collisions that occurred, their severity should also be considered. As indicated in Chapter 6.4.1.4, the overrun surface in each test drive can be used as an objective parameter for measuring the severity of the collisions that occurred. Figure 6.19 illustrates the average of this objective parameter for all three test constellations.
As can be seen, the average surface of occurred collisions was reduced for all test persons. This indicates an objective reduction in the severity of the collisions that occurred, which corresponds with an objective increase in lateral safety as a result of using the developed haptic assistance system.
However, it can also be seen that the extent to which safety was improved for each test person was different. This can be interpreted by considering the functionality of a steering assistance system, which cannot completely correct an inappropriate driving behavior. If the test person drives into a passage in an unsafe manner, the haptic assistance system warns him or her about the possibility of a lateral collision and attempts to assist him or her in avoiding the collision, but the final decision is made by the human operator. Hence, improving lateral

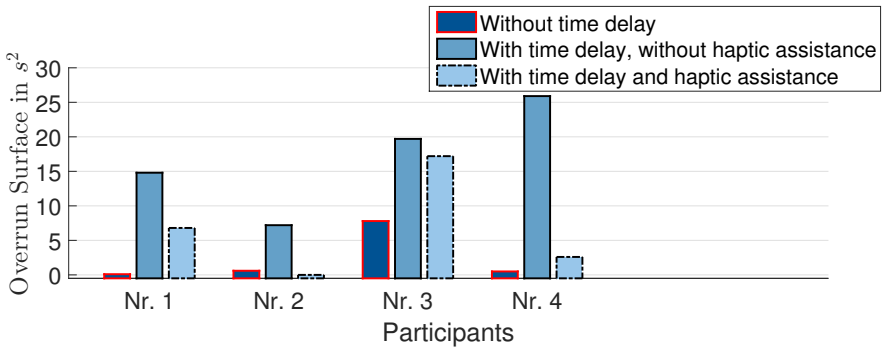

Figure 6.19 : The average overrun surface in the test scenario "Double Lane Change" by all test persons

safety by means of using a steering assistance system remains dependent on the driving performance of the operator.
Figure 6.20 illustrates the average deviation of the remote car from the centerline between the traffic cones in the double lane change test scenario. The different abilities of the test persons when it comes to controlling the remote car under the time delay can be obviously seen in this figure.

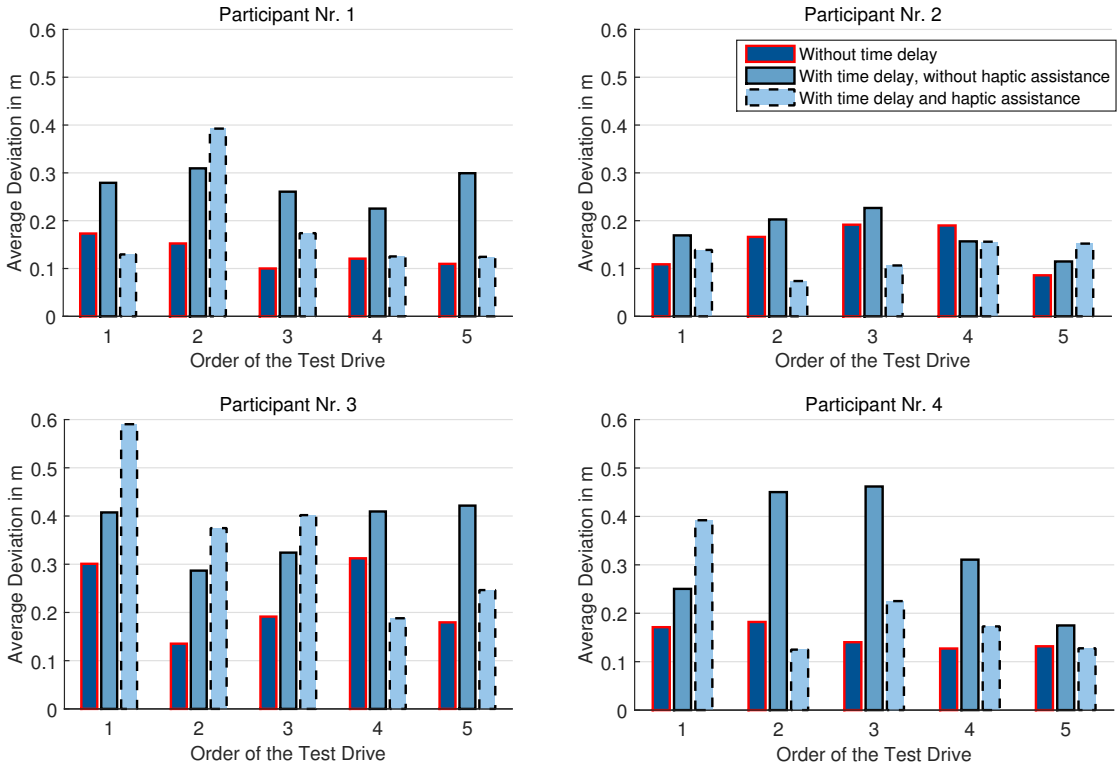

Figure 6.20 : Average deviation of the remote car from the centerline between the traffic cones in the test scenario "Double Lane Change"

These results indicate that steering assistance has a greater impact on the driving performance of more experienced test persons. As can be seen, test persons Nr. 4, Nr. 2 and Nr. 3 could drive with less deviation from the middle of the positioned traffic cones using the haptic assistance system, while no significant change in this objective parameter was demonstrated by test person Nr. 1. This could be a result of the fact that test person Nr. 1, having the least experience of teleoperated driving, needed a high level of concentration in order to handle the time delay. Any additional assistance system could not be properly used by her while driving.

6.4.2.2 **Results of the Test Scenario: Collision Evasion**

Figure 6.21 illustrates the trajectories driven by one of the test persons in the collision evasion test scenario. As can be seen in Figure 6.21(b), evading an obstacle under communication time delay, even when using the predictive display, causes fluctuation in the lateral control of the remote car. Considering that the illustrated trajectories represent the position of the center of the gravity of the remote car, a number of lateral collisions with the static obstacles located on both sides of the street can be observed.

As can be seen in Figure 6.21(c), lateral control of the car improves when the haptic assistance system is used. When drivers evaded the cut-in car, the haptic assistance system applied an assistance torque that warned the operator about the possible collision with the static obstacles located on the left side. This intervention makes it possible to avoid oversteering while evading obstacles and keeps the test person in control of the situation, meaning that he can robustly steer to the right side and guide the car into the middle of the narrow street.

Figure 6.22 illustrates the total number of lateral collisions that occurred with obstacles in the collision evasion scenario. When comparing the test drives performed under the communication time delay, the total number of collisions was significantly reduced when the haptic assistance system was used. However, there were two collisions with the haptic assistance system and even one without the time delay. The latter one again indicates the role of human as a source of failure in a vehicle's control loop.

6.4.2.3 **Subjective Impression of the Test Persons**

In order to evaluate the "impression of safety" as an important subjective parameter, after finishing all of the test drives in each test scenario, the test persons were asked whether they felt that using the proposed haptic assistance system improved lateral safety while driving. Figure 6.23 illustrates their answers to this question.

As can be seen, most of the test persons believed that lateral safety was improved as a result of using the proposed haptic assistance system. However, it should not be overlooked that test person Nr. 1 did not feel that safety was improved as a consequence of using the haptic system, although an obvious improvement in safety when using the haptic assistance system can be seen in her objective test results.

As another subjective parameter, in order to evaluate the "impression of comfort", the test persons were asked whether they felt that comfort they felt while engaged in teleoperated driving was improved as a result of using the proposed haptic assistance system. Figure 6.24 illustrates their answers to this question for both test scenarios.

As can be seen, the results mainly depended on the test scenario driven. Generally, it can be seen that the proposed haptic assistance system provides less comfort in the double lane change test scenario than in the collision evasion test scenario. It should be noted that the double lane change scenario is generally considered to be challenging and is mainly used to measure the limits of driving dynamics. Such a maneuver does not occur in normal urban scenarios. Given the answers provided by the test persons, it can be concluded that the developed system does not provide a high rate of comfort in critical driving situations. As can be seen, in the collision evasion test scenario, a higher level of comfort was provided through the use of the haptic assistance system.

In order to study their subjective impressions of the assistance provided by the developed system, the test persons were asked whether they found the level of assistance provided by the haptic assistance system to be sufficient. The answers of the test persons are illustrated in Figure 6.25. As can be seen, the difficulty levels of the driven scenarios directly affected the answers. However, an overall impact is that the test persons tended to receive a higher level of assistance. This could be realized through expanding on the proposed system by adding an autonomous trajectory planning system and using assistance torque to guide the vehicle along the planned trajectory. However, as described in Chapter 6.2, this requires a high level of environment perception, which is still a challenge in some urban environments.

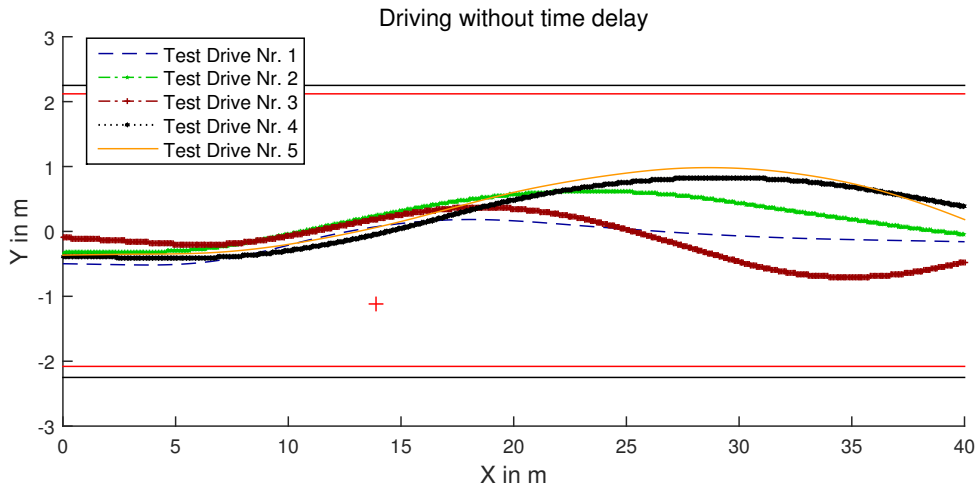

(a)

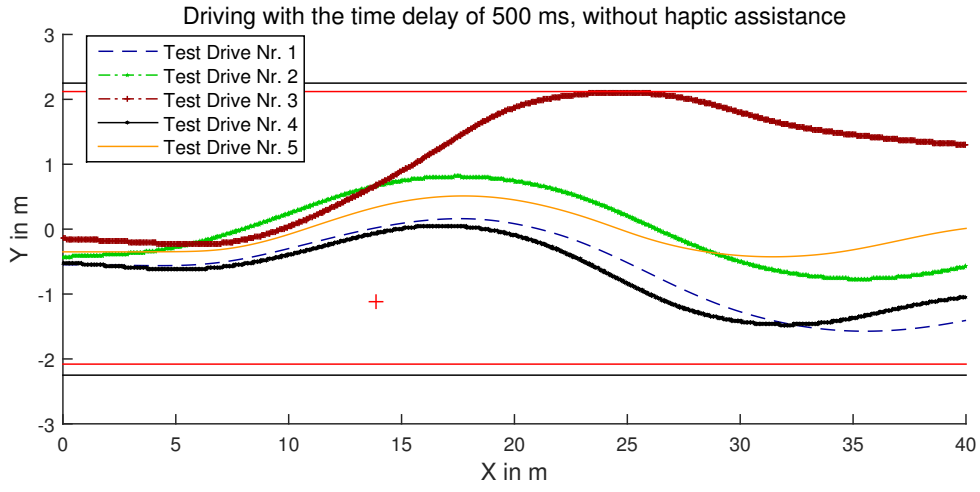

(b)

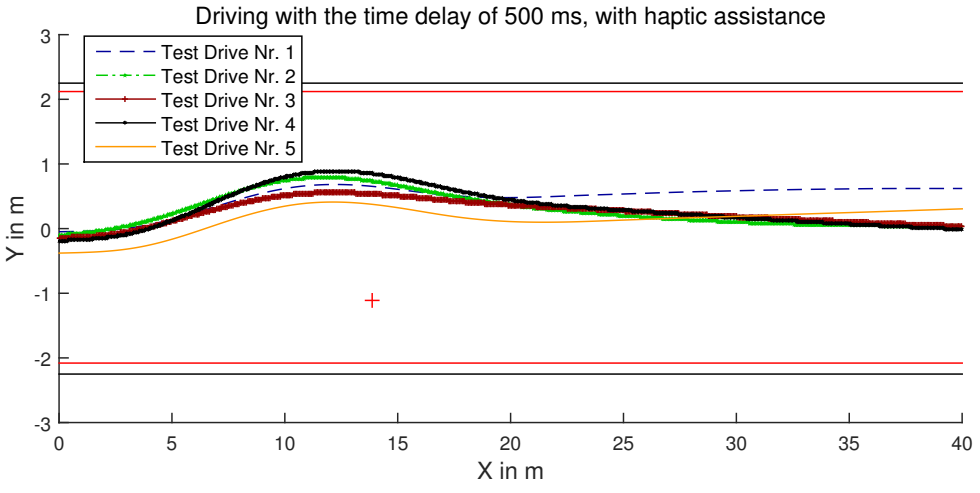

(c)

Figure 6.21 : Driving trajectory of the test person Nr. 4 within the test scenario "Collision Evasion": (a) Without time delay, (b) with the time delay of 500 ms and without haptic assistance, (c) with the time delay of 500 ms and using haptic assistance

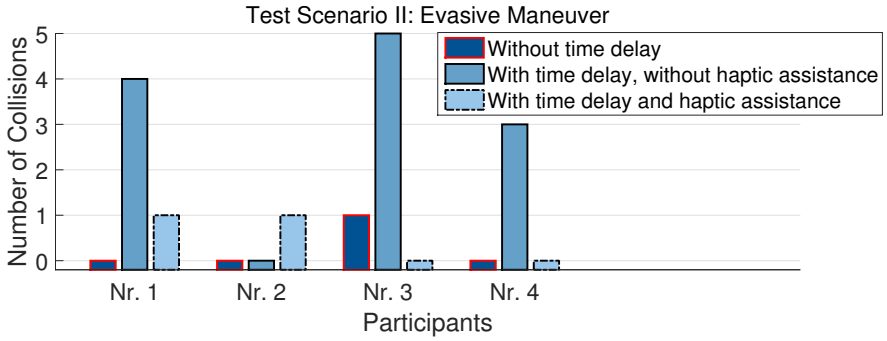

Figure 6.22 : The overall number of occurred collisions using three constellations in the test scenario "Collision Evasion"

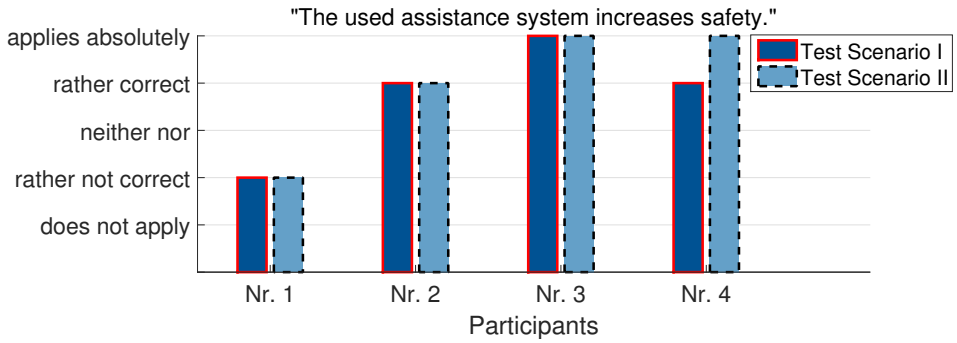

Figure 6.23 : Impressions of the test persons about "improving of safety"

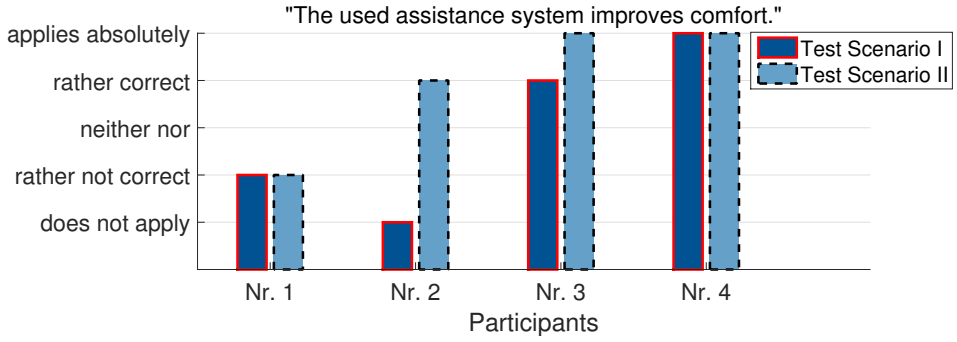

Figure 6.24 : Impressions of the test persons about "improving of comfort"

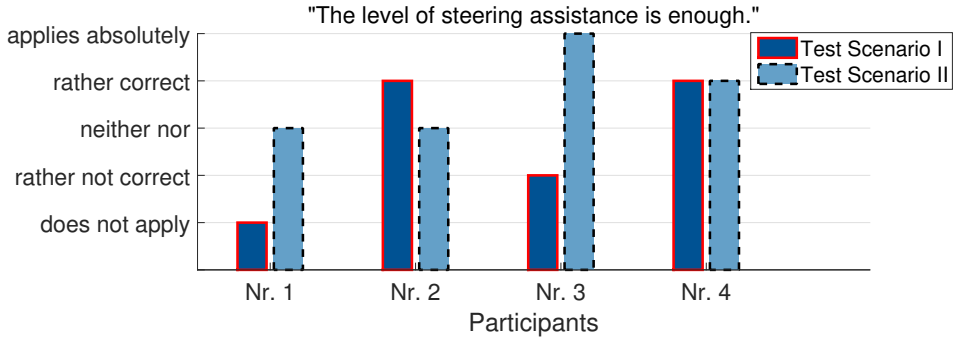

Figure 6.25 : Impressions of the test persons about the provided assistance level

6.5 Conclusion and Discussion

The objective parameters analyzed indicate a decrease in the number and severity of occurred collisions while driving in both scenarios with static and dynamic environments when

using the proposed haptic assistance system.
These results illustrate an improvement in lateral safety during teleoperated driving when using the proposed haptic assistance system, indicating that the system achieved its primary goal.
The subjective parameters analyzed suggest that the test persons tended to receive more assistance from the steering assistance system. This can be realized by combining of an autonomous trajectory planning system with the steering assistance system. As discussed within this work, this step remains a challenge in complex urban environments. In addition, should it become possible to achieve robust trajectory planning in all urban environments, a steering assistance system would no longer be required and the entire driving task could be performed autonomously.
In addition, this assistance system is not able to address all possible instabilities while an operator directly controls a remote car with a high communication time delay. Although this challenge can be partially addressed through the use of experienced operators, it would be necessary to replace the concept of direct control with shared control in order to completely overcome this difficulty.

7 Discussions on Teleoperated Driving

This chapter discusses the human-in-the-loop test drives conducted in this work to evaluate the developed concepts. In addition, two possible approaches for increasing the level of automation in teleoperated driving are briefly introduced and discussed. Finally, the communication challenges posed by the use of the fifth generation of mobile networks (5G) in teleoperated driving are discussed.

7.1 Human-in-the-Loop Test Drives

7.1.1 Simulated Test Environment vs. Real Test Environment

Employing a simulated environment for a human-in-the loop test has several advantages. One of the most important advantages is that the test drives can be repeated for all test persons under the same test conditions.
However, the results of a test drive conducted within a simulated environment may partially differ from the results of one within a real environment. These differences arise as a result of the ability of the tool used to simulate real driving conditions and from human factors.
Assuming that a tool can simulate real driving conditions with an acceptable deviation from reality, in some cases the human operator may not take the driving situation as seriously as he would when driving within a real environment. Test persons usually drive much more courageously in a simulated environment than in a real test environment, particularly in highly dynamic driving situations.
While driving within a simulated environment, the test persons are certain that their possible failures will not lead to real damage. Hence, after some training, a test person may begin to boldly drive up to the safety limits of the system or even exceed them.
Within a real test environment, test persons drive conservatively. Since they know that each minor failure may lead to fatal damage, they do not readily drive up to their safety limits. Hence, the final safety limits of the developed systems must be determined using highly dynamic test drives within real urban environments.

7.1.2 Human Factors

Although the concept of teleoperated driving benefits from the ability of the human operator to perceive the environment and make decisions, the existence of a human in the control loop can be in some cases a source of error.
As can be seen in several of the human-in-the-loop studies conducted in this research, test persons have varying levels of driving skills. Furthermore, even the same test person cannot always deliver the same driving results when repeating a test scenario.
Several parameters, such as driving experience, amount of experience with the operator's workstation and familiarity with computer games, may affect the driving performance of a human operator. A separate study would be required in order to determine the weight of each of above indicated factors as well as several other possible human factors.
This study requires a greater number of test persons with varying levels of driving experience. The most important hypotheses about safety, precision and controllability while teleoperated driving could be extracted from the results of the present work.
The test persons who participated in the conducted test drives of the present study required several initial training sessions in order to become acquainted with the operator's workstation, the HMI and the developed control concepts for teleoperated driving. After determining the average driving limits, which can affect even the best-trained test persons, it would be necessary to develop a specific exam that an individual would need to complete before being issued with a teleoperated driver's license. Using such an approach, it would be possible to ensure that human operators possess the skills required to remotely control a car in urban

traffic.

7.2 Increasing the Level of Automation in Teleoperated Driving

Using a higher level of intelligence in the remote car, the level of automation in vehicle teleoperation could be increased. This chapter introduces two possible methods for achieving this goal.

7.2.1 Automating of Teleoperated Driving Through Interactive Path Planning

The shared control concept provides an appropriate basis for increasing the level of automation of a driving task. The concept of trajectory-based control [41] represents a form of shared control between the human operator and the remote vehicle. As described in Chapter 3, lateral control of a remote car using this control concept is a challenge. In several scenarios, this challenge forces a human operator to undergo several steps: stopping the car, generating an appropriate trajectory using the steering wheel and the gas pedal and sending it to the remote car. Since this approach would result in the car occasionally coming to a halt, it would not be appropriate for driving in all urban environments.

As proposed in [143], a solution to the above-mentioned problem that does not require the use of an offline digital map would be finding appropriate paths in the occupancy grid and suggesting them to the human operator.

There are different approaches to autonomous path planning. Generally, the majority of these approaches can be divided into two categories: heuristic search algorithms and numerical optimization approaches.

The heuristic search algorithms demonstrate rapid performance but mostly do not consider vehicle dynamics. Hence, their results are normally on their own inadequate for use in automotive applications.

This category includes different approaches, such as A*, D* [122] and their variants including TWD* and E* [123], which search for the shortest path between two known positions.

Numerical optimization approaches such as MILP-based approaches [13] and model predictive control [124] consider vehicle dynamics in path planning. Although the results of these approaches are kinematically feasible, their slow convergence, as a result of dropping in multiple local minima, makes it difficult to utilize them for real-time applications.

An appropriate approach for exploiting the advantages of both of these categories while suppressing their disadvantages would be their combination in two stages. For this purpose, in the first stage, a sub-optimal solution needs to be found by means of a heuristic search algorithm. In the second stage, the solution found must be optimized using numerical optimization. Thereby, the kinematic quality and calculation speed of the path planning can be ensured.

A similar approach for path planning in a parking lot is proposed by Dolgov *et al.* [125], which in its first stage finds a sub-optimal path using the A* approach and in its second stage optimizes this path by means of numerical optimization. In this approach, the target position is predefined on a parking garage's offline map, which is necessary for path planning using the A* approach.

To plan appropriate paths during teleoperated driving without using a digital map, the target position can be predefined. Hence, most heuristic search algorithms cannot be used for this application.

The rapidly-exploring random tree (RRT) [126] is a rather new approach that does not need a predefined target position for path planning. This characteristic, as well as the fact that this tree considers vehicle dynamics in path planning, makes it an appropriate approach for increasing the level of automation in teleoperated driving without the use of a digital map.

The RRT builds a space-filling tree-structured graph in order to explore a search space. The tree grows incrementally based on the sample points or states, which are created randomly. Hence, in each step the nodes are created based on their successive nodes and expanded

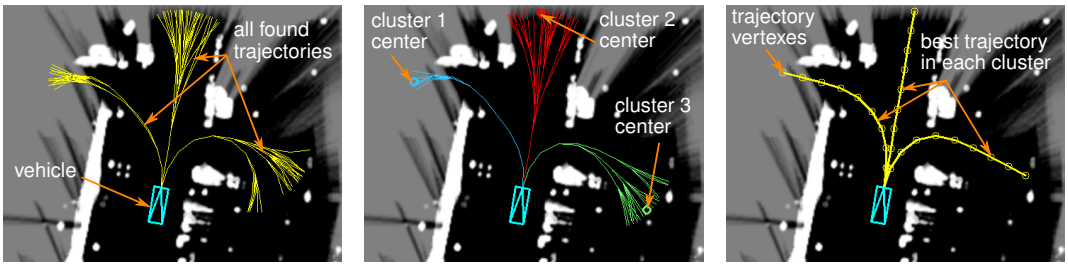

(a) (b) (c)

Figure 7.1 : Results of RRT path planning: (a) all paths found by RRT, (b) clustering of the results and (c) selection of the best paths [143]

into all of the free spaces in the search area. During this expansion, the drivability of the propagated path is proven.
Using RRT, several possible paths can be generated during teleoperated driving. However, since these paths are not optimal in some ways, they need to be optimized thereafter.
As described in [143], this procedure can be realized using a two-step approach. In the first step, a modified RRT approach is used to find, cluster and select the possible paths on the occupancy grid. Figure 7.1 illustrates the clustering and selection of the suitable paths generated by this modified RRT approach.
In the second step, the resulting paths are optimized through minimizing of the following cost function:

$$J = w_1 \cdot \sum_{k=0}^{N} \phi(x_k, y_k) + \frac{1}{2} \cdot w_2 \cdot ((x_N - x_z)^2 + \ + (y_N - y_z)^2) + \frac{1}{2} \cdot w_3 \cdot \sum_{k=1}^{N} (u_k - u_{k-1})^2,$$

in which $\phi(x_k, y_k)$ represents the potential value of the trajectory vertexes. The middle term minimizes the difference between the end point of the trajectory from RRT (x_z, y_z) and the end point of the optimized one (x_N, y_N). The last term minimizes the changes in the steering angle u as much as possible, since a smooth steering angle curve is more favorable for the vehicle control.
Through this optimization, the number of mesh vertexes in the generated trajectory is increased and the distance between the vehicle path and exsiting obstacles in the scene is optimized. Figure 7.2 shows the result of the optimization step in an example scenario.

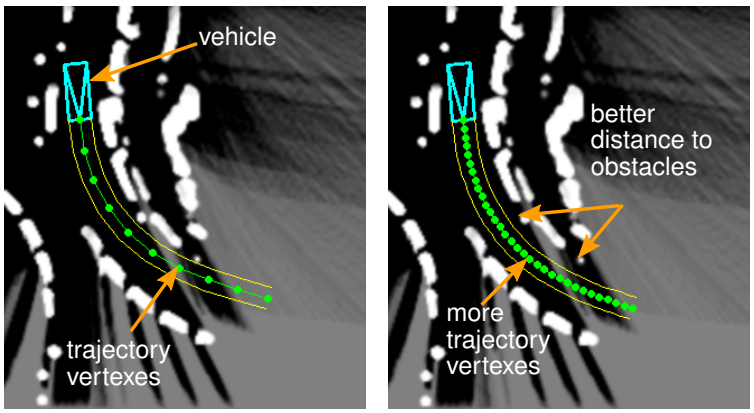

(a) (b)

Figure 7.2 : Generated trajectory without (a) and with (b) optimization step [143]

The resulting paths are then transmitted from the teleoperator to the human operator and

displayed by means of augmented reality on the operator's interface. Fig. 7.3 illustrates the projection of an example of a generated path using the above-mentioned approach from the occupancy grid into the camera image displayed on the operator's interface.

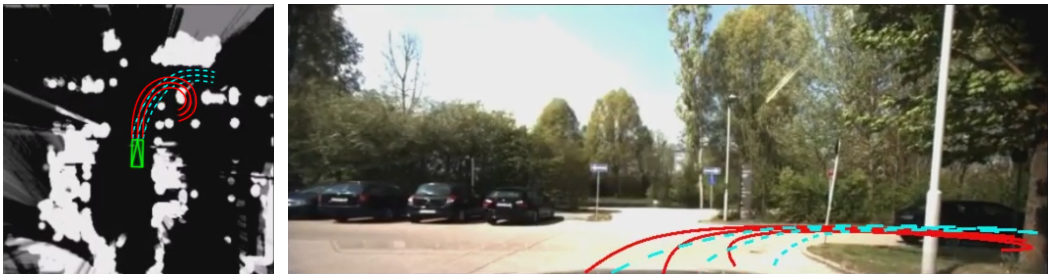

(a) (b)

Figure 7.3 : Comparison of the manually generated path (red) as well as the autonomous generated path (aqua) [143]

The red trajectory in this image is generated by the human operator using the steering wheel and gas pedal, as indicated in [41]. As can be seen, this manually generated Euler spiral is not appropriate for negotiating a curve. Using this approach, the operator would need to manually generate several short trajectories to pass a curve.
Instead of requiring these efforts, the autonomously generated path suggested by the above-mentioned approach (illustrated dashed in aqua) can be confirmed by pressing a button on the steering wheel of the operator's workspace. The remote vehicle will then autonomously follow this confirmed path.

7.2.2 Teleoperated Driving as a Backup for Driverless Driving

At a higher level of automation, teleoperated driving can be seen as a backup for driverless driving. After further development of the technologies required for environment perception, as well as the provision of frequently updated high-definition maps for all urban environments, the majority of the driving task could be performed autonomously. However, it is possible that in some cases a driverless car could not autonomously drive beyond a certain point.
A variety of different reasons may cause such inconveniences for driverless cars. For example, if due to construction the environment changes and this change has not been captured on the offline digital map, the ego-localization system of the driverless car may encounter difficulty when attempting to determine its exact position on the digital map. A similar problem may occur if a vehicle's sensor gets damaged or dusty. In addition, bad weather or poor light conditions can make the recognition of the landmarks on the digital map difficult.
Since, in such cases the car has no passenger or has a passenger who cannot be asked to solve the problem, rapid help from beyond the car would be required. Teleoperated driving would be an appropriate solution for solving such problem. After the autonomous car detects its inability to go further, it would need to bring itself to a safe state and inform the teleoperation call center of the problem. Then, a human operator could remotely drive the car to a position from which it can autonomously drive further.
Since in this use case a high-definition digital map is available, teleoperated driving can be performed at a high level of automation. If the problem confronted by the autonomous car lies in decision-making, the shared control concept seems to be a better solution than the direct control concept. Using shared control, the existing intelligence of the car can be used to relieve the human operator while he is engaged in teleoperated driving.
Should driverless cars enter the market on a large scale, a teleoperation center would need to supervise a large number of them. In this case, the "scalability" of the teleoperation service would become more important.
For this use case, it is not feasible to devote a human operator to each autonomous car, rather a single operator would be responsible for several cars. Since a human operator is unable to simultaneously control several remote cars, each car would need to be able to bring itself to a

safe state after facing a challenge to drive autonomously. The number of cars supervised by each human operator would directly depend on the amount of support that each autonomous car would require from the teleoperation center on a daily basis.
One of the most important factors when considering the scalability of teleoperation services is the amount of data transferred between the autonomous car and the teleoperation center. To enable the simultaneous supervision of several autonomous cars from a teleoperation center, it would be necessary to reduce the size of the data required for the teleoperation task as much as possible. The majority of the data transferred for the teleoperation task is accounted for by the uploading of camera images from the remote car to the operator workstation. The indicated value of approximately 3 Mbit/s to transfer three compressed camera images in this work would be too much for a high-scale teleoperation task.
This data size could be reduced through a combination of the mixed-reality HMI concept, proposed in Chapter 4, with a high-definition digital map. A high-definition digital map would provide some detailed information about the vehicle's surroundings, in addition to the information which can be gained by the vehicle's sensors. This would allow for the weight of reality within the mixed-reality environment to be reduced, which would lead to a reduction in the amount of data transferred from the remote car to the operator's workstation.
To decrease the weight of reality within the mixed-reality environment, the transmission of camera images with a lower priority, such as side camera images, would need to be minimized. Then, the missing information from these camera images would need to be reconstructed by means of virtual reality, using the existing information about the scene provided by the high-definition digital map as well as on the dynamic occupancy grid.

7.3 Communication Challenges

7.3.1 Expected Developments Using 5G

The first version of the fifth generation of the mobile communication network (5G) will be released approximately around 2020 [127], although some of its pilot versions will be tested beforehand.
At the current time, a data rate 100 times higher than that which today's wireless networks offer is targeted by this mobile communication network. In addition, it is promised that the communication jitters experienced by this standard will be significantly lower than the existing jitters in the fourth generation of the mobile communication network (LTE).
This standard will significantly affect teleoperation technology. Using this standard, the current time delay encountered when uploading camera images from a remote car to the operator's workstation be decreased. In addition, the need for compression and decompression of the images before and after transmission could be eliminated. However, the time delay will not be completely eliminated and a part of it will remain.
As described in this work, one of the main challenges in vehicle teleoperation using the existing wireless communication standards, such as 4G LTE, is the communication time delay. Using 5G, this time delay will be minimized and the current restrictions on the speed of teleoperated driving will be lifted.
However, wide coverage of this standard in all urban areas will only be provided a number of years after its first release. It is expected that, until that time, the technologies required for autonomous driving in cities will continue to enjoy great progress. This may lead to a significant combination of fully automated driving with teleoperated driving, as described in Chapter 7.2.2.

7.3.2 Communication Loss

Besides the communication time delay and lack of situation awareness, communication loss is one of the main challenges in vehicle teleoperation, whose solving was not in the focus of this work. The probability of communication loss during teleoperated driving can be reduced through the network provider ensuring a high quality of service as well as attempting to restrict

navigation of remote vehicles to areas that are completely covered by mobile communication services. However, communication loss will always remain a risk during teleoperation and cannot be completely avoided.
As can be seen in several sections of this work, such as in Figures 4.1, 5.11 and 6.1, the "free corridor" concept [128] was used in combination with predictive display in the context of the direct control concept.
Given the experiences obtained by means of several test drives, the free corridor concept does not seem to be an appropriate approach for handling the challenges posed by communication loss.
On one hand, this concept does not consider the parallel challenge of communication time delay. The operator is asked to keep a visualized brake path free while the visualized scene itself is delayed. Hence, it is possible that a dynamic obstacle could suddenly enter the visualized brake path and the operator would only perceive it after the communication time delay. Therefore, it cannot be guaranteed that the operator would always be able to keep the visualized "corridor" free.
On the other hand, this concept draws the attention of the human operator to the visualized brake path, which may lead to his becoming distracted and overlooking other traffic participants. As described previously, the predictive display concept relies completely on augmented reality to visualize the predicted positions of the remote car and other traffic participants. Adding an additional augmented reality such as the "free corridor" could lead to exceeding the limits of the augmented reality, which could be taken into account by a human operator while engaged in teleoperated driving.
In addition, full braking after a possible communication loss does not seem to be a suitable reaction in urban environments. Such a braking behavior results in inconvenience for the possible passengers of the remote car and increases the crash probability from the rear side.
The above-mentioned weaknesses of the free corridor concept illustrate the need for a more appropriate solution for ensuring the safety of a remote vehicle after a possible communication loss. This could be realized through improving the machine intelligence in the remote car. After a possible communication loss, the vehicle should autonomously bring itself to a safe state and avoid full braking as much as possible under such conditions.

8 Conclusion and Outlook

This work has aimed to improve precision and safety in teleoperated driving in urban environments. For that purpose, a package of advanced driver assistance systems is proposed that removes some existing limits of this mobility concept. This package includes a HMD-based HMI to increase precision and two safety assistance systems that autonomously intervene in the longitudinal and lateral control of the car.
The proposed HMD-based HMI provides a mixed reality environment that uses sensor data from the remote vehicle. This HMI significantly enhances situation awareness and thus the telepresence of the human operator. The mixed reality environment created simulates those parts of the vehicle surroundings that are missing from the camera images received, as well as the exact borders of the remote vehicle as a virtual reality construct. In addition, certain key parts of the operator's workstation, such as the steering wheel and pedals, are added to this virtual environment. The resulted 360° virtual environment decouples the human operator from the stationary workstation and increases the sensation of being in the remote vehicle.
As studied in several test drives, the enhancement of telepresence improves the human operator's task performance in precisely controlling the remote car. The test results show that all test persons could control the teleoperator with greater precision and safety within narrow passages.
Although the use of active safety systems is optional for car drivers, the use of these systems is necessary while teleoperated driving due to existing of communication time delay.
The predictive brake assistance proposed in this study takes into account the delayed perception of the environment by the human operator. To solve this challenge, it predicts the dynamic environment by using a stereo-vision system and autonomously intervenes in the braking task before the human operator perceives a hazard. It thus compensates for the time delay in communication and ensures the frontal safety of the remote car.
The results of several test drives conducted by experienced operators show an improvement in collision avoidance and an overall increase in TTC in hazardous scenarios when the proposed brake assistance system is used. In addition, the average of triggered brakes on a simulated urban test track shows an overall decrease in the deceleration required to avoid collisions with the proposed brake assistance system. These results illustrate increasing of safety and improving of braking behavior during teleoperated driving when using the proposed assistance system.
The proposed haptic assistance system tackles the safety hazards in the lateral control of a remote car through intervention in the steering system. The time delay in the lateral control of the remote car, even when using a predictive display and employing experienced operators, leads to an obvious instability. When driving in an urban environment with dense traffic, this instability could result in safety hazards.
To address this challenge, the proposed haptic assistance system generates an assistance torque on the steering wheel of the operator's workstation. The intervention logic of the system is based on an environment model that is created using sensor measurement data from the remote car. For that purpose, a LiDAR-based occupancy grid is created at the operator's workstation, the effect of time delay is eliminated and a virtual safety zone around the remote car is defined. Once this virtual safety zone collides with an obstacle, the assistance torque is generated and guides the human operator to avoid the danger.
Several test drives conducted in both static and dynamic environments show that the proposed haptic assistance system improves the safety of the lateral control of the remote car. Using this system, both the number of collisions and their severity decreased. The assistance torque generated increases the situation awareness of the human operator, alerting that individual to the possibility of a lateral collision. However, since the human operator remains the main decision maker in the control loop, this assistance system cannot guarantee total collision avoidance.

The proposed HMI and ADAS for teleoperated driving has been realized in an experimental test car using a sensor package consisting of radar, LiDAR, and a stereo camera system. To examine the concepts developed at the safety limits of teleoperated driving, a human-in-loop test environment with a simulated test track is employed. In the next development steps of teleoperated driving, the developed HMI and ADAS needs to be examined in real urban environments with dense traffic and at high driving velocities. To study different human factors, a large number of test persons should be used in these test drives.
It is expected that part of the identified safety challenges will be suppressed after the launch of the 5th generation of the mobile communication network (5G). However, since part of the time delay remains in the control loop, 5G technology alone cannot eliminate the need for specific safety assistance systems to control teleoperated vehicles. In addition, in the near future, with the continued development of machine intelligence, more driving tasks can be given over to the machine, which could make employing a human operator as the supervisor of several automated cars possible. These steps in the technological progress make employing the concept of teleoperated driving as a transient technology or backup solution on the path driverless driving in urban environments even more important.

List of Figures

List of Tables

Lists of Abbreviations

4G Fourth Generation of Wireless Mobile Telecommunications Technology
5G Fifth Generation of Wireless Mobile Telecommunications Technology
ABS Anti-lock Braking System
ACC Adaptive Cruise Control
ADAS Advanced Driver Assistance System
ADTF Automotive Data and Time-Triggered Framework
AEB Autonomous Emergency Braking
BASt Bundesanstalt für Straßenwesen
CAN CAN Controlled Area Network
CES Consumer Electronics Show
CMOS Complementary Metal-Oxide-Semiconductor
CNN Convolutional Neural Network
CU Collision Unavoidable
CUDA Compute Unified Device Architecture
DGPS Differential Global Positioning System
EKF Extended Kalman Filter
ESP Electronic Stability Program
FOV Field of View
GiGE Gigabit Ethernet
GNSS Global Navigation Satellite System
GPS Global Positioning System
GPU Graphics Processing Unit
GSM Global System for Mobile Communications
HMD Head-Mounted Display
HMI Human-Machine Interface
HUD Head-up Display
ITQ Immersive Tendencies Questionnaire
JIPDA Joint Integrated Probabilistic Data Association
LiDAR Light Detection and Ranging
LKA Lane Keeping Assist
LOD Level of Difficulty
LTE Long Term Evolution
MILP Mixed Integer Linear Programming
MWC Mobile World Congress
NASA The National Aeronautics and Space Administration
OPTICS Ordering Points To Identify the Clustering Structure
RCP Rapid Control Prototyping
RRT Rapidly-Exploring Random Tree

RV Reality-Virtuality

SA Situation Awareness

SAE Society of Automotive Engineers

TIT Time Integrated Time-to-Collision

TTC Time-to-Collision

TUM Technische Universität München

UDP User Datagram Protocol

UMTS The Universal Mobile Telecommunications System

V2X Vehicle-to-X

List of Symbols

Symbol	Unit	Description
v	$\frac{\mathrm{m}}{\mathrm{s}}$	Velocity
v_{diff}	$\frac{\mathrm{m}}{\mathrm{s}}$	Relative velocity of the teleoperator to the obstacle
a	$\frac{m}{s^2}$	Acceleration
D	$\frac{m}{s^2}$	Deceleration
D_{max}	$\frac{m}{s^2}$	Highest possible deceleration of the car
$D_{PartialBraking}$	$\frac{m}{s^2}$	Deceleration while partial braking
$d_{PredictedDistance}$	m	Distance of the remote vehicle to the predicted collision point
$d_{Reaction-Stopping}$	m	Distance in x-direction
$d_{FullBraking}$	m	Driven distance while full braking
d_{LC}	m	Lateral distance of the vehicle to the lane mark
t	s	Time
Δt	s	Communication time delay
t_{Total}	s	Total reaction time
t_{P-R}	s	Perception-reaction time of the human operator
t_{Video}	s	Time required to transmit the video images
$t_{Control}$	s	Time required to transmit the control signals
$t_{BrakeActivation}$	s	Activation time of the brake actuator
t_{driven}	s	Time required to drive a specific track
t_{LC}	s	Time-to-line-crossing (TLC)
t_{LA}	s	Look-ahead time
x	m	Distance in x-direction
y	m	Distance in y-direction
Ψ	°	Course angle
κ	$\frac{1}{\mathrm{m}}$	Road curvature
C_0	$\frac{1}{\mathrm{m}}$	Initial curvature of Euler spiral
C_1	$\frac{1}{\mathrm{m}^2}$	Change of curvature of Euler spiral
l	m	Path Coordinates
L	m	Length of a segment
n_{gap}	-	Absolute number of steering reversals within a driven track
t_{TC}	s	Time-to-collision (TTC)
$\mathbf{u}$	-	Two-dimensional displacement field of each image point
ϕ	°	Angle between the longitudinal axis of the vehicle and traffic lanes
ψ	°	Side slip angle
β	°	Heading angle
b	m	Car's width
u	°	Steering angle

Literature

[1] "Google self driving car testing report on disengagements of autonomous mode", IEEE Connected Vehicles, Tech. Rep., 2015.

[2] S. Gnatzig, F. Chucholowski, T. Tang, and M. Lienkamp, "A system design for teleoperated road vehicles", in *ICINCO 2013 - Proceedings of the 10th International Conference on Informatics in Control, Automation and Robotics*, 2014, pp. 231–238, ISBN: 978-989856571-6.

[3] A. Cornet, M. Mohr, F. Weig, B. Zerlin, and A. Hein, "Mobility of the future. opportunities for automotive oems", McKinsey & Company, Tech. Rep., 2012.

[4] S. Shaheen and A. Cohen, "Innovative mobility carsharing outlook - winter 2016", Innovative Mobility Research, University of California, Berkeley, Tech. Rep., 2016.

[5] F. Chucholowski, "Eine vorausschauende Anzeige zur Teleoperation von Straßenfahrzeugen", PhD thesis, Technische Universität München, München, 2015, ISBN: 978-3-8439-2480-1.

[6] F. Chucholowski, T. Tang, and M. Lienkamp, "Teleoperiertes Fahren: Sichere und robuste Datenverbindungen", *ATZelektronik*, vol. 9, no. 1, pp. 60–63, 2014, ISSN: 1862-1791. DOI: 10.1365/s35658-014-0390-z. [Online]. Available: http://dx.doi.org/10.1365/s35658-014-0390-z.

[7] *Standard J3016: Taxonomy and definitions for terms related to on-road motor vehicle automated driving systems*, 2014.

[8] M. Gasser, "Ergebnisse der Projektgruppe Automatisierung: Rechtsfolgen zunehmender Fahrzeugautomatisierung", in *7. Tagung Fahrerassistenz*, 2015.

[9] K. Bengler, K. Dietmayer, B. Färber, M. Maurer, C. Stiller, and H. Winner, "Three decades of driver assistance systems: Review and future perspectives", *Intelligent Transportation Systems Magazine, IEEE*, vol. 6, no. 4, pp. 6–22, 2014, ISSN: 1939-1390. DOI: 10.1109/MITS.2014.2336271.

[10] H. Lategahn and C. Stiller, "Vision-only localization", *IEEE Transactions on Intelligent Transportation Systems*, vol. 15, no. 3, pp. 1246–1257, 2014, ISSN: 1524-9050. DOI: 10.1109/TITS.2014.2298492.

[11] C. Szegedy, W. Liu, Y. Jia, P. Sermanet, S. Reed, D. Anguelov, D. Erhan, V. Vanhoucke, and A. Rabinovich, "Going deeper with convolutions", in *Computer Vision and Pattern Recognition (CVPR)*, 2015. [Online]. Available: http://arxiv.org/abs/1409.4842.

[12] R. Girshick, J. Donahue, T. Darrell, and J. Malik, "Rich feature hierarchies for accurate object detection and semantic segmentation", in *2014 IEEE Conference on Computer Vision and Pattern Recognition*, 2014, pp. 580–587. DOI: 10.1109/CVPR.2014.81.

[13] C. Goerzen, Z. Kong, and B. Mettler, "A survey of motion planning algorithms from the perspective of autonomous uav guidance", *Journal of Intelligent and Robotic Systems*, vol. 57, no. 1-4, pp. 65–100, 2010, ISSN: 0921-0296. DOI: 10.1007/s10846-009-9383-1. [Online]. Available: http://dx.doi.org/10.1007/s10846-009-9383-1.

[14] *Intuitive Surgical Iinc.* [Online]. Available: https://www.intuitive.com/.

[15] *The National Aeronautics and Space Administration. MSL's Curiosity: A big rover on a bold mission*, 2012. [Online]. Available: https://www.nasa.gov/centers/dryden/Features/msl_curiosity_colloquium.html.

[16] *H2000-INS/ROV (Remotely Operated Vehicle), ECA Group Hytec*, 2017. [Online]. Available: http://www.ecagroup.com/en/solutions/h2000\-ins\-rov\-remotely\-operated\-vehicle.

[17] G. T. Sunga and I. S. Gill, “Robotic laparoscopic surgery: A comparison of the da vinci and zeus systems”, *Urology*, vol. 58, no. 6, pp. 893–898, 2001.

[18] *United States Air Force. MQ-1B Predator*, 2013. [Online]. Available: http://www.af.mil/AboutUs/FactSheets/Display/tabid/224/Article/104469/mq-1b-predator.aspx.

[19] J. M. Teixeira, R. Ferreira, M. Santos, and V. Teichrieb, “Teleoperation using google glass and ar, drone for structural inspection”, in *Virtual and Augmented Reality (SVR), 2014 XVI Symposium on*, 2014, pp. 28–36. DOI: 10.1109/SVR.2014.42.

[20] S. Lichiardopol, “A survey on teleoperation”, *(DCT rapporten; Vol. 2007.155). Technische Universiteit Eindhoven.*, 2007. [Online]. Available: https://pure.tue.nl/ws/files/4419568/656592.pdf.

[21] W. Griffin and S. U. D. of Mechanical Engineering, *Shared Control for Dexterous Telemanipulation with Haptic Feedback*. Stanford University, 2003. [Online]. Available: http://books.google.de/books?id=UWwTPQAACAAJ.

[22] K. Salisbury, “Issues in human/computer control of dexterous remote hands”, *Aerospace and Electronic Systems, IEEE Transactions on*, vol. 24, no. 5, pp. 591–596, 1988, ISSN: 0018-9251. DOI: 10.1109/7.9687.

[23] T. W. Fong, “Collaborative control: A robot-centric model for vehicle teleoperation”, PhD thesis, Robotics Institute, Carnegie Mellon University, Pittsburgh, PA, 2001.

[24] F. O. Flemisch, C. A. Adams, S. R. Conway, K. H. Goodrich, M. T. Palmer, and P. C. Schutte, “The h-metaphor as a guideline for vehicle automation and interaction”, NASA Langley Research Center; Hampton, VA, United States, Tech. Rep., 2003. [Online]. Available: https://ntrs.nasa.gov/archive/nasa/casi.ntrs.nasa.gov/20040031835.pdf.

[25] T. Sheridan, “Space teleoperation through time delay: Review and prognosis”, *Robotics and Automation, IEEE Transactions on*, vol. 9, no. 5, pp. 592–606, 1993, ISSN: 1042-296X. DOI: 10.1109/70.258052.

[26] T. Tang, “Methods for improving the control of teleoperated vehicles”, PhD thesis, Technische Universität München, 2015. [Online]. Available: https://mediatum.ub.tum.de/doc/1236115/1236115.pdf.

[27] *Capio upper body exoskeleton for teleoperation, Robotics Innovation Center (RIC), DFKI GmbH*. [Online]. Available: http://robotik.dfki-bremen.de/en/research/robot-systems/exoskelett-aktiv-ca.html.

[28] D. Decker and J. A. Piepmeier, “Gaze tracking interface for robotic control”, in *2008 40th Southeastern Symposium on System Theory (SSST)*, 2008, pp. 274–278. DOI: 10.1109/SSST.2008.4480236.

[29] P. Agarwal, S. A. Moubayed, A. Alspach, J. Kim, E. J. Carter, J. F. Lehman, and K. Yamane, “Imitating human movement with teleoperated robotic head”, in *2016 25th IEEE International Symposium on Robot and Human Interactive Communication (RO-MAN)*, 2016, pp. 630–637. DOI: 10.1109/ROMAN.2016.7745184.

[30] S. Zhao, P. Xu, Z. Li, and C. Y. Su, “Brain-actuated teleoperation control of a mobile robot”, in *2015 IEEE International Conference on Robotics and Biomimetics (ROBIO)*, 2015, pp. 464–469. DOI: 10.1109/ROBIO.2015.7418811.

[31] *Mobility experiment: Remote repositioning, atlanta*, Ford Motor Company, 2015. [Online]. Available: https://media.ford.com/content/fordmedia/fna/us/en/news/2015/01/06/mobility-experiment-remote-repositioning-atlanta.html.

[32] “PRESS KIT: Nissan Intelligent Mobility at CES”, 2017. [Online]. Available: http://nissannews.com/en-US/nissan/usa/channels/us-nissan-2017-ces/releases/press-kit-nissan-intelligent-mobility-at-ces.

[33] “5G can make remote driving a reality, Telefonica and Ericsson demostrate at MWC”, 2017. [Online]. Available: https://www.telefonica.com/es/web/press-office/-/5g-can-make-remote-driving-a-reality-telefonica-and-ericsson-demostrate-at-mwc.

[34] *Basler AG*. [Online]. Available: http://www.baslerweb.com.

[35] *Oxford Technical Solutions*. [Online]. Available: www.oxts.com/.

[36] *DSPACE GmbH*. [Online]. Available: https://www.dspace.com.

[37] *SENSO-Wheel SD-LC, SENSODRIVE GmbH*. [Online]. Available: https://www.sensodrive.de/EN/products/Force-Feedback-Wheels/Senso-Wheel-SD-LC.php.

[38] *SENSODRIVE GmbH*. [Online]. Available: https://www.sensodrive.de.

[39] *EB Assist ADTF (Automotive Data and Time-Triggered Framework), Elektrobit Automotive GmbH*. [Online]. Available: https://www.elektrobit.com/products/eb-assist/adtf/.

[40] F. Chucholowski, S. Buechner, J. Reicheneder, and M. Lienkamp, “Prediction methods for teleoperated road vehicles”, in *CoFAT, Conference on Future Automotive Technology*, 2013.

[41] S. Gnatzig, “Trajektorienbasierte Teleoperation von Straßenfahrzeugen auf Basis eines Shared-Control-Ansatzes”, PhD thesis, Technische Universität München, 2015. [Online]. Available: https://mediatum.ub.tum.de/doc/1253158/1253158.pdf.

[42] *DYNA4 Framework: Automotive Simulation Software, TESIS DYNAware GmbH*. [Online]. Available: https://www.tesis-dynaware.com/en/products/dyna4-framework.

[43] *Driving simulation software SILAB, WIVW GmbH*. [Online]. Available: https://wivw.de/en/silab.

[44] *V-Model*. [Online]. Available: http://www.cio.bund.de/Web/DE/Architekturen-und-Standards/V-Modell-XT/vmodell_xt_node.html.

[45] T. B. Sheridan, “Teleoperation, telerobotics and telepresence: A progress report”, *ControlEng. Practice.*, vol. 3, no. 2, pp. 205–214, 1995. [Online]. Available: http://www.sciencedirect.com/science/article/pii/096706619400078U.

[46] F. Biocca and B. Delaney, “Communication in the age of virtual reality”, in, F. Biocca and M. R. Levy, Eds., Hillsdale, NJ, USA: L. Erlbaum Associates Inc., 1995, ch. Immersive Virtual Reality Technology, pp. 57–124, ISBN: 0-8058-1550-3.

[47] M. R. Endsley, “Situation awareness global assessment technique (sagat)”, in *Proceedings of the IEEE 1988 National Aerospace and Electronics Conference*, 1988, 789–795 vol.3. DOI: 10.1109/NAECON.1988.195097.

[48] J. V. Draper, D. B. Kaber, and J. M. Usher, “Telepresence”, *Human Factors*, vol. 40(3), pp. 354–375, 1998. DOI: 10.1518/001872098779591386.

[49] J. M. Riley, D. B. Kaber, and J. V. Draper, “Situation awareness and attention allocation measures for quantifying telepresence experiences in teleoperation”, *Human Factors and Ergonomics in Manufacturing & Service Industries*, vol. 14, no. 1, pp. 51–67, 2004, ISSN: 1520-6564. DOI: 10.1002/hfm.10050. [Online]. Available: http://dx.doi.org/10.1002/hfm.10050.

[50] D. Akin, M. I. of Technology, G. C. M. S. F. Center, U. S. N. Aeronautics, S. A. Scientific, and T. I. Branch, *Space applications of automation, robotics and machine intelligence systems (ARAMIS) - phase II*, ser. NASA contractor report v. 3. National Aeronautics, Space Administration, Scientific, and Technical Information Branch, 1983. [Online]. Available: https://books.google.de/books?id=0EB4-DGI088C.

[51] T. B. Sheridan, *Telerobotics, automation, and human supervisory control*. Cambridge, Mass. MIT Press, 1992, ISBN: 0-262-19316-7. [Online]. Available: http://opac.inria.fr/record=b1089614.

[52] J. Steuer, "Defining virtual reality: Dimensions determining telepresence", *JOURNAL OF COMMUNICATION*, vol. 42, pp. 73–93, 1992. DOI: 10.1111/j.1460-2466.1992.tb00812.x.

[53] D. Zeltzer, "Autonomy, interaction, and presence", *Presence: Teleoper. Virtual Environ.*, vol. 1, no. 1, pp. 127–132, Jan. 1992, ISSN: 1054-7460. DOI: 10.1162/pres.1992.1.1.127.

[54] B. G. Witmer and M. J. Singer, "Measuring presence in virtual environments: A presence questionnaire", *Presence: Teleoper. Virtual Environ.*, vol. 7, no. 3, pp. 225–240, Jun. 1998, ISSN: 1054-7460. DOI: 10.1162/105474698565686.

[55] C. Cruz-Neira, "Virtual reality overview", in *ACM SIGGRAPH '93 Conference*, 1993.

[56] M. R. Mine, F. P. Brooks, and C. H. Sequin, "Moving objects in space: Exploiting proprioception in virtual-environment interaction", in *SIGGRAPH '97 Proceedings of the 24th annual conference on Computer graphics and interactive techniques*, 1997, pp. 19–26. DOI: 10.1145/258734.258747. [Online]. Available: http://dx.doi.org/10.1145/258734.258747.

[57] I. E. Sutherland, "The ultimate display", in *Proceedings of the IFIP Congress*, 1965, pp. 506–508. DOI: 10.1109/MC.2005.274. [Online]. Available: http://dx.doi.org/10.1109/MC.2005.274.

[58] T. Mazuryk and M. Gervautz, "Virtual reality history, applications, technology and future", Institute of Computer Graphics and Algorithms, Vienna University of Technology, Favoritenstrasse 9-11/186, A-1040 Vienna, Austria, Tech. Rep. TR-186-2-96-06, Feb. 1996. [Online]. Available: http://www.cg.tuwien.ac.at/research/publications/1996/mazuryk-1996-VRH/.

[59] R. Dörner, W. Broll, P. Grimm, and B. Jung, Eds., *Virtual und Augmented Reality (VR/AR) - Grundlagen und Methoden der Virtuellen und Augmentierten Realität*. Springer Berlin Heidelberg, 2013.

[60] *Oculus VR*. [Online]. Available: https://www.oculus.com.

[61] R. M. Satava and S. B. Jones, "Current and future applications of virtual reality for medicine", *Proceedings of the IEEE*, vol. 86, no. 3, pp. 484–489, 1998, ISSN: 0018-9219. DOI: 10.1109/5.662873.

[62] N. Pioch, B. Roberts, and D. Zeltzer, "A virtual environment for learning to pilot remotely operated vehicles", in *Virtual Systems and MultiMedia, 1997. VSMM '97. Proceedings., International Conference on*, 1997, pp. 218–226. DOI: 10.1109/VSMM.1997.622350.

[63] L. R. Elliott, C. Jansen, E. S. Redden, and R. A. Pettitt, "Robotic telepresence: Perception, performance, and user experience", U.S. Army Research Laboratory, Tech. Rep., 2012. [Online]. Available: http://www.arl.army.mil/arlreports/2012/ARL-TR-5928.pdf.

[64] T. Bock, M. Maurer, and G. Farber, "Validation of the vehicle in the loop (vil); a milestone for the simulation of driver assistance systems", in *Intelligent Vehicles Symposium, 2007 IEEE*, 2007, pp. 612–617. DOI: 10.1109/IVS.2007.4290183.

[65] S. Kratz, J. Vaughan, and D. Kimber, "Evaluating stereoscopic video with head tracking for immersive teleoperation of mobile telepresence robots", in *Proceedings of the Tenth Annual ACM/IEEE International Conference on Human-Robot Interaction*, 2015, pp. 43–44. DOI: 10.1145/2701973.2701982.

[66] S. Livatino, G. Muscato, and F. Privitera, “Stereo viewing and virtual reality technologies in mobile robot teleguide”, *Robotics, IEEE Transactions on*, vol. 25, no. 6, pp. 1343–1355, 2009, ISSN: 1552-3098. DOI: 10.1109/TRO.2009.2028765.

[67] H. Martins, I. Oakley, and R. Ventura, “Design and evaluation of a head-mounted display for immersive 3d teleoperation of field robots”, *Robotica*, vol. 33, pp. 2166–2185, 10 Dec. 2015, ISSN: 1469-8668. DOI: 10.1017/S026357471400126X. [Online]. Available: http://journals.cambridge.org/article_S026357471400126X.

[68] Y. Wang, F. Zhong, C. Li, H. Xiang, Q. Peng, and X. Qin, “Tele-AR system based on real-time camera tracking”, in *Virtual Reality and Visualization (ICVRV), 2012 International Conference on*, 2012, pp. 19–26. DOI: 10.1109/ICVRV.2012.13.

[69] K. Kruckel, F. Nolden, A. Ferrein, and I. Scholl, “Intuitive visual teleoperation for ugvs using free-look augmented reality displays”, in *Robotics and Automation (ICRA), 2015 IEEE International Conference on*, 2015, pp. 4412–4417. DOI: 10.1109/ICRA.2015.7139809.

[70] P. Milgram, H. Takemura, A. Utsumi, and F. Kishino, “Augmented reality: A class of displays on the reality-virtuality continuum”, *Telemanipulator and Telepresence Technologies*, vol. Vol. 2351, pp. 282–292, 1994. DOI: 10.1117/12.197321.

[71] W. Hoenig, C. Milanes, L. Scaria, T. Phan, M. Bolas, and N. Ayanian, “Mixed reality for robotics”, in *2015 IEEE/RSJ International Conference on Intelligent Robots and Systems (IROS)*, 2015, pp. 5382–5387. DOI: 10.1109/IROS.2015.7354138.

[72] H. Schnädelbach, B. Keleva, M. Flintham, M. Fraser, S. Izadi, P. Chandler, M. Foster, S. Benford, C. Greenhalgh, and T. Rodden, “The augurscope: A mixed reality interface for outdoors”, in *Proceedings of the SIGCHI conference on Human factors in computing systems: Changing our world, changing ourselves*, Association for Computing Machinery, Inc., 2002, pp. 9–16. [Online]. Available: http://research.microsoft.com/apps/pubs/default.aspx?id=132662.

[73] A. Elfes, “Using occupancy grids for mobile robot perception and navigation”, *Computer*, vol. 22, no. 6, pp. 46–57, Jun. 1989, ISSN: 0018-9162. DOI: 10.1109/2.30720. [Online]. Available: http://dx.doi.org/10.1109/2.30720.

[74] G. Knappe, A. Keinath, K. Bengler, and C. Meinecke, “Driving simulator as an evaluation tool: Assessment of the influence of field of view and secondary tasks on lane keeping and steering performance”, in *20th International Technical Conference on the Enhanced Safety of Vehicles (ESV)*, Lyon , France, 2007. [Online]. Available: https://www-nrd.nhtsa.dot.gov/pdf/esv/esv20/07-0262-o.pdf.

[75] G. Knappe, “Empirische Untersuchungen zur Querregelung in Fahrsimulatoren: Vergleichbarkeit von Untersuchungsergebnissen und Sensitivitaet von Messgroessen”, PhD thesis, Uni Erlangen-Nürnberg, 2009. [Online]. Available: https://opus4.kobv.de/opus4-fau/frontdoor/index/index/year/2010/docId/1032.

[76] *The National Aeronautics and Space Administration (NASA), the NASA Task Load Index (TLX)*. [Online]. Available: https://humansystems.arc.nasa.gov/groups/tlx/.

[77] H. Winner, S. Hakuli, F. Lotz, and C. Singer, *Handbuch Fahrerassistenzsysteme*. Springer Vieweg, 2015, ISBN: 978-3-658-05734-3. [Online]. Available: https://books.google.de/books?id=UqlYIaso3yoC&redir_esc=y.

[78] N. Moshchuk, S. K. Chen, C. Zagorski, and A. Chatterjee, “Optimal braking and steering control for active safety”, in *2012 15th International IEEE Conference on Intelligent Transportation Systems*, 2012, pp. 1741–1746. DOI: 10.1109/ITSC.2012.6338640.

[79] EURO NCAP, “Mercedes-Benz PRE-SAFE Brake”, Tech. Rep., 2010. [Online]. Available: http://www.euroncap.com/en/ratings-rewards/euro-ncap-advanced-rewards/2010-mercedes-benz-pre-safe-brake/.

[80] H. Winner, “Fundamentals of collision protection systems”, in *Handbook of Driver Assistance Systems: Basic Information, Components and Systems for Active Safety and Comfort*, H. Winner, S. Hakuli, F. Lotz, and C. Singer, Eds., Springer International Publishing, 2015, ch. 46, pp. 1149–1176, ISBN: 978-3-319-12353-0.

[81] C. G. Keller, T. Dang, H. Fritz, A. Joos, C. Rabe, and D. M. Gavrila, “Active pedestrian safety by automatic braking and evasive steering”, *IEEE Transactions on Intelligent Transportation Systems*, vol. 12, no. 4, pp. 1292–1304, 2011, ISSN: 1524-9050. DOI: 10.1109/TITS.2011.2158424.

[82] S. Buzzi, M. Lops, and L. Venturino, “Track-before-detect procedures for early detection of moving target from airborne radars”, *Aerospace and Electronic Systems, IEEE Transactions on*, vol. 41, no. 3, pp. 937–954, 2005, ISSN: 0018-9251. DOI: 10.1109/TAES.2005.1541440.

[83] S. Baker, D. Scharstein, J. P. Lewis, S. Roth, M. J. Black, and R. Szeliski, “A database and evaluation methodology for optical flow”, *International Journal of Computer Vision*, vol. 92, no. 1, pp. 1–31, 2011, ISSN: 1573-1405. DOI: 10.1007/s11263-010-0390-2. [Online]. Available: http://dx.doi.org/10.1007/s11263-010-0390-2.

[84] J. Sanchez Perez, E. Meinhardt-Llopis, and G. Facciolo, “TV-L1 Optical Flow Estimation”, *Image Processing On Line*, vol. 3, pp. 137–150, 2013. DOI: 10.5201/ipol.2013.26.

[85] C. Rabe, “Detection of moving objects by spatio-temporal motion analysis”, PhD thesis, University of Kiel, Kiel, Germany, 2011, ISBN: 978-3-8381-3219-8. [Online]. Available: https://books.google.de/books?id=fPd-uAAACAAJ.

[86] C. Rabe, T. Müller, A. Wedel, and U. Franke, “Dense, Robust, and Accurate Motion Field Estimation from Stereo Image Sequences in Real-Time”, in *Proceedings of the 11th European Conference on Computer Vision*, K. Daniilidis, P. Maragos, and N. Paragios, Eds., ser. Lecture Notes in Computer Science, vol. 6314, Springer, 2010, pp. 582–595. DOI: 10.1007/978-3-642-15561-1_42. [Online]. Available: https://doi.org/10.1007/978-3-642-15561-1_42.

[87] C. Zach, T. Pock, and H. Bischof, “A duality based approach for realtime TV-L1 optical flow”, in *Proceedings of the 29th DAGM conference on Pattern recognition*, 2007, pp. 214–223. DOI: 10.1007/978-3-540-74936-3_22. [Online]. Available: https://doi.org/10.1007/978-3-540-74936-3_22.

[88] H. Hirschmüller, “Accurate and efficient stereo processing by semi-global matching and mutual information”, in *Proceedings of the 2005 IEEE Computer Society Conference on Computer Vision and Pattern Recognition (CVPR’05) - Volume 2 - Volume 02*, ser. CVPR ’05, Washington, DC, USA: IEEE Computer Society, 2005, pp. 807–814, ISBN: 0-7695-2372-2. DOI: 10.1109/CVPR.2005.56. [Online]. Available: http://dx.doi.org/10.1109/CVPR.2005.56.

[89] A. Geiger, J. Ziegler, and C. Stiller, “Stereoscan: Dense 3d reconstruction in real-time”, in *2011 IEEE Intelligent Vehicles Symposium (IV)*, 2011, pp. 963–968. DOI: 10.1109/IVS.2011.5940405.

[90] *Vienna Convention on Road Traffic*, 1968. [Online]. Available: https://www.unece.org/fileadmin/DAM/trans/conventn/crt1968e.pdf.

[91] *Report of the sixty-eighth session of the working party on road traffic safety.* 2014. [Online]. Available: https://www.unece.org/fileadmin/DAM/trans/doc/2014/wp1/ECE-TRANS-WP1-145e.pdf.

[92] *NVIDIA GeForce GTX 780 Ti*. [Online]. Available: http://www.geforce.com/hardware/desktop-gpus/geforce-gtx-780-ti.

[93] A Geiger, P Lenz, C Stiller, and R Urtasun, “Vision meets robotics: The KITTI dataset”, *International Journal of Robotics Research (IJRR)*, vol. 32, no. 11, pp. 1231–1237, Sep. 2013, ISSN: 0278-3649. DOI: 10.1177/0278364913491297. [Online]. Available: http://dx.doi.org/10.1177/0278364913491297.

[94] T. Vaudrey, C. Rabe, R. Klette, and J. Milburn, “Differences between stereo and motion behaviour on synthetic and real-world stereo sequences”, in *Image and Vision Computing New Zealand, 2008. IVCNZ 2008. 23rd International Conference*, 2008, pp. 1–6. DOI: 10.1109/IVCNZ.2008.4762133.

[95] M. M. Minderhoud and P. H. Bovy, “Extended time-to-collision measures for road traffic safety assessment”, *Accident Analysis & Prevention*, vol. 33, no. 1, pp. 89 –97, 2001, ISSN: 0001-4575. DOI: http://dx.doi.org/10.1016/S0001-4575(00)00019-1. [Online]. Available: http://www.sciencedirect.com/science/article/pii/S0001457500000191.

[96] M. McClelland and M. E Campbell, “Anticipation as a method for overcoming time delay in control of remote systems”, *American Institute of Aeronautics and Astronautics (AIAA). Guidance, Navigation, and Control Conference*, 2010. [Online]. Available: enu.kz/repository/2010/AIAA-2010-7730.pdf.

[97] Y. Zheng, M. Brudnak, P. Jayakumar, J. Stein, and T. Ersal, “An experimental evaluation of a model-free predictor framework in teleoperated vehicles”, *13th IFAC Workshop on Time Delay Systems TDS 2016*, vol. 49, no. 10, pp. 157–164, 2016.

[98] S. Hirche and M. Buss, “Human-oriented control for haptic teleoperation”, *Proceedings of the IEEE*, vol. 100, no. 3, pp. 623–647, 2012, ISSN: 0018-9219. DOI: 10.1109/JPROC.2011.2175150.

[99] T. Fong, F. Conti, S. Grange, and C Baur, “Novel interfaces for remote driving: Gesture, haptic and pda”, *Proceedings of the SPIE Telemanipulator and Telepresence Technologies Conference, Boston, MA*, 2000. [Online]. Available: https://infoscience.epfl.ch/record/29981/files/SPIE00-TF.pdf.

[100] L. B. Rosenberg, “Virtual fixtures: Perceptual tools for telerobotic manipulation”, in *Proceedings of IEEE Virtual Reality Annual International Symposium*, 1993, pp. 76–82. DOI: 10.1109/VRAIS.1993.380795.

[101] D. A. Abbink, M. Mulder, and E. R. Boer, “Haptic shared control: Smoothly shifting control authority?”, *Cognition, Technology & Work*, vol. 14, no. 1, pp. 19–28, 2012, ISSN: 1435-5566. DOI: 10.1007/s10111-011-0192-5. [Online]. Available: http://dx.doi.org/10.1007/s10111-011-0192-5.

[102] P. Marayong and A. M. Okamura, “Speed-accuracy characteristics of human-machine cooperative manipulation using virtual fixtures with variable admittance”, *Human Factors*, vol. 46, no. 3, pp. 518–532, 2004. [Online]. Available: https://www.ncbi.nlm.nih.gov/pubmed/15573549.

[103] T. M. Lam, H. W. Boschloo, M. Mulder, and M. M. van Paassen, “Artificial force field for haptic feedback in uav teleoperation”, *IEEE Transactions on Systems, Man, and Cybernetics - Part A: Systems and Humans*, vol. 39, no. 6, pp. 1316–1330, 2009, ISSN: 1083-4427. DOI: 10.1109/TSMCA.2009.2028239.

[104] B. Forsyth and K. MacLean, “Predictive haptic guidance: Intelligent user assistance for the control of dynamic tasks”, *Visualization and Computer Graphics, IEEE Transactions on*, vol. 12, no. 1, pp. 103–113, 2006, ISSN: 1077-2626. DOI: 10.1109/TVCG.2006.11.

[105] P. G. Griffiths and R. B. Gillespie, “Sharing control between humans and automation using haptic interface: Primary and secondary task performance benefits”, *Human Factors*, vol. 47, no. 3, pp. 574–590, 2005.

[106] D. Katzourakis, M. Alirezaei, J. C. F. de Winter, M. Corno, R. Happee, A. Ghaffari, and R. Kazemi, “Shared control for road departure prevention”, in *2011 IEEE International Conference on Systems, Man, and Cybernetics*, 2011, pp. 1037–1043. DOI: 10.1109/ICSMC.2011.6083811.

[107] M. Flad, J. Otten, S. Schwab, and S. Hohmann, “Steering driver assistance system: A systematic cooperative shared control design approach”, in *Systems, Man and Cybernetics (SMC), 2014 IEEE International Conference on*, 2014, pp. 3585–3592. DOI: 10.1109/SMC.2014.6974486.

[108] “BMW Blog, BMW develops a Narrow-Passage Assistant”, 2010. [Online]. Available: http://www.bmwblog.com/2010/03/27/bmw-develops-a-narrow-passage-assistant/.

[109] S. Scholz, S. Chlosta, S. Freter, and F. Schuldt, “Prototypische umsetzung eines bau- und engstellenassistenten”, in *Automatisierte Systeme, Assistenzsysteme und eingebetette Systeme fuer Transportmittel, AAET 2014*, 2014, pp. 292–304. [Online]. Available: https://www.ifr.ing.tu-bs.de/static/files/forschung/papers/download_pdf.php?id=736.

[110] T. Michalke, C. Gläser, L. Bürkle, and F. Niewels, “The narrow road assistant - next generation advanced driver assistance in inner-city”, in *Intelligent Transportation Systems - (ITSC), 2013 16th International IEEE Conference on*, 2013, pp. 2173–2180. DOI: 10.1109/ITSC.2013.6728550.

[111] T. P. Michalke, C. Gläser, L. Bürkle, and F. Niewels, “The narrow road assistant - evolution towards highly automated driving in inner city”, in *2016 IEEE Intelligent Vehicles Symposium (IV)*, 2016, pp. 1192–1198. DOI: 10.1109/IVS.2016.7535541.

[112] *Project UR:BAN, Urbaner raum: Benutzergerechte Assistenzsysteme und Netzmanagement*. [Online]. Available: http://urban-online.org/de/urban.html.

[113] S. Pietzsch, “Modellgestützte Sensordatenfusion von Laserscanner und Radar zur Erfassung komplexer Fahrzeugumgebungen”, PhD thesis, Technische Universität München, 2015. [Online]. Available: https://mediatum.ub.tum.de/doc/1236700/1236700.pdf.

[114] M. Darms, “Eine Basis-Systemarchitektur zur Sensordatenfusion von Umfeldsensoren für Fahrerassistenzsysteme”, PhD thesis, Technische Universität, Darmstadt, 2007. [Online]. Available: http://tuprints.ulb.tu-darmstadt.de/914/.

[115] M. Ankerst, M. M. Breunig, H. peter Kriegel, and J. Sander, “Optics: Ordering points to identify the clustering structure”, ACM Press, 1999, pp. 49–60. [Online]. Available: https://www.dbs.ifi.lmu.de/Publikationen/Papers/OPTICS.pdf.

[116] W. Zhonghong, S. Zhangsong, W. Yaoping, and H. Jiawei, “Line extraction method based on distance weighted least squares and self-adaption segmentation”, in *2015 7th International Conference on Intelligent Human-Machine Systems and Cybernetics*, vol. 2, 2015, pp. 452–455. DOI: 10.1109/IHMSC.2015.159.

[117] Y. Bar-Shalom, F. Daum, and J. Huang, “The probabilistic data association filter”, *IEEE Control Systems*, vol. 29, no. 6, pp. 82–100, 2009, ISSN: 1066-033X. DOI: 10.1109/MCS.2009.934469.

[118] D. Musicki and R. Evans, “Joint integrated probabilistic data association: Jipda”, *IEEE Transactions on Aerospace and Electronic Systems*, vol. 40, no. 3, pp. 1093–1099, 2004, ISSN: 0018-9251. DOI: 10.1109/TAES.2004.1337482.

[119] M. Alirezaei, M. Corno, D. Katzourakis, A. Ghaffari, and R. Kazemi, “A robust steering assistance system for road departure avoidance”, *Vehicular Technology, IEEE Transactions on*, vol. 61, no. 5, pp. 1953–1960, 2012, ISSN: 0018-9545. DOI: 10.1109/TVT.2012.2191001.

[120] S. de Nijs, M. Mulder, and D. Abbink, “The value of haptic feedback in lane keeping”, in *Systems, Man and Cybernetics (SMC), 2014 IEEE International Conference on*, 2014, pp. 3599–3604. DOI: 10.1109/SMC.2014.6974488.

[121] *ISO/DIS 3888-1, Passenger cars - Test track for a severe lane-change manoeuvre - part 1: Double lane-change*. [Online]. Available: http://www.iso.org/iso/catalogue_detail.htm?csnumber=67973.

[122] D. Ferguson, M. Likhachev, and A. Stentz, “A guide to heuristic-based path planning”, in *Proceedings of the International Workshop on Planning under Uncertainty for Autonomous Systems, International Conference on Automated Planning and Scheduling (ICAPS)*, 2005. [Online]. Available: https://www.cs.cmu.edu/~maxim/files/hsplanguide_icaps05ws.pdf.

[123] M. Cikes, M. Dakulovic, and I. Petrovic, “The path planning algorithms for a mobile robot based on the occupancy grid map of the environment; a comparative study”, in *Information, Communication and Automation Technologies (ICAT), 2011 XXIII International Symposium on*, 2011, pp. 1–8. DOI: 10.1109/ICAT.2011.6102088.

[124] S. Anderson, S. Karumanchi, and K. Iagnemma, “Constraint-based planning and control for safe, semi-autonomous operation of vehicles”, in *Intelligent Vehicles Symposium (IV), 2012 IEEE*, 2012, pp. 383–388. DOI: 10.1109/IVS.2012.6232153.

[125] D. Dolgov, S. Thrun, M. Montemerlo, and J. Diebel, “Path planning for autonomous vehicles in unknown semi-structured environments”, *The International Journal of Robotics Research*, vol. 29, no. 5, pp. 485–501, Apr. 2010, ISSN: 0278-3649. DOI: 10.1177/0278364909359210.

[126] S. LaValle and J. Kuffner J.J., “Randomized kinodynamic planning”, in *Robotics and Automation, 1999. Proceedings. 1999 IEEE International Conference on*, vol. 1, 1999, 473–479 vol.1. DOI: 10.1109/ROBOT.1999.770022.

[127] J. Boyd, “5G Coming Sooner, Not Later”, IEEE Spectrum, Tech. Rep., 2016.

[128] T. Tang, P. Vetter, S. Finkl, K. Figel, and M. Lienkamp, “Teleoperated road vehicles - the free corridor as a safety strategy approach”, in *2nd International Conference on Mechanical Design and Power Engineering, ICMDPE 2013*, Applied Mechanics and Materials Volume 490-491, 2014, pp. 1399–1409. DOI: 10.4028/www.scientific.net/AMM.490-491.1399.

Supervised Theses

This work contains the results of the following final theses, which have been supervised by the author of the present dissertation:

[129] R. Forster, “Weiterentwicklung und Umsetzung eines HMI-Konzepts mit Hilfe von Head-Mounted-Display zur präzisen Steuerung von teleoperierten Straßenfahrzeugen”, Master’s thesis, Technische Universität München, 2017.

[130] J. Porer, “Weiterentwicklung und Erprobung eines haptischen Assistenzsystems für teleoperiertes Fahren in innerstädtischen Umgebungen”, Master’s thesis, Technische Universität München, 2016.

[131] A. Rotar, “Weiterentwicklung und echtzeitfähige Umsetzung eines Stereo-Vision-basierten Bewegungsprädiktionssystems für die aktive Sicherheit von teleoperierten Fahrzeugen”, Master’s thesis, Technische Universität München, 2016.

[132] I. Janscha, “Entwicklung einer dynamischen Belegungskarte mit Hilfe von LiDAR-Sensoren für teleoperierte Fahrzeuge”, Master’s thesis, Technische Universität München, 2016.

[133] J. Sabielny, “Design und Umsetzung eines Bedienkonzepts zur präzisen Steuerung von teleoperierten Fahrzeugen mit Hilfe eines Head-Mounted Displays”, Master’s thesis, Technische Universität München, 2015.

[134] R. Kutka, “Entwicklung eines aktiven Sicherheitssystems für teleoperierte Straßenfahrzeuge”, Master’s thesis, Technische Universität München, 2015.

[135] F. Richthammer, “Entwicklung eines Assistenzsystems zur präzisen lateralen Steuerung teleoperierter Fahrzeuge unter Nutzung von haptischem Feedback”, Master’s thesis, Technische Universität München, 2015.

[136] S. Bauer, “Objektdetektion und Bewegungsprädiktion mittels eines Stereokamerasystems beim teleoperierten Fahren”, Master’s thesis, Technische Universität München, 2014.

[137] T. Wiedemann, “Interaktive Bahnplanung zur indirekten Steuerung von teleoperierten Fahrzeugen”, Master’s thesis, Technische Universität München, 2014.

[138] C. Vortmann, *Teleoperiertes Fahren - Untersuchung von Grenzen des Bedienkonzeptes Direkte Steuerung*, Diplomarbeit, Technische Universität München, 2015.

[139] S. Tsoukalas, *Realisierung eines Stereo Vision Systems für teleoperierte Fahrzeuge*, Semesterarbeit, Technische Universität München, 2014.

[140] T. Lieb, “Regelungstechnische Modellierung des menschlichen Fahrverhaltens beim teleoperierten Fahren”, Master’s thesis, Technische Universität München, 2014.

Own Publications

[141] P. M. d'Orey, A. Hosseini, J. Azevedo, F. Diermeyer, M. Ferreira, and M. Lienkamp, "Hail-a-drone: Enabling teleoperated taxi fleets", in *2016 IEEE Intelligent Vehicles Symposium (IV)*, 2016, pp. 774–781. DOI: 10.1109/IVS.2016.7535475.

[142] A. Hosseini, D. Bacara, and M. Lienkamp, "A system design for automotive augmented reality using stereo night vision", in *2014 IEEE Intelligent Vehicles Symposium Proceedings*, 2014, pp. 127–133. DOI: 10.1109/IVS.2014.6856484.

[143] A. Hosseini, T. Wiedemann, and M. Lienkamp, "Interactive path planning for teleoperated road vehicles in urban environments", in *Intelligent Transportation Systems (ITSC), 2014 IEEE 17th International Conference on*, 2014, pp. 400–405. DOI: 10.1109/ITSC.2014.6957723.

[144] A. Hosseini and M. Lienkamp, "Enhancing telepresence during the teleoperation of road vehicles using hmd-based mixed reality", in *2016 IEEE Intelligent Vehicles Symposium (IV)*, 2016, pp. 1366–1373. DOI: 10.1109/IVS.2016.7535568.

[145] A. Hosseini and M. Lienkamp, "Fahrerassistenzsysteme zur präzisen und sicheren Steuerung von teleoperierten Straßenfahrzeugen in innerstädtischen Umgebungen", in *7. Tagung Fahrerassistenz*, 2015. [Online]. Available: https://mediatum.ub.tum.de/doc/1290714/1290714.pdf.

[146] A. Hosseini and M. Lienkamp, "Predictive safety based on track-before-detect for teleoperated driving through communication time delay", in *2016 IEEE Intelligent Vehicles Symposium (IV)*, 2016, pp. 165–172. DOI: 10.1109/IVS.2016.7535381.

[147] A. Hosseini, F. Richthammer, and M. Lienkamp, "Predictive haptic feedback for safe lateral control of teleoperated road vehicles in urban areas", in *2016 IEEE 83rd Vehicular Technology Conference (VTC Spring)*, 2016, pp. 1–7. DOI: 10.1109/VTCSpring.2016.7504430.